

THE EFFECT OF LIFELONG MATERNAL OBESITY ON PREGNANCY  
OUTCOMES AND PLACENTAL DEVELOPMENT

By

EMILY K. HAYES, H.B.Sc.

A Thesis

Submitted to the School of Graduate Studies

in Partial Fulfillment of the Requirements

for the Degree

Master of Science

McMaster University

© Emily K. Hayes, March 2012

MASTER OF SCIENCE (2012)  
(Medical Sciences)

McMaster University  
Hamilton, Ontario

TITLE: The Effect of Lifelong Maternal Obesity on Pregnancy Outcomes and Placental Development

AUTHOR: Emily K. Hayes, H.B.Sc (McMaster University)

SUPERVISOR: Dr. Sandeep Raha

NUMBER OF PAGES: xvii, 123

## **ABSTRACT**

Maternal obesity is associated with an increased risk of pregnancy complications, including preeclampsia, miscarriage, birth of small for gestational age (SGA) babies, and stillbirth. Placental dysfunction has been implicated in all of these complications; however, the mechanisms by which maternal obesity influences placental development and function are not well understood. Female Sprague-Dawley rats were fed either a control diet (CON; 16% kcal from fat) or a high fat diet (HF; 45% kcal from fat) for 16 weeks beginning at weaning and were then mated with age-matched CON-fed males. This model emulates life-long obesity prior to pregnancy, a situation which is clinically relevant. Prior to pregnancy, HF-fed dams were 36% heavier and had significantly more abdominal fat. Dams were sacrificed at either gestational day (GD) 15 or GD18 to collect placental tissues. The remaining females were allowed to give birth naturally. HF-fed dams showed evidence of increased intrauterine death at GD15 and GD18. At birth, smaller litter sizes, offspring with reduced birthweight, and more stillbirths were observed in the HF-fed group. Placentas from HF-fed dams exhibited morphological changes at GD15, including an increased area covered by the labyrinth zone, an increase in blood vessel density and decrease in blood vessel maturity in the labyrinth layer, as well as increased carbonic anhydrase staining, indicative of hypoxia. These changes were associated with increased vascular endothelial growth factor (VEGF) protein levels and decreased placental growth factor (PIGF) protein levels. Both interstitial and endovascular trophoblast invasion into the maternal mesometrial triangles were increased

at GD15. While these differences were no longer evident by GD18, placental morphometry demonstrated that the area covered by the labyrinth layer remained significantly greater in the HF-fed compared to CON-fed dams. Placental oxidative stress, which is often associated with placental dysfunction, was not observed at statistically significant levels at GD15. The early dysregulation of placental structure in HF-fed dams, which is normalized later in gestation, may play a role in the development of pregnancy complications associated with maternal obesity.

## **ACKNOWLEDGEMENTS**

I would like to thank Dr. Sandeep Raha for his patience, guidance and expertise. I would also like to thank Dr. Alison Holloway and Dr. Bernardo Trigatti for their helpful advice, as well as our collaborators Dr. Jim Petrik and his lab at the University of Guelph, and Dr. Andree Gruslin and her lab at the University of Ottawa; particularly Daniel Tessier for his knowledge of placental biology. I would like to thank Dr. Alison Holloway, Dr. Warren Foster, Dr. Mark Tarnopolsky, and Dr. Thomas Hawke and all their labs for allowing me to use their equipment and providing advice on experimental procedures. Previous members of the Raha lab, including Anna Lechowicz, Yaryna Storozhuk, Milosz Kaczmarczyk, Andy Liu, Margaret Mansell, Michael Percival, Kara Grace, and Hannah Aikman, were essential to this project and their work is greatly appreciated. Finally, I appreciate the support of many family members and friends, including Rick Hayes, Lillian Robson, Natasha Sarin, Glynnis Lee, and Ben Somer.

## TABLE OF CONTENTS

DESCRIPTIVE NOTES	ii
ABSTRACT	iii
ACKNOWLEDGEMENTS	v
TABLE OF CONTENTS	vi
LIST OF FIGURES	xi
LIST OF TABLES	xiv
LIST OF ABBREVIATIONS	xv
1. INTRODUCTION	1
1.1 The prevalence and impact of maternal obesity	1
1.1.1 The obesity epidemic	1
1.1.2 Physiological consequences of obesity	1
1.1.3 Obesity during pregnancy	3
1.1.4 The rat as a model to study human placentation	4
1.2 The placenta	5
1.2.1 Functions of the placenta	5
1.2.2 The structure of the rat placenta	6
1.2.3 The structure of the human placenta	9
1.2.4 The rat as a model of human placentation	11
1.3 Development of the placenta	12

1.3.1 Early gestation: implantation and formation of the placenta proper	12
1.3.2 Establishment and development of the placental vasculature	13
1.3.3 Trophoblast invasion into the mesometrial triangle	16
1.3.4 Remodelling of the maternal spiral arteries by invasive trophoblast cells	17
1.3.5 Role of hypoxia in placental development	19
1.3.6 Role of oxidative stress in placental development	21
1.4 The role of the placenta in pregnancy complications	24
1.4.1 Preeclampsia	24
1.4.2 Small for gestational age and intrauterine growth restriction	29
1.4.3 Miscarriage and stillbirth	30
1.5 Maternal obesity and placental dysfunction	31
2. STUDY OBJECTIVES	33
2.1 Hypothesis	33
2.2 Objectives	33
3. MATERIALS AND METHODS	34
3.1 Study design	34
3.1.1 Mating and pregnancy	34
3.1.2 Sample preparation and storage	35
3.2 CT scanning and analysis	36
3.3 Measures of obstetric outcomes	36
3.3.1 Fertility and mating outcomes	36

3.3.2 Pregnancy and birth outcomes	37
3.4 Measures of systemic oxidative stress and inflammation	38
3.4.1 Creatinine colorimetric assay	38
3.4.2 8-Isoprostanes ELISA	38
3.4.3 8-hydroxy-2'-deoxyguanosine ELISA	38
3.4.4 Monocyte chemoattractant protein-1 (MCP-1) ELISA	38
3.5 Placental tissue preparations	39
3.5.1 Tissue homogenization	39
3.5.2 Preparation of mitochondrially enriched fractions	39
3.5.3 Bicinchoninic acid protein assay	40
3.6 Protein quantification by Western blot	40
3.6.1 SDS-PAGE	40
3.6.2 Ponceau-S Stain	40
3.6.3 Western blotting	41
3.7 Immunohistochemistry	42
3.7.1 Tissue processing and slide preparation	42
3.7.2 Immunohistochemical staining	43
3.7.3 Hematoxylin and eosin staining	44
3.8 Imaging and quantification of stained slides	44
3.8.1 Analysis of placental morphology	44
3.8.2 Analysis of blood vessel density and maturity in the labyrinth	45
3.8.3 Analysis of carbonic anhydrase staining intensity	45

3.8.4 Analysis of interstitial trophoblast invasion	46
3.8.5 Analysis of endovascular trophoblast invasion	46
3.8.6 Analysis of spiral artery remodelling	46
3.8.8 Analysis of intensity of nitrotyrosine staining	48
3.9 Measurement of protein carbonyls	48
3.9.1 Protein carbonyl OxyBlot	48
3.9.2 Protein carbonyl ELISA	48
3.10 Gelatin zymography	49
3.11 Statistical analysis	49
4. RESULTS	51
4.1 Maternal weight gain and body fat distribution	51
4.2 Maternal systemic inflammation and oxidative stress	54
4.3 Maternal fertility and fetal and neonatal health outcomes	56
4.4 Placental vascular structure, morphometry of the implantation site, and cell death	60
4.5. Mechanisms behind the alterations in blood vessel structure and morphometry of the placenta: angiogenic growth factors and hypoxia	66
4.6 Trophoblast invasion and blood vessel remodelling in the mesometrial triangle	69
4.7 Markers of placental oxidative stress	77
5. DISCUSSION	84
5.1 The model of lifelong maternal obesity	84

5.1.1 Maternal weight gain, distribution of adipose tissue, systemic oxidative stress and inflammation	86
5.2 Fertility and pregnancy outcomes	88
5.3 Structural perturbations in the placenta proper	90
5.4 Trophoblast invasion into the mesometrial triangle	92
5.5 Temporal changes in the placenta	93
5.6 Spiral artery remodelling in the mesometrial triangle	94
5.7 Matrix metalloproteinases 2 and 9 in the junctional zone	98
5.8 Placental oxidative stress	98
6. FUTURE DIRECTIONS	100
REFERENCES	101
APPENDIX	123

## LIST OF FIGURES

<b>Figure 1.</b>	Structure of the rat placental labyrinth	6
<b>Figure 2.</b>	The structure of the rat placenta at GD15 of gestation.	8
<b>Figure 3.</b>	Comparing the structure of the human and rat placentas	10
<b>Figure 4.</b>	Structure of the blastocyst at the time of implantation	13
<b>Figure 5.</b>	The structure of the maternal spiral arteries in normal human pregnancy in the human.	18
<b>Figure 6.</b>	The structure of the maternal spiral arteries in preeclampsia in the human	26
<b>Figure 7.</b>	Body weight of CON and HF-fed dams prior to pregnancy	52
<b>Figure 8.</b>	Amount of abdominal adipose tissue is increased in HF-fed dams prior to pregnancy and at GD15	53
<b>Figure 9.</b>	Labyrinth layers of placentas from HF-fed dams exhibit an increased density of CD31-positive blood vessels at GD15 but not GD18.	62
<b>Figure 10.</b>	Labyrinth layers of placentas from HF-fed dams exhibit fewer SMA positive blood vessels at GD15 but not GD18.	63
<b>Figure 11.</b>	Placental morphometric parameters are altered in HF-fed vs CON-fed dams at gestational days 15 and 18	64
<b>Figure 12.</b>	The number of apoptotic cells per area is not significantly different in the labyrinth and junctional zones of placentas from	65

	CON and HF-fed dams at GD15.	
<b>Figure 13.</b>	VEGF protein levels are increased and PlGF levels are decreased in HF GD15 placentas.	67
<b>Figure 14.</b>	Labyrinth layers of placentas from HF-fed dams exhibit increased carbonic anhydrase staining intensity at GD15 but not GD18.	68
<b>Figure 15.</b>	Area covered by interstitial trophoblast cells in the mesometrial triangle is higher in HF-fed dams at gestational day 15 but not 18 of pregnancy.	70
<b>Figure 16.</b>	The percentage of blood vessels invaded by endovascular trophoblast cells in the entire mesometrial triangle is higher in HF-fed dams at GD15 but not GD18.	71
<b>Figure 17.</b>	The degree of spiral artery remodeling is not significantly different between CON and HF-fed dams at GD15 or GD18	73
<b>Figure 18.</b>	MMP2 protein and activity levels in junctional zones of placentas from HF and CON-fed dams are not significantly different at GD15.	74
<b>Figure 19.</b>	MMP9 protein and activity levels are lower in junctional zones of placentas from HF-fed dams at GD15.	75
<b>Figure 20.</b>	Levels of antioxidant enzymes are similar in the placentas of CON and HF-fed dams at GD15.	78
<b>Figure 21.</b>	Levels of lipid peroxidation are similar in the placentas of	79

	GD15 CON and HF-fed dams.	
<b>Figure 22.</b>	Levels of nitrotyrosine are similar in the placentas of GD15 CON and HF-fed dams.	80
<b>Figure 23.</b>	Levels of oxidative damage in mitochondrially enriched fractions isolated from the whole placentas of CON and HF-fed dams at GD15.	81
<b>Figure 24.</b>	Immunohistochemical analysis of nitrotyrosine in the placentas of GD15 and GD18 CON and HF-fed dams shows no significant difference.	82
<b>Figure 25.</b>	Nitrotyrosine immunostaining in endovascular trophoblasts at GD15 is not significantly higher in HF-fed dams.	83
<b>Supplemental Figure 1.</b>	Decreased VSMC coverage is associated with increased lumen area in invaded blood vessels.	122

## LIST OF TABLES

<b>Table 1.</b>	Important cytokines and their effects	53
<b>Table 2.</b>	Markers of systemic inflammation and oxidative stress in CON and HF-fed dams at gestational day 15.	55
<b>Table 3.</b>	Mating and fertility outcomes of CON and HF-fed dams	58
<b>Table 4.</b>	Parameters of fetal health in CON and HF-fed dams.	58
<b>Table 5.</b>	Parameters of neonatal health in CON and HF-fed dams	59
<b>Table 6.</b>	Levels of protein carbonyls in the placentas of GD15 CON and HF-fed dams	79

## LIST OF ABBREVIATIONS

BCA	Bicinchoninic acid
BMI	Body mass index
BMP	Bone morphogenic protein
BSA	Bovine serum albumin
CD31	Cluster of differentiation 31
CON	Control
CuZnSOD	Copper/Zinc superoxide dismutase
COX	Cytochrome <i>c</i> oxidase
DNPH	Dinitrophenylhydrazine
ETC	Electron transport chain
ECL	Enhanced chemiluminescence
EGF	Epidermal growth factor
ELISA	Enzyme-linked immunosorbent assay
EVT	Endovascular trophoblast
FGF	Fibroblast growth factor
GD	Gestational day
GPx	Glutathione peroxidase
HF	High fat
H <sub>2</sub> O <sub>2</sub>	Hydrogen peroxide

8-OHdG	8-hydroxydeoxyguanosine
OH <sup>•</sup>	Hydroxyl radical
4-HNE	4-hydroxynoneal
ICM	Inner cell mass
IL	Interleukin
IST	Interstitial trophoblast
IUGR	Intrauterine growth restriction
JZ	Junctional zone
LGA	Large for gestational age
MDA	Malondialdehyde
MMP	Matrix metalloproteinase
MMT	Mesometrial triangle
MnSOD	Manganese superoxide dismutase
mtDNA	Mitochondrial deoxyribonucleic acid
NAD <sup>+</sup>	Nicotinamide adenine dinucleotide
NADH <sub>2</sub>	Nicotinamide adenine dinucleotide dehydrogenase
NO	Nitric oxide
NTyr	Nitrotyrosine
OONO <sup>•</sup>	Peroxynitrite
PIGF	Placental growth factor
PAGE	Polyacrylamide gel electrophoresis
PBS	Phosphate buffered saline

PND	Postnatal day
ROS	Reactive oxygen species
SA	Spiral artery
SGA	Small for gestational age
SMA	Smooth muscle actin
SNAT	Sodium-coupled neutral amino acid transporter
SDS	Sodium dodecyl sulfate
O <sub>2</sub> <sup>•</sup>	Superoxide
SOD	Superoxide dismutase
TBST	Tris-buffered saline
TNF	Tumour necrosis factor
VSMC	Vascular smooth muscle cell
VEGF	Vascular endothelial growth factor
H <sub>2</sub> O	Water
WHO	World Health Organization

## **1.1 The prevalence and impact of maternal obesity**

### *1.1.1 The obesity epidemic*

Industrialized and developing countries are currently experiencing a rapid increase in the prevalence of obesity. Obesity has been declared an epidemic by the World Health Organization (World Health Organization, 2000) and women of reproductive age are not exempt from this trend. According to the Canadian Community Health Survey released in 2005, the measured obesity rate among women aged 25-34, the age group that is responsible for 62% of childbirths, was 17% (Tjempkema, 2006). Obesity is also increasingly frequent in the younger population. More than 27% of Canadian youth aged 2-17 were considered overweight or obese in 2004, a number which has more than tripled in the last 25 years (Shields et al, 2006). Many of the females in this group are likely to remain obese through their childbearing years (Eriksson et al, 2001).

### *1.1.2 Physiological consequences of obesity*

Research conducted in the last fifteen years has highlighted the fact that obesity is more complex than a simple excess of fat. Fat is stored in adipose tissue, which also functions as an endocrine organ, secreting many signaling molecules that affect processes throughout the body. When produced by adipose tissue, these molecules are termed *adipokines* and include peptide and steroid hormones (leptin, adiponectin, estrogen), cytokines (TNF $\alpha$ , IL-6, IL-8, IL-1 $\beta$ ), and chemokines (MCP-1) (Despres et al, 2008). Processes affected by these and other adipokines include glucose and lipid metabolism, vascular function, angiogenesis, immune function, and reproduction (Bohler et al, 2010). The secretion of adipokines by adipose tissue is dysregulated in obesity, resulting in

systemic changes in signalling proteins and hormones and a state of chronic inflammation. A state of systemic oxidative stress (defined as an imbalance in the ratio of oxidants to antioxidants in favour of the oxidants, at a level which may cause cellular damage) also occurs with obesity. This oxidative stress may be caused by increased metabolism of fatty acids, elevated oxygen consumption, and the reactive oxygen species (ROS)-producing effects of certain inflammatory cytokines on macrophages and monocytes (Furukawa et al, 2004; Fernandez-Sanchez et al, 2011). These systemic changes may be part of the connection between obesity and its comorbidities, which include type 2 diabetes, dyslipidemia, cardiovascular disease, fatty liver disease, and cancer (Guh et al, 2009).

The World Health Organization (WHO) defines obesity as abnormal or excessive fat accumulation that may impair health (World Health Organization, 2011); clinically, an individual is classified as obese if they have a body mass index (BMI) of  $>30 \text{ kg/m}^2$ . The BMI measurement does not take into account the distribution of excess fat, but this may affect health: an excess of intra-abdominal or visceral fat is associated with the most severe metabolic derangements, while an excess of subcutaneous fat is associated with a more normal metabolic phenotype. The cellular structure of adipose tissue also affects the pathogenicity of obesity: *hypertrophic* obesity (characterized by an increase in adipocyte size) is more strongly associated with inflammation and metabolic stresses than *hyperplastic* obesity (where the number of adipocytes is higher) (Veilleux et al, 2011; Smith et al. 2006).

### *1.1.3 Obesity during pregnancy*

Obesity has detrimental effects on both fertility and pregnancy in women. Obese women have more difficulty conceiving naturally (Metwally et al, 2007) and are more likely to seek fertility treatment (Vahratian and Smith, 2009), yet the pregnancy rate with assisted reproductive technologies (ART) is lower (Petanovski et al, 2011; Souter et al, 2011). The situation does not improve once pregnancy occurs, as maternal obesity increases the risk of nearly every pregnancy complication, including gestational diabetes, preeclampsia, miscarriage, stillbirth, intrauterine growth restriction and both large for gestational age and small for gestational age babies (Norman and Reynolds, 2011); (Rajasingam et al, 2009; Perlow et al, 1992). Babies born to obese women are also predisposed to a variety of health issues later in life, including obesity and the metabolic syndrome (Armitage et al, 2008).

There has been an abundance of epidemiological studies documenting the increased incidence of these complications with maternal obesity, but the mechanisms underlying these connections have not been fully elucidated. Systemic inflammation and oxidative stress as well as the metabolic changes occurring in obese individuals persist during pregnancy, and may contribute to the development of complications (Stewart et al, 2007; Szarka et al, 2010; Rajasingam et al, 2009). Many of the cytokines, hormones and growth factors that are dysregulated in obesity also have important roles in the development of the placenta. Placental dysfunction is implicated in most of the poor pregnancy outcomes associated with maternal obesity, and is also known to be involved in developmental

programming of later-life diseases (Bilbo et al, 2011; Reynolds et al, 2010; Ray et al. 2005). The effects of obesity on placental development and function have not yet been examined, and may prove to be the connection between maternal obesity and pregnancy complications.

#### *1.1.4 The rat as a model of maternal obesity*

To study the placenta in the context of maternal obesity, our lab has developed a model of lifelong high fat diet-induced obesity in the Sprague-Dawley rat (described in Hayes et al, 2011; in press), an outbred strain with greater genetic diversity than inbred rat strains. This strain, like the human population, responds to a high fat diet with varying degrees of weight gain. The rat placenta is very similar to the human placenta in a number of ways, making rats one of the most commonly utilized models for understanding human placentation (Caluwaerts et al, 2005). In order to understand the potential effects of obesity on placental development and function, a background understanding of placental biology is necessary.

## **1.2 The Placenta**

### *1.2.1. Functions of the placenta*

The placenta is the first organ to develop during mammalian embryogenesis (Rossant and Cross, 2001). It is essential for successful pregnancy in mammals and carries out many functions, including gas and nutrient exchange, fluid regulation, elimination of waste, and production of hormones (Donnelly and Campling, 2008). It serves as a central regulator of fetal and maternal metabolism during pregnancy. Failure of the placenta to develop and function properly will directly affect the fetus and can lead to poor fetal

growth or death. Detrimental effects of poor placental formation and function do not end at birth; placental dysfunction is associated with later cardiovascular disease (Thornburg et al, 2010), and growth-restricted or macrosomic infants (a consequence of a failure of the placenta to regulate growth) are more likely to grow up to be predisposed to metabolic disorders, including obesity and diabetes (McMillen and Robinson, 2005).

Although placentas of different species differ structurally, there are elements that remain conserved. All placentas contain a highly vascularized region that brings the maternal and fetal blood supplies into close proximity. Exchange occurs across a cell barrier, keeping maternal and fetal blood separate. The placentas of non-human primates and rodents are most similar to the human placenta. The placentas of these species have the same four basic structural elements: 1) the highly vascularised section where exchange occurs; 2) a structure connecting the exchange surface with the maternal tissues; 3) the maternal decidual layer that directly contacts the placenta; and 4) the underlying mesometrium of the uterus. Invasion of trophoblast cells from the placenta into the maternal tissues is also common to these species; trophoblast cells invade either along the spiral artery lumen (endovascular trophoblast cells) or through the tissue (interstitial trophoblast cells).

### *1.2.2 The structure of the rat placenta*

In the rat placenta, the region of nutrient and gas exchange is called the *labyrinth zone*. This region plus the *junctional zone* at the maternal-fetal border comprise the placenta proper. The labyrinth zone is named for the intricate maze-like structure of its vasculature. The blood vessels in the labyrinth consist of embryo-derived endothelial

cells and underlying vascular smooth muscle cells, which are covered by a sheath of trophoblast cells: two layers of syncytiotrophoblast (multinucleated, fused cell layers across which exchange occurs); and scattered cytotrophoblast stem cells which provide proliferative capacity (Figure 1). There are no cells of maternal origin in the labyrinth; maternal blood flows in through the spiral arteries that pass through the decidua and fills the sinusoidal spaces between labyrinthine vessels, bathing the syncytiotrophoblasts in blood. This type of placenta is called a *hemochorial* placenta (from Greek, heme = blood, chorion = trophoblastic membrane), meaning that the blood directly contacts the trophoblast (Soares and Hunt, 2006).

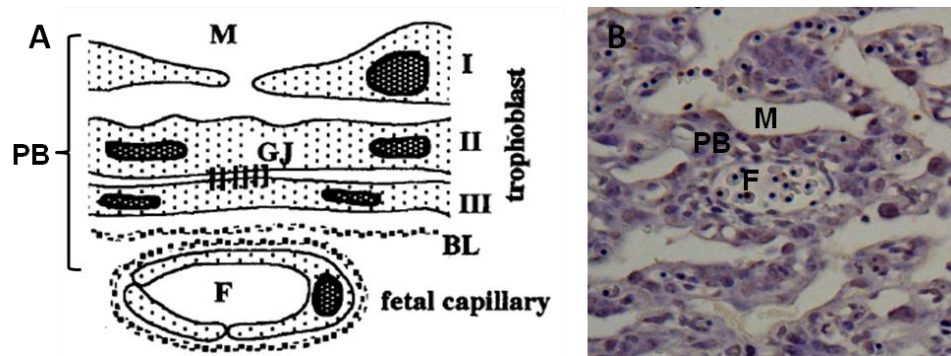


**Figure 1. Structure of the rat placental labyrinth.** Panel A shows the cellular structure of the rat placental labyrinth (adapted from Takata et al, 1997). Trophoblast layer I is composed of cytotrophoblast cells, while layers II and III are multinucleated syncytiotrophoblast cells. F = fetal blood, M= maternal sinusoidal space, BL = basal lamina, GJ = gap junctions, PB = placental barrier. Panel B shows an image of the rat labyrinth stained with hematoxylin to show morphology. Fetal blood (F) can be distinguished from maternal blood (M) by the presence of nucleated red blood cells. The placental barrier (PB) is also labelled.

The junctional zone, which lies between the labyrinth and maternal tissues, has structural and endocrine functions (Rossant and Cross, 2001; Soares and Hunt, 2006) It contains three main cell types: trophoblast giant cells, spongiotrophoblast cells, and glycogen cells (Figure 2B, C). Trophoblast giant cells are based at the border of the junctional zone and the maternal decidua. They are characterized by a large volume of cytoplasm as well as large polyploid nuclei and are thought to have endocrine function (Hu and Cross, 2010). Spongiotrophoblasts make up the bulk of the junctional zone and provide structural support for the developing labyrinth layer (Rossant and Cross, 2001). Glycogen cell islands are interspersed between groups of spongiotrophoblasts. These cells accumulate glycogen during the last week of gestation and can release glucose when circulating stores are low to maintain a constant supply to the fetus. They are thought to give rise to the majority of the cells that invade into the mesometrial triangle by the interstitial pathway (Caluwaerts et al, 2005). Trophoblast cells that invade into the mesometrial triangle by the endovascular pathway also come from the junctional zone, although the cell type that they originate from is unknown.

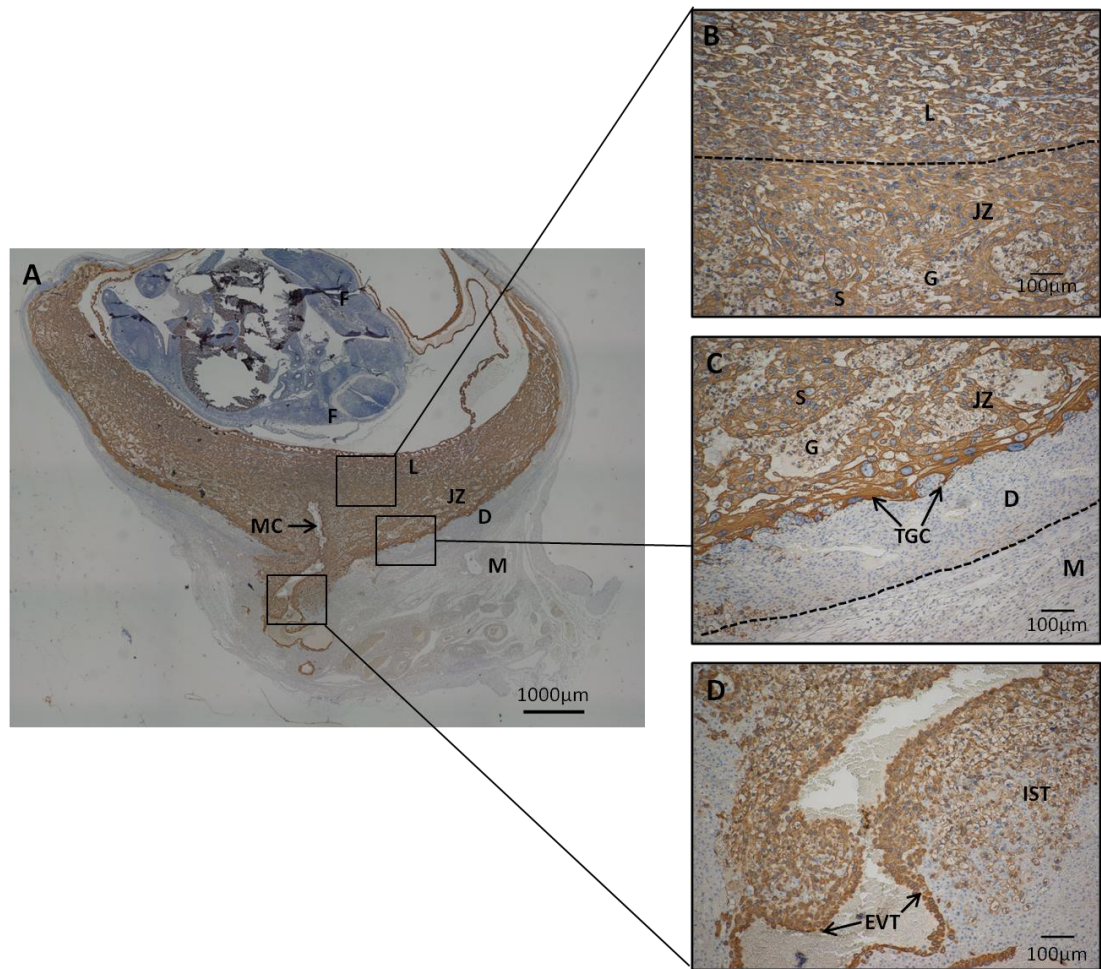


**Figure 2. The structure of the rat placenta at gestational day 15.** A central section (5  $\mu\text{m}$  thick) of a rat placenta containing a cross-section of a maternal channel (MC) was stained with the trophoblast cell marker cytokeratin (1:300). Panel **A** shows a scan of the entire implantation site at 4x magnification. Panels **B**, **C** and **D** show magnification of pertinent areas of the placenta, taken at 10x magnification, highlighting the four sections of the placenta: L, labyrinth; JZ, junctional zone; D, decidua; M, mesometrial triangle. The fetus (F) is also labelled. Identifiable trophoblast cell types are indicated as well: S, spongiotrophoblast; G, glycogen cells; TGC, trophoblast giant cells; IST, interstitial trophoblast cells; EVT, endovascular trophoblast cells.

Directly underlying the junctional zone is the maternal decidua (Figure 2C). Contact with the blastocyst initiates ‘decidualization’ of the stromal cells of the outer mesometrium, leading to the formation of the decidual layer between the mesometrial triangle and the junctional zone of the placenta proper. These cells are specialized to contact the trophoblast cells; they have endocrine and paracrine functions and also contain glycogen (de Rijk et al, 2002).

The mesometrial triangle is the region of the uterus directly underlying the decidua. This area grows during pregnancy and is composed of stromal cells, blood vessels, maternal immune cells, and, later in gestation, invasive trophoblast cells (Soares and Hunt, 2006); the cell composition and size of this compartment change significantly with gestation (Picut et al, 2009). The mesometrial triangle was previously called the ‘metrial gland’; although this term is relatively obsolete now, the discovery of the hormone-secreting functions of invasive trophoblasts in the mesometrium does support the nomenclature of this structure as a ‘gland’ (Ain et al, 2003; Ain and Soares, 2004).

### *1.2.3 The structure of the human placenta*

The human placenta is similar to the rat placenta in many ways, but there are also structural differences. In the human placenta, the vasculature of the exchange surface is organized into branching structures called chorionic villi (Figure 3). Exchange occurs across a single layer of multinucleated syncytiotrophoblasts in the human placenta, compared with the double layer in the rat. There is no junctional zone in the human placenta; instead, column cytotrophoblast cells anchor chorionic villi to the decidua, carrying out a function similar to that of the spongiotrophoblast cells of the junctional

zone (Figure 3; (Caniggia et al, 2000)). Despite these differences, the invasion of endovascular and interstitial trophoblast cells into the mesometrium in rats is remarkably similar to humans.

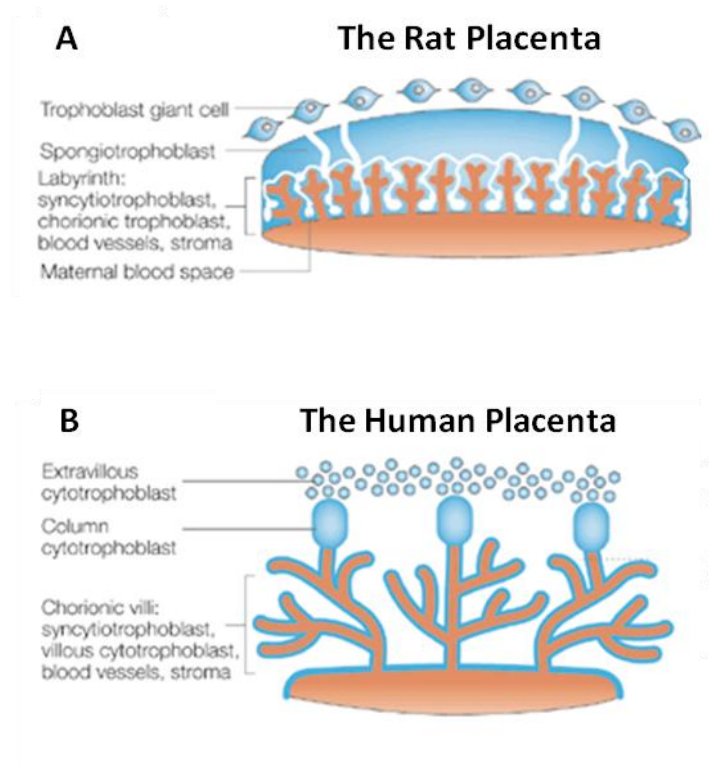


**Figure 3. Comparing the structure of the human and rat placenta.** Panel **A** shows a representation of the rat placenta, while Panel **B** shows a representation of the human placenta (adapted from Rossant and Cross, 2001). Blue: trophoblast cells, orange: fetal-derived cells, white: maternal blood space. Notable differences include the structure of the exchange surface (labyrinth in the rat vs. chorionic villi in the humans), and the lack of the junctional zone in the human placenta..

#### *1.2.4 The rat as a model to study human placentation*

Placentas are generally classified in two ways: by the shape of the placenta, and by the types of cells that make up the barrier between maternal and fetal circulation. Humans share the discoid placental shape with only non-human primates and rodents. The hemochorial structure, where maternal blood comes in direct contact with trophoblast cells, is also shared only between primates and rodents. There are pros and cons to using either of these as a model of human placentation.

The non-human primate (particularly Old World monkeys including macaques and baboons) shares the same structure of the exchange surface (chorionic villi) and invasion of endovascular trophoblast to remodel maternal spiral arteries. They are phylogenetically closest to humans and their pregnancies are very similar in length of gestation and number of offspring. However, there is no interstitial trophoblast invasion in the monkey, and there are also the problems of a long generation time and ethical concerns regarding use of primates in research (Carter et al, 2007).

Mice and rats are the most common rodent models, and of these rats are by far the superior for studying placentation. The main differences between the mouse and rat placentas lie in the invasion of trophoblast cells into maternal tissues. Both endovascular and interstitial patterns of invasion occur in humans and rats, with a very similar pattern and mechanism (Caluwaerts et al, 2005; Vercruyssen et al, 2006) but only interstitial invasion occurs in the mouse (Rossant and Cross, 2001). The depth of invasion also differs; interstitial trophoblasts invade only as far as the proximal decidua in the mouse,

compared with the deep mesometrium in the rat and human (Ain et al, 2003). The remodelling of the spiral arteries of the uterus is carried out by these invading trophoblasts in humans and rats, whereas in the mouse placenta remodelling is carried out by uterine natural killer (uNK) cells of the maternal immune system (Ain et al, 2003).

### **1.3 Development of the placenta**

#### *1.3.1 Early gestation: implantation and formation of the placenta proper*

Implantation in rats occurs 4-6 days post-fertilization (Lee and DeMayo, 2004). At the time of implantation, the conceptus is at the blastocyst stage, consisting of the inner cell mass (ICM), which will give rise to the fetus, and the trophectoderm, which will give rise to all trophoblast lineages of the placenta (Figure 4). Polar trophectoderm cells (those not in contact with the ICM) differentiate into trophoblast giant cells, the first terminally differentiated placental cells to form. Implantation begins with the contact of the blastocyst with uterine epithelial cells. Uterine epithelial cells at the site of implantation undergo apoptosis, and their cell fragments are phagocytosed by trophoblasts (Parr et al, 1987). Trophoblast cells immediately start secreting autocrine and paracrine factors, initiating the decidualization of stromal cells of the uterus in rats and pacifying the maternal immune system (Hu and Cross, 2010). There is significant cross-talk between the cell types to allow this to happen. Trophoblast cells also begin secreting chorionic gonadotropin into the maternal circulation, which stimulates the corpus luteum in the ovary to produce progesterone and by this informs the mother's body that a pregnancy has occurred.

Successful implantation requires both a healthy blastocyst and a receptive uterine environment. The receptivity of the uterus depends on cytokine and hormone levels, and changes in local or systemic immunologic factors have been implicated in implantation failures (Kwak-Kim et al, 2010).

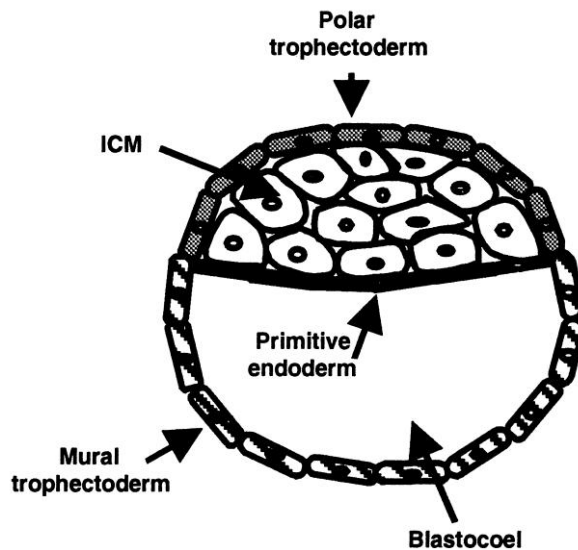


**Figure 4. Structure of the blastocyst at the time of implantation.** Trophoblast cells give rise to the placenta and are essential for pregnancy from the beginning, as they are the cells that drive implantation (adapted from Carayannopoulos et al, 2000).

### 1.3.2 Establishment and development of the placental vasculature

The placental vasculature begins to form around day 8.5-10, when an ICM-derived structure called the allantois aligns with the trophoblast-derived chorion. The allantois contains mesenchymal cells that are precursors to the endothelial and vascular smooth muscle cells in the placenta, while the chorion consists of trophoblastic precursors of all lineages of trophoblast except trophoblast giant cells. Thus the rat and human placentas are referred to as 'chorioallantoic' placentas. Immediately after these structures align, cells from the allantois begin to form tubes that grow into the chorion, eventually

forming blood vessels that are 'coated' with trophoblasts - the vasculature of the labyrinth (Rossant and Cross, 2001). This process is called vasculogenesis. Failure of this initial vasculogenesis leads to early loss of the embryo (Watson and Cross, 2005). Genes involved include the bone morphogenic proteins (BMPs), fibroblast growth factor (FGF), epidermal growth factor (EGF), Notch, and the Wnt signaling pathway (Watson and Cross, 2005). Spongiotrophoblast cells differentiate at this point to provide structural support for the developing labyrinth, and branching angiogenesis and formation of the multinucleated syncytiotrophoblasts layers occurs. Mice with mutations that lead to defects in branching angiogenesis die between day 10.5 and 12.5 (Watson and Cross, 2005). Finally, non-branching angiogenesis takes over later in gestation. The placenta grows rapidly and carries out most of its growth over the first half of gestation (Reynolds et al, 2005). During the latter half of gestation the vasculature of the placenta increases in density, allowing for an increase in efficiency of exchange relative to placental size and permitting the near-exponential fetal growth that occurs during this time. If the labyrinth is not appropriately vascularized with suitable vessel patterning, branching, and dilation, placental perfusion is impaired, resulting in poor oxygen and nutrient diffusion (Pardi et al, 2002).

Several growth factor families are implicated in controlling angiogenesis in the placenta, including FGFs, angiopoietins, and importantly, the VEGF family (Reynolds et al, 2005). The VEGF family of growth factors consists of seven members: VEGF-A through F and PlGF. The two members known to be important in placental vascular development are VEGF-A and PlGF.

VEGF-A is the most potent member of the VEGF family and is important for vasculogenesis, angiogenesis, vasodilation and vascular permeability (Demir 2007). This protein binds to two tyrosine kinase receptors: VEGFR-1 (Flt-1) and VEGFR-2 (Flk-1). The proangiogenic effects of VEGF-A are exerted through VEGFR-2; VEGFR-1 has twice the affinity for VEGF-A, but its intracellular kinase domain has only a tenth of the activity of VEGFR-2. Eliminating the tyrosine kinase domain of VEGFR1 allows for normal embryonic development, suggesting that the main role of this receptor may be to sequester VEGF-A (Hiratsuka et al, 1998).

PlGF is a member of the VEGF family of growth factors, with 53% homology to VEGF-A (Maglione et al, 1991). The mechanism of action of PlGF is twofold. PlGF binds exclusively to VEGFR-1 and its soluble analog, the decoy receptor sFlt-1, and probably exerts most of its proangiogenic effects by displacing VEGF-A from these receptors. VEGF-A is then free to bind and activate VEGFR-2. Some angiogenic effects may also be transduced directly through activation of the VEGFR-1 tyrosine kinase domain, including the vasodilation of uterine arteries (Osol et al, 2008). However, these functions can also be carried out by VEGF-A.

A knockout of even one allele of VEGF leads to early embryonic death (Carmeliet et al, 1996). PlGF knockout mice show no deficiencies in embryonic angiogenesis, likely due to a compensatory increase in total VEGF levels, allowing free VEGF levels to remain unchanged (Carmeliet et al, 2001). Placental development of the PlGF<sup>-/-</sup> mouse has been examined briefly (Tayade et al, 2007). The most striking observations were a smaller placenta and delayed remodelling of the spiral arteries in the maternal decidua.

The vasculature of the labyrinth has not yet been examined in this knockout mouse model.

### *1.3. Trophoblast invasion into the mesometrial triangle*

Spiral arteries are found in the mesometrium and decidua of rats and humans and provide blood to the placenta. They are named for their unique spiralling shape, which helps to prevent placental injury by decreasing the pressure of blood as it approaches the placenta (Pijnenborg et al, 2006). During pregnancy in rats and humans, these arteries undergo modifications from high-resistance, low-capacity vessels to low-resistance, high-capacity vessels; this process is largely driven by invasive trophoblasts and is characterized by the replacement of maternal endothelial cells with endovascular trophoblast cells and loss of the underlying smooth muscle layer (Figure 5). Failure of trophoblast invasion and spiral artery remodelling is associated with both growth restriction and preeclampsia (Naicker et al, 2003; Khong et al, 1986).

Trophoblast invasion has been studied extensively in humans due to this link with preeclampsia. The rat shows very similar patterns of invasion and spiral artery conversion and the time-course of invasion and regression of trophoblasts is better understood in rats, as most placental bed biopsies in humans are taken either during the first trimester (from elective abortions) or during the third trimester, at delivery. Endovascular and interstitial trophoblast invasion in the rat begins at GD14. Endovascular trophoblasts migrate from the placenta along the lumen of the maternal spiral arteries, beginning at the central maternal artery channel (Caluwaerts et al, 2005). By GD20, endovascular trophoblast levels start to decline as endovascular trophoblasts are replaced by maternal endothelial

cells to prepare for delivery (Geusens et al, 2010). Interstitial trophoblast cells initially appear surrounding the central maternal artery channel, but spread out to cover about 40 % of the mesometrial triangle by their peak at GD18 (Vercruysse et al, 2006).

Trophoblast invasion is regulated by a number of factors including the local oxygen tension, cytokine environment, the type of cell adhesion molecules expressed by the interacting cells, and the matrix metalloproteinases (including MMP2 and MMP9) released by both trophoblast and maternal cells. Many *in vitro* experiments using cultured cells have noted that treatment with cytokines leads to varying changes in trophoblast invasion and migration (summarized in Table 1). However, *in vivo* examinations of the effects of these molecules on trophoblast migration have not yet been carried out. In the body, the net effect of systemic changes in many cytokines (such as the changes observed in obesity) remains unknown.

#### *1.3.4 Remodelling of maternal spiral arteries by invasive trophoblast cells*

Spiral artery remodelling refers to the change from a high-resistance, low-capacity vessel to a low-resistance, high-capacity vessel, and is mediated by the replacement of maternal endothelial cells by trophoblasts and the loss of underlying vascular smooth muscle cells (VSMCs; Figure 5). Like trophoblast invasion, this process is mediated by tightly regulated signalling between maternal cells in the mesometrial triangle, the maternal immune system, and trophoblast cells, and may be affected by the changes that are present with maternal obesity. Endovascular trophoblasts migrating down the lumen of spiral arteries replace CD31-positive maternal endothelial cells soon after contact with them. This loss of endothelial cells occurs by apoptosis and requires contact with

trophoblast cells (Chen et al, 2005). VSMCs, on the other hand, can either be lost due to apoptosis or can undergo a process of dedifferentiation, where they move from a ‘functional’, contractile phenotype to a proliferative and migratory cell, a process which is associated with loss of contractile proteins including smooth muscle actin (Whitley and Cartwright, 2010). Loss of VSMCs due to apoptosis is mediated in part by the release of FasL by trophoblast cells, which binds in a paracrine manner to the death receptors on VSMCs (Harris et al, 2006). This process may also depend on maternal factors including the presence of uterine natural killer cells. Therefore loss of vascular smooth muscle cells is dependent on the proximity but not direct contact of EVT’s with smooth muscle cells (Vercruyse et al, 2006).

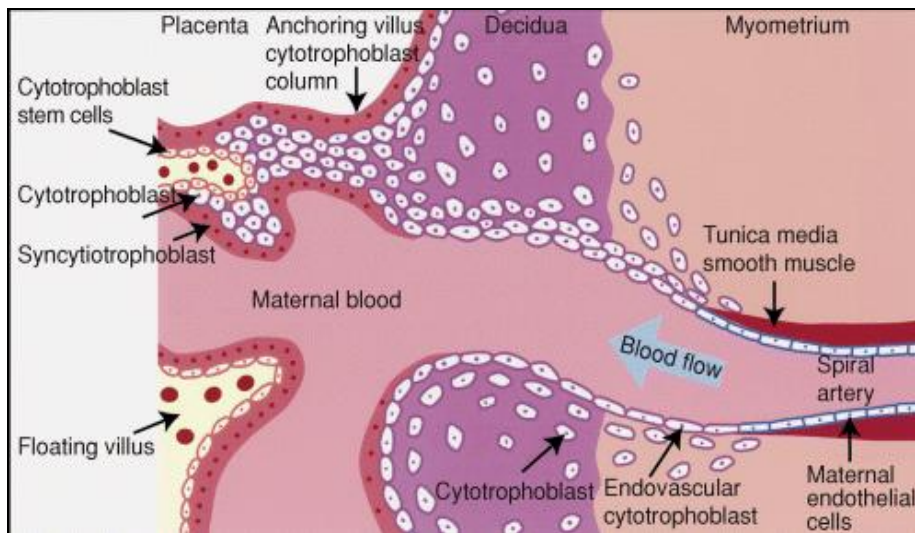


**Figure 5. The structure of the maternal spiral arteries in normal pregnancy in the human.** In normal pregnancy, invading trophoblast cells replace the maternal endothelial cells, which is associated with loss of underlying vascular smooth muscle cells; this serves to convert the spiral arteries into flaccid, high-capacity vessels (adapted from Lam et al, 2005).

### *1.3.5 Role of hypoxia in placental development*

Oxygen tension in the conceptus follows a distinct pattern over gestation, and maintenance of the proper level of oxygen is important for a successful pregnancy. Uteroplacental hypoxia occurs normally at certain time periods during pregnancy, and is essential for placental and embryonic development (Dunwoodie, 2009). On the other hand, dysregulation of placental oxygen levels has been implicated in the pathogenesis of pregnancy complications, including IUGR, preeclampsia, and miscarriage (Kingdom and Kaufmann, 1999).

Prior to the establishment of maternal-fetal circulation, oxygen tension in the fetoplacental unit is low, which reduces the exposure of the placenta and fetus to reactive oxygen species during this critical early period in fetal growth (Burton and Caniggia, 2001). Early fetal and placental vascular development also depends strongly on hypoxia-driven expression of VEGF (Dunwoodie, 2009). Hypoxia influences cell fate decisions as well, increasing differentiation and invasion of endovascular trophoblasts (Rosario et al, 2008). Trophoblast proliferation may also be affected by hypoxia, but there are inconsistencies in the literature as to whether it stimulates or inhibits the process (Caniggia et al, 2000; Genbacev and Miller, 2000); these inconsistencies are likely due to variations in the degree of hypoxia and timing of exposure in each experimental protocol, and may suggest that hypoxia has different effects on proliferation at different windows of exposure.

These responses to hypoxia are driven by oxygen-sensitive signalling molecules, including the hypoxia-inducible factor (HIF) family of transcription factors. These proteins play an important role in rescuing the early embryo and placenta from the pathological effects of hypoxia as well as their effects on the development of placental and embryonic morphology. A knockout of the HIF 1 $\beta$  gene results in embryonic death in the mouse by GD10.5, caused by malformed placentas which exhibit reduced labyrinthine vascularisation, increased numbers of giant cells and decreased numbers of spongiotrophoblasts (Cowden Dahl et al, 2005; Adelman et al, 2000).

Excessive placental hypoxia persisting after circulation is established can have detrimental effects on pregnancy outcomes. There are several manifestations of excessive hypoxia in pregnancy. *Preplacental* hypoxia occurs when both the mother and fetus are hypoxic; the best example is in high altitude pregnancies, but maternal anemia and maternal smoking also lead to reduced whole-body tissue oxygenation (Pfarrer et al, 1999). *Uteroplacental* hypoxia occurs in preeclampsia and IUGR, and is likely a consequence of poor placental development, although it also contributes to the pathology of these conditions (Soleymanlou et al, 2005). Finally, *post-placental* (fetal) hypoxia occurs secondary to defective placentation (Kingdom and Kaufmann, 1999).

In general, excessive hypoxia is associated with reduced fetal growth. Low oxygen tension *in vitro* leads to vasoconstriction in human and rat placental arteries and is thought to be part of the mechanism leading to this hypoxia-induced growth restriction (Howard et al, 1987; Thaete et al 2004). Placental phenotypes observed with hypoxia depend on the cause of the hypoxia. Preplacental hypoxia in women (caused by living at

a high altitude during pregnancy) is associated with increases in vascularity of the placenta (Khalid et al, 1997) and reduced remodelling of decidual spiral arteries (Tissot van Patot et al, 2003). In the rat, preplacental hypoxia leads to increases in trophoblast invasion, though spiral artery remodelling has not been assessed (Rosario et al, 2008). The placental phenotype in uteroplacental hypoxia varies depending on the initial causes of the placental dysfunction, and can be a consequence of reduced blood flow to the placenta (due to reduced trophoblast invasion or spiral artery remodelling) or within the placenta (due to altered development of the vasculature of the exchange surface) (Kingdom and Kaufmann, 1999; Sebire and Talbert, 2001).

### *1.3.6 Role of oxidative stress in placental development*

Oxidative stress has been defined as an imbalance in the levels of prooxidants and antioxidants in favour of the oxidants, at a level that may lead to damage to cellular components (Burton and Jauniaux, 2011). Like hypoxia, oxidative stress occurs naturally in the placenta at certain times in gestation, but can also be present in excess in many pregnancy complications (including preeclampsia, growth restriction and miscarriage) and may contribute to the pathology of these conditions. Obesity is also associated with oxidative stress, and this is thought to be part of the link between maternal obesity and the increased incidence of these pregnancy complications (Zavalza-Gomez, 2011).

The term 'reactive oxygen species' includes both free radicals (containing one or more unpaired electron) and other non-radical but reactive molecules. Free radicals include superoxide ( $O_2^{\cdot-}$ ), the hydroxyl radical ( $OH^{\cdot}$ ), and peroxynitrite ( $ONOO^{\cdot}$ ), derived from the interaction between nitric oxide and superoxide (Burton and Jauniaux,

2011). Hydrogen peroxide ( $\text{H}_2\text{O}_2$ ) is an important non-radical reactive molecule. These reactive molecules are generated by normal cellular processes, with the bulk of ROS production occurring in the mitochondria. ROS can affect signalling pathways and are important for cellular function, but can also lead to damage if they are present in excess.

Antioxidant enzymes are present in the cell to mitigate the damaging effects of reactive oxygen species. Common antioxidant enzymes in the cell convert  $\text{O}_2^{\cdot-}$  to  $\text{H}_2\text{O}_2$  (including the superoxide dismutase enzymes, CuZnSOD and MnSOD) and  $\text{H}_2\text{O}_2$  to  $\text{H}_2\text{O}$  (including glutathione peroxidase (GPx) and catalase). These proteins are regulated by multiple factors including reactive oxygen species (Yoshioka et al, 1994), oxygen tension (Hass et al, 1989), and cytokines (Visner et al, 1992).

When present in excess, ROS can react with almost any cellular component, leading to protein oxidation (forming protein carbonyls and malondialdehyde), lipid oxidation (forming 4-hydroxynonenal and isoprostanes), and DNA damage (forming 8-hydroxy-2-deoxyguanosine). Oxidative and nitrate damage to proteins can affect their function, and proteins that have been damaged by ROS are eventually targeted for destruction by the proteasome (Grune et al, 1996). The increased degradation of these damaged proteins puts additional stress on the cell, and oxidative stress is often associated with endoplasmic reticulum (ER) stress (Liu et al, 2011; Zhang et al, 2010) which leads to decreased protein synthesis (Yung et al, 2008). Lipid peroxidation is associated with loss of membrane fluidity and function (Burton and Jauniaux, 2011). Oxidative damage to mitochondrial DNA can perpetuate the cycle of oxidative stress by reducing the efficiency of the electron transport chain. Damage occurs in a diffusion-

limited manner from the site of ROS production, so the mitochondria are often the site of the most extensive oxidative damage (Burton and Jauniaux, 2011). Apoptosis can occur if this mitochondrial damage is high enough (Green and Reed, 1998).

Mitochondrial ROS production occurs as a byproduct of oxidative phosphorylation, due to leakage of electrons from the electron transport chain to molecular oxygen. The amount of ROS produced by the mitochondria is affected by many factors. Elevated ROS production can occur when oxidative phosphorylation is increased due to high metabolic demand. Alterations in the nutrient balance can also cause ROS production, with excessive lipid and glucose levels both leading to oxidative stress (Han et al, 2005; Bournat and Brown, 2010). Oxidative stress occurs upon exposure to hyperoxia, when there are many O<sub>2</sub> molecules available to accept electrons leaking from the ETC (Gore et al, 2010). Paradoxically, hypoxic conditions can also lead to oxidative stress (Park et al, 1991; Kolamunne et al, 2011). This may be due to the slowing of passage of electrons along the ETC, increasing the likelihood that they will be picked up by molecular oxygen.

Cells have actually evolved to utilize these ROS as important mediators of normal cellular functions by activating or inhibiting redox-sensitive proteins. Proteins activated by ROS include the transcription factors NFκB, AP-1 and the hypoxia inducible factor (HIF) family (Hensley et al, 2000). These transcription factors activate genes to produce antioxidant enzymes, proinflammatory cytokines (TNFα, among others), cell adhesion molecules and matrix metalloproteases, including MMP-2 and MMP-9 (Fujiwara et al, 2007).

The increased metabolic demands of pregnancy lead to a state of oxidative stress higher than that present in nonpregnant individuals, in the placenta as well as other organs (Belo et al, 2004; Myatt and Cui, 2004). During early gestation, before maternal-fetal circulation is established, the conceptus is exposed to low oxygenation and low oxidative stress; the sudden increase in oxygen tension when maternal-fetal circulation is established causes a burst of oxidative stress at this time (Jauniaux et al, 2000). Oxidative stress naturally increases over gestation, coinciding with an increase in placental mitochondrial function; in the rat, the expression of placental MnSOD, CuZnSOD and GPx all increased over gestation (Jones et al, 2010). This increase in antioxidant levels also occurs in the human placenta (Watson et al, 1998). Excessive placental oxidative stress is present in preeclampsia, IUGR and miscarriage, and may contribute to the pathology of these conditions by affecting protein structure and function, diminishing transfer capabilities of trophoblast cells, and increasing trophoblast cell apoptosis (Burton and Jauniaux, 2011). Systemic oxidative stress may also inhibit invasion of trophoblast cells, which could contribute to the development of these complications (Staff et al, 2000).

## **1.4 The role of the placenta in pregnancy complications associated with maternal obesity**

### *1.4.1 Preeclampsia*

Preeclampsia is a life-threatening medical condition unique to humans that endangers both mother and child. It is diagnosed by the presence of a set of symptoms, including pregnancy-induced hypertension (BP >140/90 mmHg) and proteinuria (random

urinary protein/creatinine ratio >30 mg/mmol creatinine or 0.3 g protein excreted per day) occurring after gestational week 20. The syndrome is strongly associated with maternal obesity; those with a BMI>35 have a four-fold increased risk of developing preeclampsia (Sohlberg et al, 2012). Preeclampsia can lead to reduced fetal growth and fetal death; when left untreated it can progress to eclampsia, which is characterized by maternal seizures and may lead to coma and death.

Preeclampsia originates in shallow implantation of the placenta, characterized by reduced trophoblast invasion into the spiral arteries and maintenance of the muscular layer of the arteries (Figure 6); this leads to altered uteroplacental blood flow, placental hypoxia, and placental oxidative stress (Soleymanlou et al, 2005; Hutchinson et al, 2009; Siddiqui et al, 2010). The high-pressure blood flow through unremodelled spiral arteries can cause rupture of the delicate villous structures, affecting maternal immune function (Burton et al, 2009). Circulating levels of the antiangiogenic VEGF-A decoy receptor sFlt1 (sFlt-1) are higher in preeclampsia due to production by the hypoxic placenta; this elevated sFlt-1 is thought to cause the maternal renal and endothelial dysfunction characteristic of preeclampsia by reducing the vasodilatory effects of VEGF and PlGF (Maynard et al, 2003).

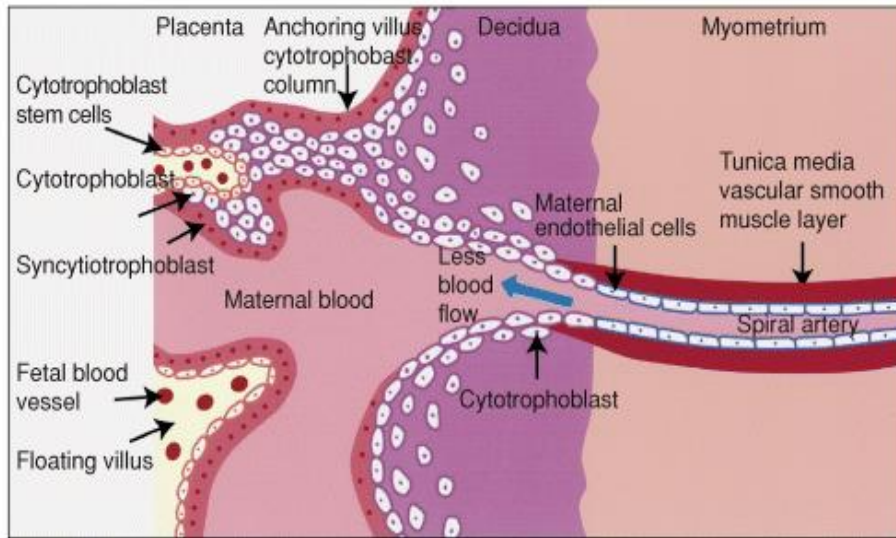


**Figure 6. The structure of the maternal spiral arteries in preeclampsia in the human.** The invasion of trophoblasts into the maternal spiral arteries is compromised in preeclampsia, leading to retention of the maternal endothelial cells and underlying vascular smooth muscle cells (adapted from Lam et al, 2005).

The initial cause of the failure of trophoblast cells to invade and remodel spiral arteries in preeclampsia is not fully understood; however, maternal immune dysfunction likely plays a role. There is evidence to support the role of the maternal immune system in the development of preeclampsia, as maternal health conditions that are characterized by systemic inflammation (including both responses to infections and autoimmune diseases such as systemic lupus erythematosus and rheumatoid arthritis) are associated with an increased risk of developing the disease (Conde-Agudelo et al, 2008; Chakravarty et al, 2006). Altered levels of circulating cytokines are also present when preeclampsia occurs in otherwise healthy women, though it is difficult to determine whether this is a cause of decreased trophoblast invasion or a consequence of the resulting placental dysfunction and inflammation (Szarka et al, 2010).

Many of the cytokines that are altered systemically in preeclampsia are also altered in obesity. These molecules can affect trophoblast invasion *in vitro*, with some stimulating and some inhibiting the process (summarized in Table 1). The cumulative effects of systemic changes in these cytokines on trophoblast invasion *in vivo* remains unknown, but it is possible that the effects of obesity-associated systemic inflammation on trophoblast invasion *in vivo* may be part of the connection between obesity and preeclampsia.

<b>Adipokine</b>	<b>Obesity</b>	<b>Preeclampsia</b>	<b>Trophoblast Invasion</b>	<b>MMP Expression</b>
<b>Leptin</b>	+ (Gautron and Elmquist, 2011)	+ (Sucak et al, 2010)	+ (Schulz and Widmaier, 2004)	+ (Schulz and Widmaier, 2004)
<b>Adiponectin</b>	- (Arita et al, 1999)	?	+ (Benaitreau et al, 2010)	+ MMP2 + MMP9 (Benaitreau et al, 2010)
<b>MCP-1</b>	+ (Catalan et al, 2007)	+ (Szarka et al, 2010)	?	?
<b>TNF<math>\alpha</math></b>	+ (Catalan et al, 2007)	+ (Szarka et al, 2010)	- (Bauer et al, 2004)	+ MMP9 (Bauer et al, 2004)
<b>IL-1<math>\beta</math></b>	+ (Um et al, 2004)	+ (Kalinderis et al, 2011)	+ (Librach et al, 1994)	+ MMP9 (Librach et al, 1994)
<b>IL-6</b>	+ (Eder et al, 2009)	+ (Lockwood et al, 2008)	+ (Jovanovic and Vicovac, 2009)	+ MMP2 + MMP9 activity (Meisser et al, 1999)
<b>IL-8</b>	+ (Strackowski et al, 2002)	+ (Szarka et al, 2010)	+ (Jovanovic et al, 2010)	+ MMP2 + MMP9 (Jovanovic et al, 2010)

**Table 1. Levels of adipokines in obesity and preeclampsia and their effects on trophoblast invasion and MMP expression.** Circulating levels of each adipokine in obesity and preeclampsia are expressed as being increased (+) or decreased (-) compared to levels in healthy women. Their effects on trophoblast invasion and MMP2 and 9 expression by trophoblast cells *in vitro* are also listed.

#### *1.4.2 Small for gestational age and intrauterine growth restriction*

It is common for babies born to obese mothers to be heavier due to increased nutrient transfer to the fetus; however, there is also an increased likelihood that obese mothers will give birth to a smaller baby (Seed et al, 2011). The birth of pathologically smaller babies can often be traced back to placental dysfunction.

There are two terms used to describe small babies at birth: small for gestational age (SGA) and intrauterine growth restriction (IUGR). The definitions of these terms overlap somewhat. SGA refers to all babies that fall in the lowest tenth centile for their gestational age at birth; these babies may be genetically smaller and have reached their full growth potential, or may be pathologically smaller (Figueras and Gardosi, 2011). Conversely, IUGR specifically refers to pathologically growth restricted infants that have failed to reach their full growth potential (Pardi et al, 2002). At birth, IUGR is defined by a birthweight of less than 2500 g (5 lb, 8 oz), and evidence of ill health: malnutrition, fetal hypoxia, and growth abnormalities. The similarities between these two definitions have led to a blurring of the literature, as babies defined as SGA may include IUGR babies. Thus both terms are associated with maternal obesity, though the majority of the SGA births are likely pathological in nature (Perlow et al, 1992; Figueras and Gardosi, 2011).

Growth restriction may arise for several different reasons. Fetal growth is affected by three factors: the genetic growth potential of the fetus, the ability of the placenta to support fetal growth, and the mother's ability to provide nutrients and oxygen for transfer. Fetal and maternal causes (fetal abnormalities, maternal malnutrition, infection,

or hypoxia) are usually easily identifiable, but placental causes of IUGR may not be identified without microscopic examination of the placenta and thus are often categorized as idiopathic (Cetin and Antonazzo, 2009).

In general, idiopathic growth restriction is associated with placental insufficiency (Apel-Sarid et al, 2010), placental oxidative stress (Turpa et al, 2007), and trophoblast apoptosis (Heazell et al, 2011). Some cases of growth restriction are associated with reduction in trophoblast invasion and spiral artery remodelling without the development of preeclampsia (Khong et al, 1986). The effect of IUGR on the vascular structure of the placenta varies. Severe early-onset IUGR usually presents with a deficit of villous development, which may actually be due to relative hyperoxia in the intervillous space, reducing the hypoxia-induced angiogenesis early in gestation (Khaliq et al, 1999). Growth restriction associated with severe preeclampsia also presents with a reduced vascularization of the placenta (Mayhew et al, 2003). However, some cases of idiopathic growth restriction occur with increased villous vascularization and may reflect the development of abnormalities later in gestation (Sibley et al, 2005). The specific placental phenotypes of obesity-associated growth restriction have not been examined.

#### 1.4.3 *Miscarriage and Stillbirth*

Miscarriage and stillbirth both refer to intrauterine fetal death, and are both associated with maternal obesity (Sirimi and Goulis, 2010). The term ‘miscarriage’ describes fetal death occurring prior to the 20<sup>th</sup> week of gestation, and ‘stillbirth’ describes fetal death after the 20<sup>th</sup> week of gestation (Robinson, 2011). These complications show overlapping etiologies, and when obvious fetal abnormalities are

ruled out, many cases of intrauterine fetal death may be due to poor placental development. 65% of recurrent pregnancy losses are due to immunologic factors which prevent normal development of the placenta; in these cases, pregnancy loss usually occurs in the first trimester and inflammation is present in placentas (Srinivas et al, 2008). Pregnancies complicated by miscarriage are more likely to show higher blood flow to the placenta between 7 and 11 weeks, suggesting that premature establishment of maternal blood flow to the placenta may cause some miscarriages, likely due to oxidative stress (Jauniaux et al, 2003). On the other hand, late sporadic miscarriage/stillbirth is associated with abnormalities in spiral artery transformation and trophoblast invasion (Ball et al, 2006). Preeclampsia and uteroplacental insufficiency are major causes of fetal death later in gestation (Stillbirth Collaborative Research Network Writing Group, 2011).

### **1.5 Maternal obesity and placental development**

The potential effects of maternal obesity on placental development are multivariate. Adipose tissue is an endocrine organ whose secretory functions are altered in obesity, affecting processes throughout the body including metabolism, vascular function, and the immune system. These effects persist throughout pregnancy (Stewart et al, 2007). Placental development is a finely tuned process that may be affected by these physiological changes, leading to the development of pregnancy complications. Examination of the structure of placentas of obese women remains unexplored, though placentas from obese women are known to exhibit increased macrophage infiltration and production of proinflammatory cytokines (Challier et al, 2008) and evidence of nitrate stress (Roberts et al, 2009). There are hints that maternal obesity may be affecting the

placenta in animal models as well: in baboons, obesity is associated with decreased uteroplacental blood flow and stillbirth (Frias et al, 2011); in rats, maternal obesity leads to reduced placental and fetal weight (Akyol et al, 2009). In addition to these observations, the work covered in this thesis suggests that the structure of the placenta, from the exchange surface to the invasion of the spiral arteries, may be affected by maternal obesity. These changes may contribute to the development of pregnancy complications in the obese mother.

## **2. STUDY OBJECTIVES**

### **2.1 Hypothesis:**

The systemic changes that occur with maternal obesity (including inflammation and oxidative stress) affect placental development, leading to changes in placental structure and affecting trophoblast invasion and remodelling of spiral arteries. Oxidative stress may be present in trophoblast cells and may contribute to their dysfunction.

### **2.2 Objectives:**

The objectives of the present study are to assess the impact of lifelong diet-induced maternal obesity on pregnancy outcomes and placental development in the rat. I will first characterize the development of obesity in the model (weight gain, body fat distribution, and systemic inflammation and oxidative stress) and will examine fertility and pregnancy outcomes in HF-fed dams. I will examine the effect of the lifelong HF diet on the vasculature and morphology of the placenta proper, and assess trophoblast function by studying trophoblast invasion into the maternal mesometrial triangle and remodelling of maternal spiral arteries. Finally, I will assess markers of oxidative stress as a potential mechanism leading to altered trophoblast function and poor pregnancy outcomes

### **3. MATERIALS AND METHODS**

#### **3.1 Study design**

All animal procedures for this study were approved by the McMaster University Animal Research Ethics Board (Animal Utilization Protocol 07-07-40). Female Sprague-Dawley rats aged 21 days (84-100g) were purchased from Charles River Laboratories (Wilmington, MA). Rats were maintained under controlled lighting (12-hr light – dark cycle) and temperature (22°C) with *ad libitum* access to food and water. Dams were randomly assigned to receive either standard rat chow (CON) (16% kcal fat, 3.82 kcal/g; Harlan Teklad, Madison, WI) or a high fat (HF) diet (45% kcal fat, 4.70 kcal/g; Research Diets, New Brunswick, NJ). Details on the composition of each diet are located in Appendix 1. Dams were maintained on their respective diets for 19 weeks before being mated with age-matched Sprague-Dawley males fed the CON diet.

##### **3.1.1 Mating and pregnancy**

Mating was carried out by pairing one male and one female per cage. Vaginal flushes were performed to assess the presence of sperm before 9am each morning. A glass eye dropper was used to flush the vagina with sterile saline (Baxter, Mississauga, ON), and the effluent was placed on a glass slide, coverslipped and examined under a microscope for sperm. The presence of sperm indicated day 0 of pregnancy, and the male was removed from the cage. Successful males were paired with another dam until all were pregnant, with separate groups of males for the CON-fed and HF-fed dams. Mating pairs were left together for up to eight days if no sperm-positive flush was

observed. After eight days without a positive, the male was removed and replaced with another male. Fertility data was calculated using only the first eight-day period of mating.

Pregnant dams were divided into three groups: one group was sacrificed at GD15, one group was sacrificed at GD18, and the remainder were allowed to give birth naturally. Eight to ten pregnant dams for each diet group were included in each group. HF and CON-fed dams underwent laparotomy at the GD15 and GD18 timepoints, exposing the abdominal cavity. Urine samples were taken from the bladder with a 26g syringe. Both sides of the uterine horn were then clamped to minimize uterine blood loss. The uterine horns were removed and placentas were harvested as described below. Blood sampling was performed by cardiac puncture prior to euthanasia.

### **3.1.2 Sample preparation and storage**

Whole placentas were dissected out and placed in 10% formalin for immunohistochemical analysis. The two placentas at the position second from the cervix on each side of the uterus as well as one additional placenta from the third or fourth position from the cervix were collected and preserved for histological analysis. Remaining placentas to be used for protein analysis were removed and either left whole or dissected into the junctional zone and labyrinth layers. These samples were snap-frozen in liquid nitrogen before they were transferred to -80°C for long-term storage.

### **3.2 CT scanning and analysis**

To determine the amount of visceral and subcutaneous fat accumulation in the abdominal area, a subset of the dams in the second cohort were fasted for 16 hr at 19 weeks of age prior to pregnancy (CON=7 and HF=7) and CT scanning was carried out using the X-SPECT small animal imaging system (Gamma Medica, Northridge, CA, USA). The midsection of the rat was scanned and the area between the bottom of the lungs and the top of the sacroiliac joint was selected for fat quantification. This area contained approximately 100 slices, each 0.5 mm thick. Densitometric quantification of fat was carried out using Amira software with attenuation thresholds of -450 to -150 Hounsfield units (HU) to select for fat tissue. Air bubbles in the intestines were first removed from the image, and the total fat (subcutaneous + abdominal) was then quantified by integrating all voxels (a 3-dimensional pixel) between -450 and -150 HU. The abdominal muscle surrounding the internal organs was highlighted, and the fat within this region was denoted as abdominal fat. The amount of subcutaneous fat was thus determined by subtracting the value of abdominal fat from the total fat.

### **3.3 Measures of obstetrical outcomes**

#### **3.3.1 Fertility and mating outcomes**

A number of obstetrical outcomes including average time to copulation (number of days cohabited to achieve a sperm positive vaginal flush), mating success (sperm positive dams/total number of cohabiting pairs), and fertility index (number of confirmed

pregnancies/sperm positive dams) were determined using data collected during the first round of mating for each dam.

### **3.3.2 Pregnancy and birth outcomes**

Fetal resorption sites (visible as either a partially resorbed conceptus or an empty area along the uterus where a conceptus has been fully resorbed) were counted at GD15. Fetal and placental weight was recorded for the two most distal conceptuses in each horn of the uterus (total of 4 conceptuses). The fetal:placental weight ratio was calculated using paired fetal:placental units. Values for fetal and placental weight as well as fetal:placental weight ratio were averaged to obtain average fetal and placental weight per dam; the final data is presented as an average of the values for all dams in a group.

The number of offspring per litter was calculated by counting all offspring born to each dam on the morning of birth, including stillbirths. A stillborn pup was defined as one that was not viable on the morning of birth. The percentage of dams in each group that gave birth to at least one stillborn pup was calculated, as well as the live birth index (number of live pups/total number of pups for each litter), and litter size. Pups were sexed and weighed on the morning following their birth (postnatal day 1, PND1). We determined the number of pups that were either large for gestational age (LGA; birth weight greater than 2 standard deviations above the average birth weight of control pups) or small for gestational age (SGA; birthweight less than 2 standard deviations below the average birthweight of control pups). Survival to PND4 was calculated as the percentage of offspring per litter that survived to PND4.

### **3.4 Measures of systemic inflammation and oxidative stress**

#### **3.4.1 Creatinine colorimetric assay**

The creatinine content of maternal urine collected at GD15 was measured using a colorimetric detection kit (Enzo Life Sciences, Farmingdale, NY) according to the manufacturer's instructions. Creatinine content was used to control for the concentration of the urine in other analyses. The assay is based on the reaction of creatinine with alkaline picrate to form a red complex. Sample was diluted 1:30 and 5  $\mu$ l were used for quantification.

#### **3.4.2 8-Isoprostanes ELISA**

The concentration of 8-isoprostanes in urine collected from dams at GD15 was quantified using an ELISA kit (Cayman Chemical, Ann Arbor, MI) according to the manufacturer's instructions. Samples were diluted 1:15 for the assay and values were normalized to urinary creatinine.

#### **3.4.3 8-hydroxy-2'-deoxyguanosine ELISA**

The amount of 8-OHdG in urine from HF and CON dams at GD15 was quantified using an ELISA kit (Cell Biolabs, San Diego, CA) according to the manufacturer's instructions. Samples were diluted 1:30 and values were normalized to urinary creatinine.

#### **3.4.4 Monocyte chemoattractant protein-1 (MCP-1) ELISA**

Total MCP-1 in serum from HF and CON dams at GD15 was quantified using a rat MCP-1 ELISA kit (Pierce, Rockford, IL, USA) according to the manufacturer's instructions. Serum samples were diluted 1:25 for the assay.

### **3.5 Placental tissue preparations**

#### **3.5.1 Tissue homogenization**

40-50 mg of placental tissue was homogenized in homogenization buffer (5 mM HEPES, 100 mM KCl, 70 mM sucrose, 220 mM mannitol, 1 mM EGTA) at a tissue:buffer ratio of 1:25. Protease inhibitor cocktail tablets (Roche Diagnostics, Indianapolis, IN) were added to the homogenization buffer at a concentration of 1 tablet per 10 ml buffer immediately before buffer use. Tissue was homogenized using a Polytron homogenizer (PT1300D; Kinematica, Tokyo, Japan). The homogenate was then centrifuged at 800 x g for 5 minutes to remove any particulate from the solution, and the supernatant stored at -80 C.

#### **3.5.2 Preparation of mitochondrially enriched fractions**

Placental tissues were homogenized at a ratio of 1:5 with homogenization buffer (5mM HEPES, pH 7.2, 100mM KCl, 70mM sucrose, 220mM mannitol, 1mM EGTA, 2mg/mL fatty acid free BSA) plus protease inhibitor cocktail tablets (Roche, Indianapolis, IN; 1 tablet/20ml) for 20 sec using a Polytron homogenizer. These homogenates were then homogenized manually using a dounce homogenizer (Wheaton, Millville, NJ), and centrifuged (Avanti J-301, Beckman Coulter, Fullerton, CA) at 1200 x g for 10 minutes at 4°C. The supernatant was centrifuged at 12,000 x g for 10 minutes at 4°C. The pellet was then resuspended in 1mL of homogenization buffer without 2mg/mL BSA and centrifuged at 12,000 x g for 10 minutes twice. The final pellet was

resuspended in 250µl of homogenization buffer without BSA and stored at frozen at -80°C

### **3.5.3 Bicinchoninic acid protein assay**

The concentration of protein in each sample of homogenized tissue or mitochondrially enriched fraction was determined using a bicinchoninic acid (BCA) protein assay kit (Thermo Fisher Scientific, Rockford, IL) according to the manufacturer's instructions. Tissue homogenate samples were diluted 1:10 in ddH<sub>2</sub>O and 25µl of diluted sample or BSA standard were assayed in duplicate.

## **3.6 Protein quantification by Western blot**

### **3.6.1 SDS-PAGE**

SDS-PAGE was used to separate proteins by size. Loading samples were prepared at a concentration of 0.5 or 1 µg/µl by dilution in 2x Laemmli loading buffer (0.5 M Tris-HCl, pH 6.0, 1% w/v SDS, 10% v/v glycerol, 5% v/v 2-mercaptoethanol ) and ddH<sub>2</sub>O. 10 µg of protein was separated on a 12.5% polyacrylamide gel (100V for 1.5 hr). Proteins were then transferred to a nitrocellulose membrane for 1.5 hr at 100V.

### **3.6.2 Ponceau-S Stain**

The immunoblot was stained with Ponceau-S (Sigma-Aldrich, St Louis, MO; 0.5% w/v in 5% v/v acetic acid) and imaged for quantification using an optical scanner (CanoScan LiDE 70, Lake Success, NY).

### 3.6.3 Western blotting

Blots were blocked overnight in 3% milk or 5% BSA in TBST and incubated with the following primary antibodies for at least 2 hours at room temperature:

<b>Protein</b>	<b>Source</b>	<b>Dilution</b>	<b>Blocking/Antibody Conditions</b>
<b>MnSOD</b>	Abcam, Cambridge, MA	1:50 000	3% milk
<b>CuZnSOD</b>	Abcam, Cambridge, MA	1:100 000	3% milk
<b>Catalase</b>	Abcam, Cambridge, MA	1:20 000	3% milk
<b>GPx</b>	Abcam, Cambridge, MA	1:2000	3% milk
<b>NTyr</b>	Millipore, Billerica, MA	1:5000	5% BSA
<b>4-HNE</b>	Abcam, Cambridge, MA	1:2000	5% BSA
<b>VEGF</b>	Santa Cruz Biotechnology, Santa Cruz, CA	1:2000	3% milk
<b>PIGF</b>	Cell Biolabs, San Diego, CA	1:2000	3% milk
<b>MMP2</b>	Abcam, Cambridge, MA	1:5000	3% milk
<b>MMP9</b>	Abcam, Cambridge, MA	1:20000	3% milk

Following incubation with primary antibody, blots were washed in TBST and incubated with horseradish peroxidase-conjugated anti-mouse or anti-rabbit secondary antibody (1:5000; GE Healthcare, Piscataway, NJ) in the same conditions as the primary

antibody for 1 hour at room temperature. Blots were again washed and developed using enhanced chemiluminescence (Millipore, Billerica, MA) then exposed to X-ray film (Kodak XAR, Carestream Health, Rochester, NY). Protein bands were quantified using ImageJ software (Version 1.37; NIH, Bethesda, MD). Images of Ponceau-S stained nitrocellulose were also analyzed with densitometry to assess equal protein loading per lane, with the region between 25 and 75 kDa selected for analysis.

### **3.7 Immunohistochemistry**

#### **3.7.1 Tissue processing and slide preparation**

Placental tissue was fixed in 10% formalin for 24 hours after harvesting and transferred to 70% ethanol for at least 48 hours. Samples were processed using a Leica TP1020 paraffin tissue processor (Leica Microsystems Inc, Buffalo Grove, IL) and embedded upright with the fetal side of the placental disc perpendicular to the cross-sectional plane using a Leica EG1160 embedder (Leica Microsystems Inc, Buffalo Grove, IL). 5µm sections were cut from the central area of the placenta using a Leica RM 2125 RT microtome equipped with Accu-Edge low-profile microtome blades (Sakura Finetek, Torrance, CA) and mounted on Superfrost Plus microslides (VWR, Mississauga, ON).

Analyses of trophoblast invasion and spiral artery remodelling were performed on slices from the central area of the placenta containing a main maternal spiral artery which crossed the decidua. This central artery is visible during slicing. Parallel slides containing this artery were stained with the antibodies used in the analysis (cytokeratin, CD31, and

SMA). Morphometric analysis was performed on slices from the thickest cross-section of the placenta (measured from the maternal to fetal side). All other staining was carried out on slices from near the central region of the placenta, containing all relevant tissue sections (labyrinth, junctional zone, decidua and mesometrial triangle).

### **3.7.2 Immunohistochemical staining**

Immunohistochemistry (IHC) was performed to determine localization and expression of the protein or antigen of interest within placental and uterine tissue. Slides were deparaffinized in xylene and rehydrated in graded alcohol solutions. Endogenous peroxidase activity was inhibited with 3% hydrogen peroxide in methanol for 15 minutes at RT. Antigen retrieval was achieved by immersing slides in citrate-based antigen unmasking solution (Vector Laboratories, Burlingame, CA), pH 6, and microwaving in a pressure cooker for 8 minutes. Tissues were blocked using 1% BSA with normal donkey serum for 1 hour at RT and incubated with anti-pan cytokeratin (1:300; Sigma-Aldrich, St Louis, MO) or anti-nitrotyrosine (1:300; Millipore, Billerica, MA) overnight at 4°C in a humidity chamber. The following day, sections were incubated with anti-mouse biotinylated secondary antibody (Millipore, Billerica, MA) for 2 hours at RT. Tissues were then exposed to AB reagents (Vector Laboratories, Burlingame, CA) for 1 hour at RT and antibodies were visualized using DAB (Sigma-Aldrich Canada Ltd., Oakville, ON). Slides was counterstained with hematoxylin (Harris hematoxylin solution, Sigma-Aldrich, St Louis, MO), dehydrated and coverslipped.

For anti-CD31 (1:250; BD Biosciences, San Diego, CA), anti-SMA (1:300; Sigma-Aldrich, St Louis, MO), and anti-carbonic anhydrase (1:500; Abcam, Cambridge,

MA), endogenous peroxidase activity was blocked in 1% hydrogen peroxide in methanol for ten minutes, and antigen retrieval was achieved by immersing slides in 10 mM citrate buffer at 90 C for 12 minutes. Blocking was carried out for ten minutes in 5% BSA. The rest of the protocol was carried out as described above.

Slides were imaged using a Nikon Eclipse 90-I confocal microscope equipped with a Nikon DS Fi1C camera; quantification was carried out on the NIS Elements software (Nikon Instruments Inc, Melville, NY) except where noted.

### **3.7.3 Hematoxylin and eosin (H&E) staining**

Hematoxylin and eosin staining was used to visualize placental morphology. Slides from the thickest region of the placenta were deparaffinised in xylene and rehydrated in a series of graded alcohol solutions. Slides were stained with hematoxylin (Harris hematoxylin solution, Sigma-Aldrich, St Louis, MO) for twenty seconds, rinsed with tap water and destained in acid alcohol for two seconds. Slides were rinsed again and stained with eosin for 30 seconds, then dehydrated and coverslipped.

## **3.8 Imaging and quantification of stained slides**

### **3.8.1 Analysis of placental morphology**

H&E stained slides were scanned with the ScanScope™ system (Aperio, Vista, CA). Morphology analysis was done with Aperio ImageScope™ software. The boundaries of the labyrinth, junctional zone, decidua and mesometrial triangle were traced and their surface areas measured. A blinded observer performed morphometric analyses.

### **3.8.2 Analysis of blood vessel density and maturity in the labyrinth**

Smooth muscle actin (SMA) was used as a marker of vascular smooth muscle cells, indicative of blood vessel maturity (Furuya et al, 2008). The number of SMA-positive blood vessels in the labyrinth layer at GD15 (n=5 CON, 7 HF) and GD18 (n=5 CON, 4 HF) was quantified by selecting the immunopositive pixels (brown) with the Threshold tool in Nikon Elements software. Nonspecific background stains were filtered out with the 'Clean' function. The labyrinth layer was selected and the number of 'objects' in this area (the SMA-positive blood vessels) was counted with the Automated Measurements toolbar. Data are presented as the number of blood vessels/ $10^4$   $\mu\text{m}$ .

The same protocol was used to quantify blood vessel density using the endothelial cell marker CD31 at GD18; blood vessel density at GD15 was determined by counting the number of CD31-positive blood vessels per field of view.

### **3.8.3 Analysis of intensity of carbonic anhydrase staining**

Carbonic anhydrase staining was quantified in each section of the implantation site (mesometrium, decidua, junctional zone and labyrinth) at GD15 and GD18 as a marker of hypoxia (Said et al, 2007). The carbonic anhydrase stain was selected using a threshold analysis; the same threshold was used for each image. The boundaries of each area to be analyzed were traced and the percentage area covered by carbonic anhydrase staining was calculated for each area.

### **3.8.4 Analysis of interstitial trophoblast invasion**

Analysis of interstitial trophoblast invasion was carried out on slides containing a cross-section of the central maternal artery, as previously described (Vercruysse et al, 2006). The entire mesometrial triangles of sections stained for cytokeratin were scanned at 4x magnification and cytokeratin-positive cells in the mesometrial triangle were selected using a threshold analysis. The same threshold was used for every image following illumination of non-specific binding. The area of the entire mesometrial triangle was then manually delineated and quantified. IST-covered area was reported as a percentage of the area of the entire mesometrial triangle.

### **3.8.5 Analysis of endovascular trophoblast invasion**

Analysis of endovascular trophoblast invasion was carried out on slides containing a cross-section of the central maternal artery, as previously described (Geusens et al, 2008). The entire mesometrial triangles of sections stained for cytokeratin were scanned at 4x magnification, and the total number of partially and fully invaded as well as non-invaded arteries were counted. Values were reported as the percentage of arteries invaded by endovascular trophoblasts.

### **3.8.6 Analysis of spiral artery remodelling**

Analysis of maternal spiral artery remodeling was carried out on slides containing a cross-section of the central maternal artery, as previously described (Verlohren et al, 2010). Parallel or near-parallel slides to those stained with cytokeratin were stained with CD31 (an endothelial cell marker) and smooth muscle actin (SMA; a vascular smooth

muscle cell marker). Cytokeratin, CD31 and SMA slides were all scanned at 4x objective with the same resolution. Each spiral artery containing endovascular trophoblast cells was identified in the parallel CD31 and SMA-stained slides.

To analyse the elimination of endothelial cells by contact with trophoblast cells, spiral arteries partially or fully invaded by endovascular trophoblasts were identified on the slides stained for CD31, using morphology and the parallel cytokeratin slides to confirm the presence of trophoblast cells. The artery contour lengths covered by EVT (the 'sub-EVT' contour lengths) were traced for each artery; the 'extra-EVT' contour of partially invaded spiral arteries (the contour not directly underlying EVT) was not analyzed, as loss of CD31-positive endothelial cells depends on contact with trophoblast cells. The persistence of CD31-positive maternal endothelial cells in the sub-EVT contour was quantified by tracing the CD31-positive sub-EVT contour. The percentage of sub-EVT contour covered by CD31 was calculated for each artery. All arteries in each implantation site were averaged to give an average % CD31-positive sub-EVT contour for each dam, and a two-tailed T-test was performed on these values (Figure 17).

SMA-positive vascular smooth muscle cells are lost in spiral arteries containing trophoblasts in a contact independent manner (Harris et al, 2006; Caluwaerts et al, 2005). Therefore the SMA-positive contour length (including both sub-EVT and extra-EVT) of partially or fully invaded spiral arteries was quantified, and compared to the total artery contour for each vessel. Values for % invaded artery contour covered by SMA were calculated for each artery; average % invaded artery contour covered by SMA was calculated for each dam and a two-way ANOVA was performed on these averages.

### **3.8.7 Analysis of intensity of nitrotyrosine staining**

Slides stained for nitrotyrosine were scanned, a region of interest was drawn around the boundaries of the area to be analyzed (mesometrium, decidua, junctional zone and labyrinth) and the intensity of each region was quantified. Nitrotyrosine staining was also assessed specifically in EVT's by selecting these cells as a region of interest and measuring staining intensity.

## **3.9 Measurement of protein carbonyls**

### **3.9.1 Protein carbonyl OxyBlot**

Relative protein carbonyl levels in mitochondrially enriched fractions of whole placentas were determined using a commercially available kit (Oxyblot Protein Oxidation Detection Kit S7150, Chemicon International, Inc, Temecula, CA, USA). Briefly, 5  $\mu$ l of 12% SDS and 10  $\mu$ L of DNPH were added to 5  $\mu$ l of mitochondrially enriched placental homogenate, and incubated for 15 min at room temperature. 8.5  $\mu$ l of neutralizing solution were added to the samples followed by the addition of 3  $\mu$ l  $\beta$ -mercaptoethanol (1:1.7 dilution with ddH<sub>2</sub>O). Proteins were resolved on 12.5% SDS-PAGE and transferred onto a Hybond<sup>®</sup> ECL nitrocellulose membrane (Amersham, Piscataway, NJ). Relative intensities of the protein bands were digitally quantified (ImageJ, Version 1.37, NIH, Bethesda, MD, USA).

### **3.9.2 Protein carbonyl ELISA**

Total protein carbonyl content in the mesometrium, labyrinth and junctional zone was quantified using a commercially available ELISA (Cell Biolabs, San Diego, CA)

according to the manufacturer's instructions. Briefly, sample was diluted to a concentration of 10 µg/ml and allowed to adsorb to the wells before being derivatized by reaction with dinitrophenylhydrazine (DNPH) to produce DNP hydrazone. The primary antibody used in the ELISA was specific for DNP. An HRP-conjugated secondary antibody was used and the absorption read at a wavelength of 450 nm.

### **3.9 Gelatin zymography**

Gelatin zymography was performed to assess activity levels of MMP-2 and MMP-9. 25 µg of junctional zone homogenate from GD15 and GD18 CON and HF-fed rats were subjected to 10% SDS-polyacrylamide gel electrophoresis, in which 1mg/ml gelatin (type A from porcine skin; Sigma-Aldrich, St Louis, MO) was incorporated. Following electrophoresis, the gels were washed in incubation buffer (50 mM Tris, 1 µM ZnCl<sub>2</sub>, 2.5% Triton X-100, pH 7.6 four times for 15 minutes each to remove SDS. The gels were then incubated in developing buffer (50 mM Tris, 0.15mM NaCl, 5 mM CaCl<sub>2</sub>, pH 7.8) for 24 h at 37 C, stained with Coomassie Brilliant Blue (Sigma-Aldrich, 0.1% in a solution of 30% isopropanol and 10% acetic acid), and destained with 10% methanol and 5% acetic acid in water. Lack of blue staining is indicative of proteolytic activity. Relative enzymatic activities were quantified using ImageJ software. MMPs were identified based on their molecular weights.

### **3.10 Statistical analysis**

Statistical analyses were performed in Microsoft Excel (Microsoft Canada, Mississauga, ON) or GraphPad Prism (GraphPad Software Inc, La Jolla, CA). Continuous outcome variables were analysed by two-tailed Student's T-tests, except data

on endovascular and interstitial trophoblast invasion and loss of VSMCs in the spiral arteries, which were analyzed by a two-way analysis of variance (ANOVA). The variables used in the two-way ANOVAs were diet and age; Bonferroni's post-hoc testing was performed if an interaction effect of these variables was observed. For the analysis of weight gain over time, Bonferroni's correction (stating that a difference is determined to be significant at a p value of  $\alpha$ /number of measures) was used to allow for multiple measures. Data for SGA/LGA, mating success and fertility index was analyzed using Fisher's Exact Test. For analyses of birth weight, fetal and placental weight and fetal and placental weight ratio, survival to PND4 and live birth index, each litter was considered a statistical unit. For immunohistochemical analysis of trophoblast invasion and vessel remodelling, one implantation site was examined for each dam, and each implantation site was considered a statistical unit. Values that were outside of a range of two standard deviations from the means were considered outliers and were removed from the analyses. A p value of  $<0.05$  was considered statistically significant.

## **RESULTS**

### **4.1 Maternal weight gain and fat distribution**

The average body weight of HF-fed dams was significantly higher than CON-fed dams by 5 weeks of age; by 19 weeks of age, the HF-fed group were 36% heavier (Figure 7;  $p < 0.001$ ). The amount and distribution of body fat in HF and CON-fed dams was assessed via CT scanning. At 19 weeks of age, CT scanning showed that HF-fed dams had a significantly higher volume of intra-abdominal fat (Figure 8C;  $p < 0.01$ ). The volume of subcutaneous fat was 2.5 times higher in HF-fed dams and trended towards significance (Figure 8D;  $p = 0.091$ ). Rats were not CT scanned during pregnancy to avoid complications due to administration of anaesthetics; instead, intra-abdominal fat was weighed at sacrifice at gestational day 15. The total weight of abdominal fat was significantly higher in HF-fed dams at GD15 (Figure 8E;  $p < 0.01$ ).

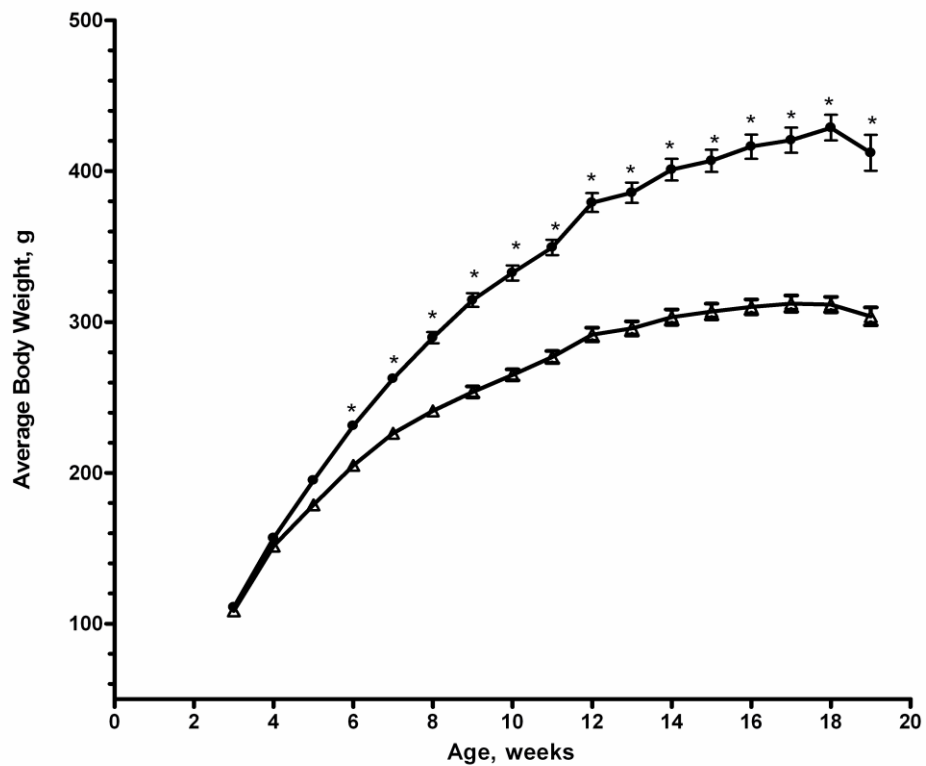


**Figure 7. Body weight of CON- and HF-fed dams prior to pregnancy.** Dams were weighed weekly from 3 weeks of age.  $\Delta$  = CON-fed dams;  $\bullet$  = HF-fed dams. Values represent mean  $\pm$  SEM. P values were calculated using a two-tailed Student's T-test with Bonferroni's correction for multiple comparisons. \*  $p < 0.05/\text{number of measures}$ , therefore \*  $p < 0.0029$ ;  $n \geq 29$  per group.

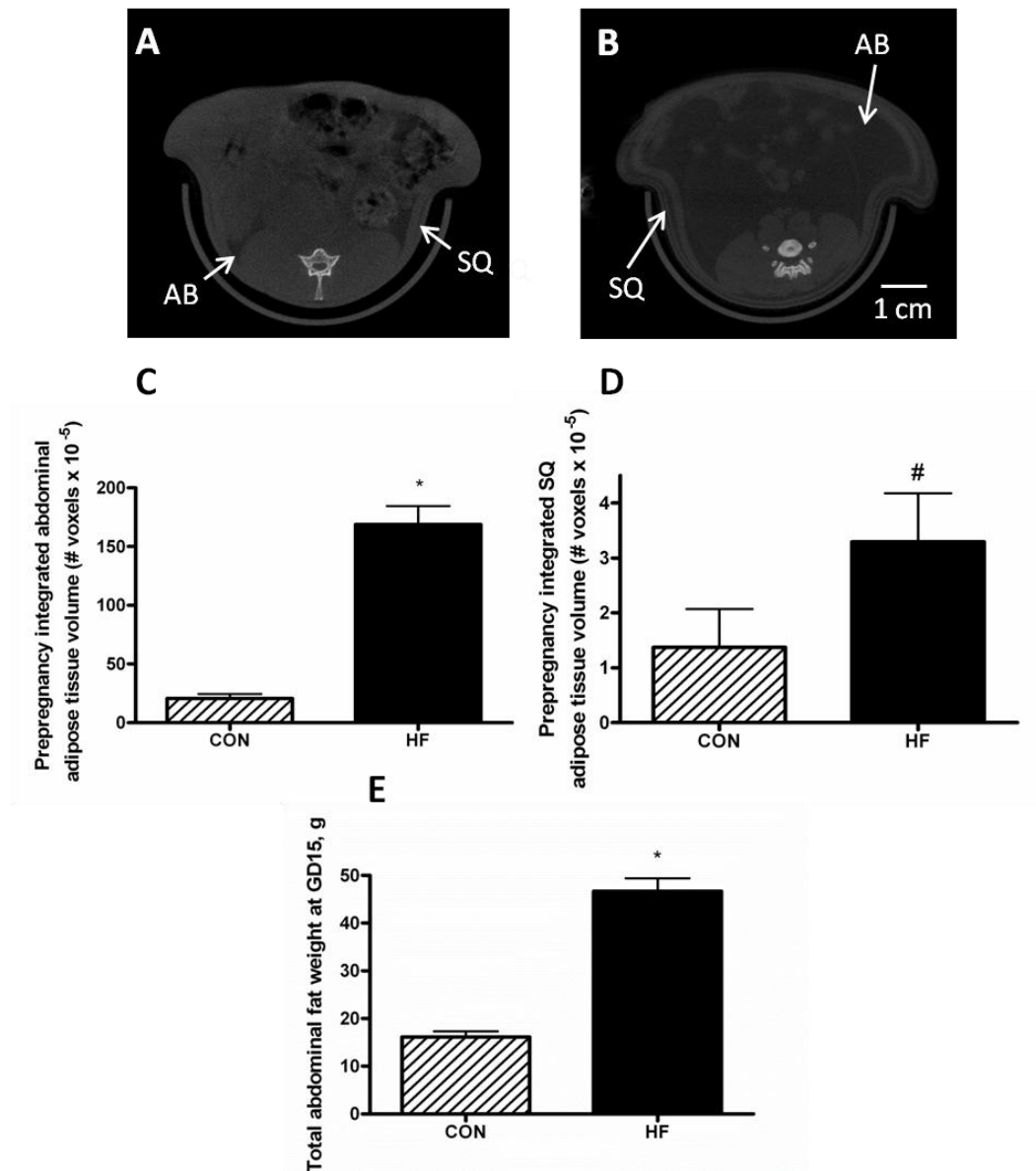


**Figure 8. Amount of abdominal adipose tissue is increased in HF-fed dams prior to pregnancy and at GD15.** Fasted rats were subjected to CT scanning under gaseous anaesthetic at 19 weeks of age prior to pregnancy. Subcutaneous and abdominal adipose tissue volume was quantified in the area between the bottom of the lungs and the top of the sacroiliac joint. Representative CT scans of CON-fed (A) and HF-fed (B) dams are shown. Adipose tissue is characterized by a lower intensity signal (darker regions on the image). The volume occupied by the abdominal fat (AB) and subcutaneous fat (SQ) are indicated. Average abdominal adipose tissue volume (C) and average subcutaneous adipose tissue volume (D) are shown; n=7 in each group. The total abdominal adipose tissue was removed and weighed at sacrifice on GD15 n $\geq$  18 in each group (E). All values represent mean  $\pm$  SEM. P values were calculated using two-tailed Student's T-tests; \* p<0.01, # p<0.10.

## **4.2 Maternal systemic oxidative stress and inflammation**

In humans, obesity is associated with a state of systemic oxidative stress, which may persist through pregnancy (Rajasingam et al, 2009). Therefore markers of systemic oxidative stress were examined in the urine of dams collected during sacrifice at GD15. 8-hydroxy-2-deoxyguanosine (8-OHdG) is an oxidized nucleoside that can be detected in the urine. While the mean level of 8-OHdG was approximately 30% greater in the HF-fed dams, the difference did not reach statistical significance (Table 2;  $p=0.10$ ). 8-isoprostanes are a marker of lipid peroxidation and were also measured in the urine of dams at GD15. There was no significant difference in isoprostane levels as measured by ELISA between CON and HF-fed dams, although values were 33% higher in HF-fed dams (Table 2;  $p=0.20$ ).

Obesity is also associated with a state of chronic inflammation which persists through pregnancy (Stewart et al, 2007). We used an ELISA kit to detect monocyte chemoattractant protein 1 (MCP-1), a chemokine which is released by stressed adipose cells in obesity and is used as a marker of inflammation (Lam et al, 2011; Madan et al, 2009). MCP-1 was significantly higher at GD15 of pregnancy (Table 2;  $p<0.01$ ).

Analyte	CON	HF	p
8-OHdG (ng/mg creatinine)	2.44 ± 0.17	3.73 ± 0.76	0.10
Isoprostanes (pg/mg creatinine)	25.20 ± 2.44	33.50 ± 5.46	0.21
MCP-1 (ng/ml)	6.76 ± 0.61	9.74 ± 0.77	<0.01

**Table 2. Markers of maternal systemic inflammation and oxidative stress in CON and HF-fed dams at gestational day 15.** 8-hydroxy-2-deoxyguanosine (8-OHdG) and 8-isoprostanes were measured in urine collected at sacrifice and normalized to creatinine in urine, measured by a colorimetric assay kit. MCP-1 was measured in non-fasted serum collected at sacrifice. P values were calculated using two-tailed Student's T-tests; n ≥ 7 per group.

### 4.3. Maternal fertility and fetal and neonatal health outcomes

Maternal mating and fertility outcomes were assessed for CON and HF-fed dams (Table 3). The average time to copulation was 46% longer for HF-fed dams ( $p=0.03$ ), the mating success (percentage of dams that had sperm-positive flushes) was reduced by 33% in HF-fed dams ( $p=0.004$ ), and the fertility index (percentage of sperm-positive females that resulted in pregnancy) was 22% lower in HF-fed dams ( $p=0.03$ ).

Parameters of fetal health were also examined (Table 4). At GD15, the number of resorption sites, indicative of *in utero* fetal loss, was significantly higher in HF-fed dams ( $p<0.05$ ). Fetal and placental weight were not significantly different at GD15; however, the fetal:placental weight ratio was 12% lower in HF-fed dams ( $p = 0.03$ ). By GD18, there was a trend towards a significant increase in the number of resorption sites in HF-fed dams ( $p=0.07$ ). Fetal weight was still not significantly different at GD18, but there was a trend towards a reduced placental weight in HF-fed dams ( $p=0.06$ ). The fetal:placental weight ratio was no longer significantly different at GD18.

Parameters of neonatal health were assessed in animals that were allowed to give birth (Table 5). The number of pups born per litter was decreased in HF-fed dams ( $p<0.01$ ). The live birth index (the percentage of pups that were alive on the morning of birth) was 11% lower in HF-fed dams ( $p=0.03$ ). Pups were weighed and separated to male and female pups; both male and female pups born to HF-fed dams were about 10% lighter at birth ( $p<0.001$ ). The number of pups born as large for gestational age (top tenth percentile of the average CON weight) and small for gestational age (bottom tenth percentile of the average CON weight) was also calculated; there were fewer LGA pups

born to HF-fed dams and more SGA pups born to HF-fed dams ( $p < 0.001$ ). The percentage of pups surviving to PND4 was calculated for each dam and was significantly lower in the HF group, with only 45% of offspring of HF-fed dams surviving compared to nearly 100% of controls ( $p < 0.01$ ).

<b>Fertility Outcome</b>	<b>CON-fed Dams</b>	<b>HF-Fed Dams</b>	<b>p</b>
Average time to copulation (d)	2.59 ± 0.39	3.80 ± 0.41	0.03
Mating success (%)	100	67.6	<0.01
Fertility Index (%)	73.8	51.7	0.03

**Table 3. Mating and fertility outcomes of CON and HF-fed dams.** The average time to copulation indicates the number of days the female was cohabited with the male before a sperm-positive vaginal flush was observed. Mating success was determined as the percent of cohabited dams that resulted in a sperm-positive vaginal flush. Fertility index was determined as the percentage of sperm-positive females that resulted in a confirmed pregnancy. The p value for average time to copulation was calculated using a two-tailed Student's T-test, and p values for mating success and fertility index were calculated using Fisher's exact tests; n= 22 for CON, 28 for HF.

<b>Outcome measured</b>	<b>GD15</b>			<b>GD18</b>		
	<b>CON</b>	<b>HF</b>	<b>p</b>	<b>CON</b>	<b>HF</b>	<b>p</b>
Number of resorption sites	0.67 ± 0.19	2.20 ± 2.28	<0.01	0.22 ± 0.22	1.00 ± 0.33	0.07
Fetal weight	0.29 ± 0.02	0.28 ± 0.06	0.70	1.48 ± 0.10	1.38 ± 0.07	0.41
Placental weight	0.27 ± 0.01	0.26 ± 0.01	0.52	0.48 ± 0.03	0.41 ± 0.03	0.06
Fetal:placental weight ratio	1.13 ± 0.05	0.99 ± 0.04	0.03	3.13 ± 0.03	3.50 ± 0.25	0.27

**Table 4. Parameters of fetal health in CON and HF-fed dams.** The number of resorption sites, indicating fetal loss, was counted at sacrifice. Four fetuses and their corresponding placenta were weighed at sacrifice. Fetal:placental weight ratio was calculated for each of the four fetoplacental units. Average fetal weight, placental weight and fetal:placental weight ratio were calculated for each dam. Data is expressed as the mean of these averages. P values were calculated using two-tailed Student's T-tests; n ≥ 8 dams per group.

<b>Outcome measured</b>	<b>CON-fed Dams</b>	<b>HF-Fed Dams</b>	<b>p</b>
Number of pups per litter	14.0 ± 0.7	10.5 ± 1.0	<0.01
Live birth index	98.9 ± 0.6	87.7 ± 4.9	0.03
Weight at birth (M)	6.9 ± 0.2	6.2 ± 0.2	<0.001
Weight at birth (F)	6.6 ± 0.2	5.9 ± 0.2	<0.001
LGA	11/383	0/234	<0.001
SGA	3/383	11/234	<0.001
Survival to PND4 (%)	97.8 ± 1.6	45.0 ± 13.7	<0.01

**Table 5. Parameters of neonatal health in CON and HF-fed dams.** Live birth index is reported as # of live pups at birth / total # of pups at birth. Live pups were separated by sex and weighed on the morning of birth. Large for gestational age (LGA) is defined as the number of pups with birth weight greater than the average of the control group plus 2 standard deviations; small for gestational age (SGA) is defined as the number of pups of birth weight lower than the control group minus 2 standard deviations. Survival to PND4 is reported as the percentage of live pups born that were still alive at PND4. For number of pups per litter, live birth index, weight at birth, and survival to PND4, mean values were calculated for each dam and two-tailed T-tests were performed on these means; n = 32 CON and 25 HF. Pup weights from all CON and all HF-fed dams were pooled and Fisher's exact test was used to calculate p values for LGA/SGA analysis; n= 383 pups born to CON-fed dams and 234 pups born to HF-fed dams.

#### **4.4 Placental vascular structure, morphometry of the implantation site, and cell death**

Changes in the structure of the placenta (which could include alterations in the vasculature or changes in gross placental morphology) compromise nutrient flow to the fetus and may be associated with reduced fetal growth and health (Furukawa et al, 2011). We hypothesized that the obese maternal environment would be associated with changes in placental structure; therefore vascular and morphometric parameters of the placenta were examined.

The density of blood vessels in the labyrinth of placentas was examined by immunostaining for the endothelial cell marker CD31. CD31 staining showed an increased number of blood vessels per area in the labyrinth layer of placentas from HF-fed dams at GD15 ( $p < 0.05$ ) but not at GD18 ( $p = 0.22$ ).

Blood vessel maturity was also examined by immunostaining for smooth muscle actin (SMA), a vascular smooth muscle cell marker. The number of SMA-positive vessels per area in the labyrinth layer was quantified. There were 22% fewer SMA-positive vessels per area in the labyrinth layer of placentas from HF-fed dams at GD15 ( $p < 0.01$ ), but by GD18 this trend was abolished and no difference in the number of mature vessels was observed ( $p = 0.76$ ).

We also assessed the sizes of the different regions of both the placenta proper (labyrinth and junctional zone) and the maternal portion of the implantation site (decidua and mesometrial triangle) to assess whether the observed vascular changes were associated with morphometric changes. H&E staining was performed on slices from the

thickest region of the placenta for this analysis. At GD15, the labyrinth layer of placentas from HF-fed dams covered 23% more area than in controls (Figure 11C;  $p < 0.05$ ). The area covered by the junctional zone was not significantly different ( $p = 0.27$ ), but the total area of the placenta was trending towards a significant increase in HF-fed dams (15% higher in HF;  $p = 0.06$ ). By GD18, the labyrinth covered 16% more area (Figure 11D;  $p < 0.01$ ) and the junctional zone was again unchanged ( $p = 0.90$ ); the increase in size of the labyrinth led to a trend towards a higher total placental area in the HF group at GD18 (11% higher in HF;  $p = 0.053$ ). The area of the decidua was not significantly different at GD15 (Figure 11E;  $p = 0.31$ ) but at GD18 was 25% larger in placentas from HF-fed dams (Figure 11F;  $p < 0.05$ ). The area covered by the mesometrial triangle was not significantly different at either timepoint ( $p = 0.37$  at GD15;  $p = 0.32$  at GD18).

The change in the size of the placenta may be a consequence of decreased apoptosis; therefore we assessed the number of apoptotic cells per area in the labyrinth and junctional zone at GD15 (Figure 12). There was no significant difference in the number of TUNEL-positive cells per area in either the labyrinth ( $p = 0.62$ ) or the junctional zone ( $p = 0.18$ ).

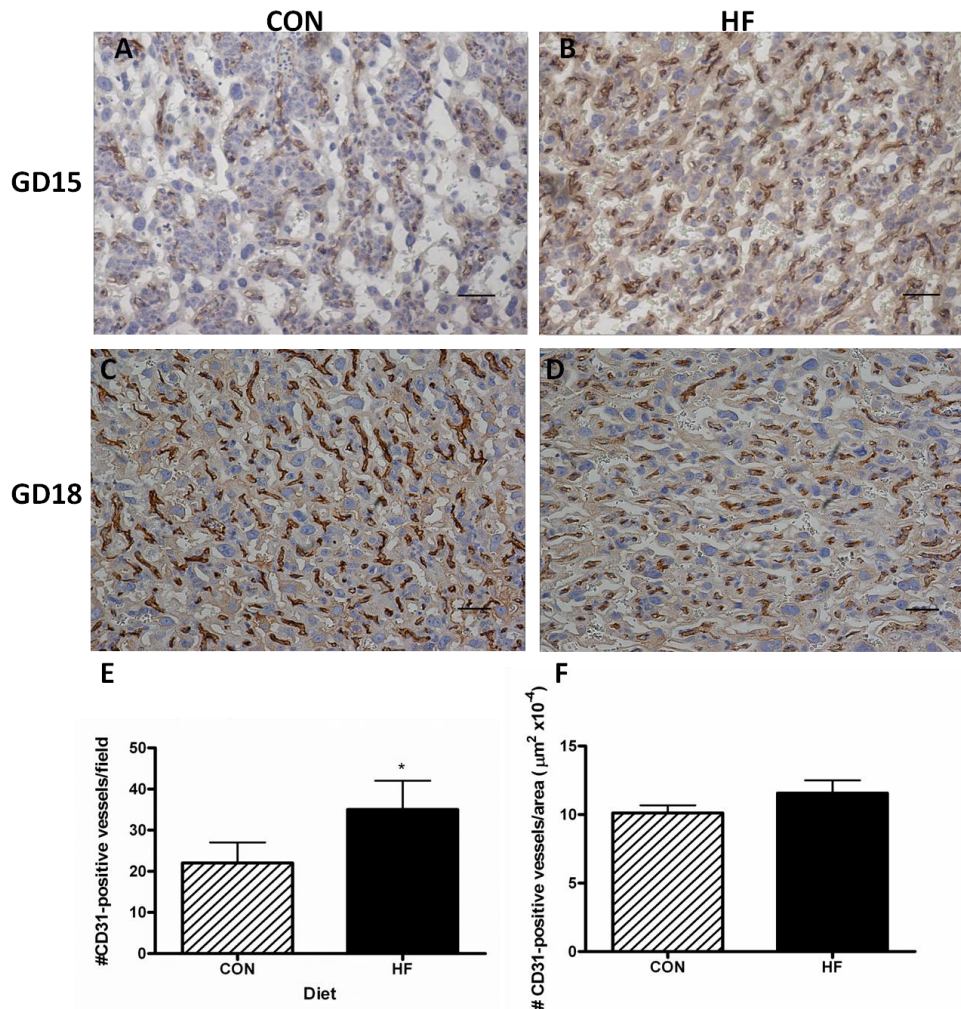


**Figure 9. Labyrinth layers of placentas from HF-fed dams exhibit an increased density of CD31-positive blood vessels at GD15 but not GD18.** 5  $\mu\text{m}$  slices were taken from the central region of each placenta and immunohistochemistry was carried out using an anti-CD31 antibody (1:250). Representative images of GD 15 placenta from CON-fed (A) and HF-fed (B) dams and GD18 placentas from CON-fed (C) and HF-fed (D) dams are shown. Scale bar: 50  $\mu\text{m}$ . At GD15, the number of CD31-positive blood vessels per field was counted in five fields of view taken from across the entire labyrinth. At GD18, the number of CD31-positive vessels in the entire labyrinth was quantified using Nikon Elements software and compared with the area of the labyrinth. E, average number of CD31-positive vessels per field of view in CON and HF placentas at GD15; F, average number of CD31-positive vessels/ $10^4 \mu\text{m}^2$  in CON and HF placentas at GD18. All values represent mean  $\pm$  SEM. P values were calculated using two-tailed Student's T-tests; \* $p < 0.05$ ,  $n \geq 5$  dams per group.

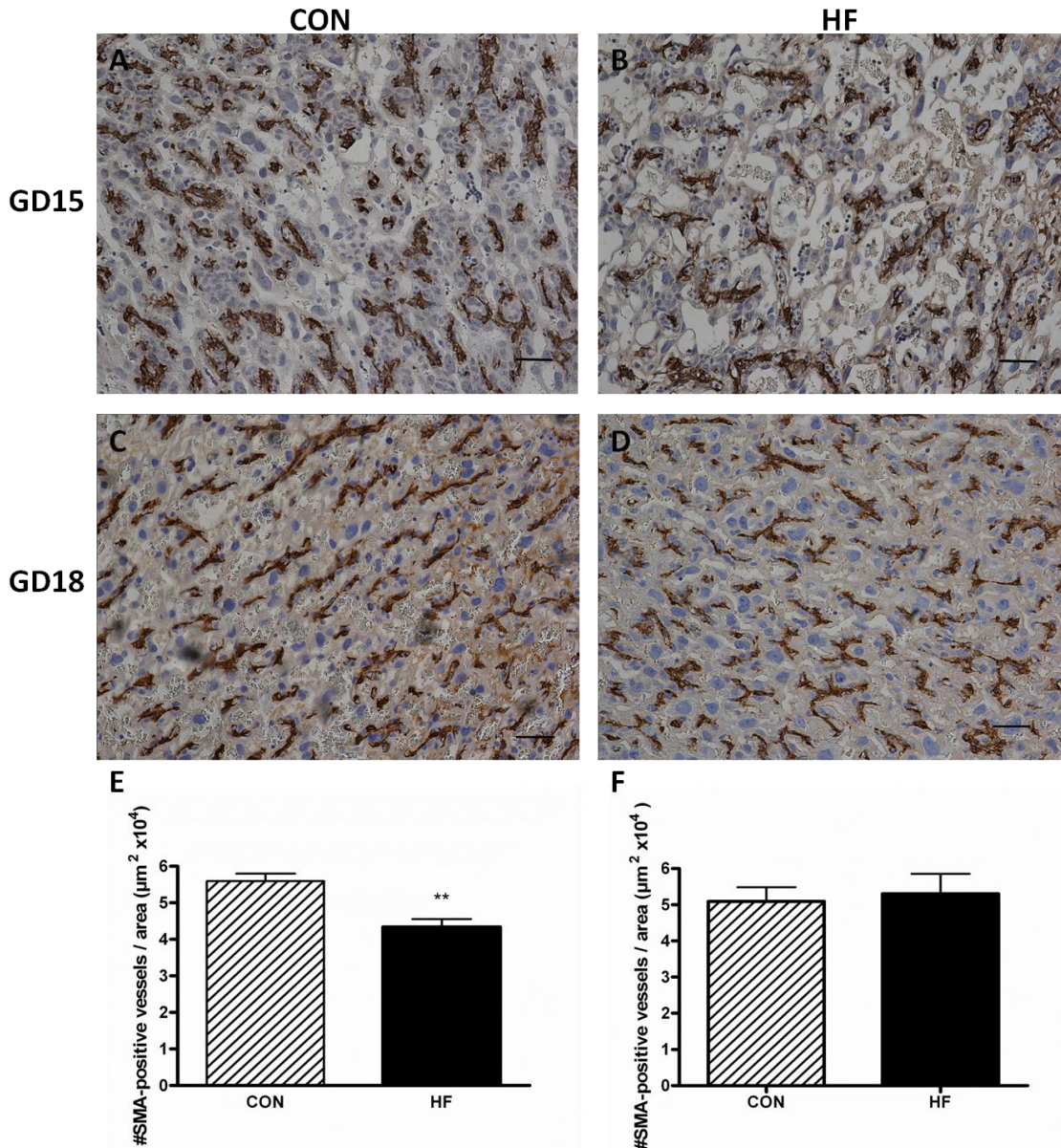


**Figure 10. Labyrinth layers of placentas from HF-fed dams exhibit fewer SMA positive blood vessels at GD15 but not GD18.** 5  $\mu\text{m}$  slices were taken from the central region of each placenta and immunohistochemistry was carried out using an anti-SMA antibody. Representative images of GD15 placentas from CON-fed (A) and HF-fed (B) dams, and GD18 placentas from CON-fed (C) and HF-fed (D) dams are shown. Scale bar: 50  $\mu\text{m}$ . The number of SMA positive vessels in the labyrinth was counted using Nikon Elements software and compared with the area of the labyrinth. E, average number of SMA-positive vessels/ $10^4 \mu\text{m}^2$  in CON and HF placentas at GD15; F, average number of SMA-positive vessels/ $10^4 \mu\text{m}^2$  in CON and HF placentas at GD18. All values represent mean  $\pm$  SEM. P values were calculated using two-tailed Student's T-tests; \* $p < 0.01$ ,  $n \geq 5$  dams per group.

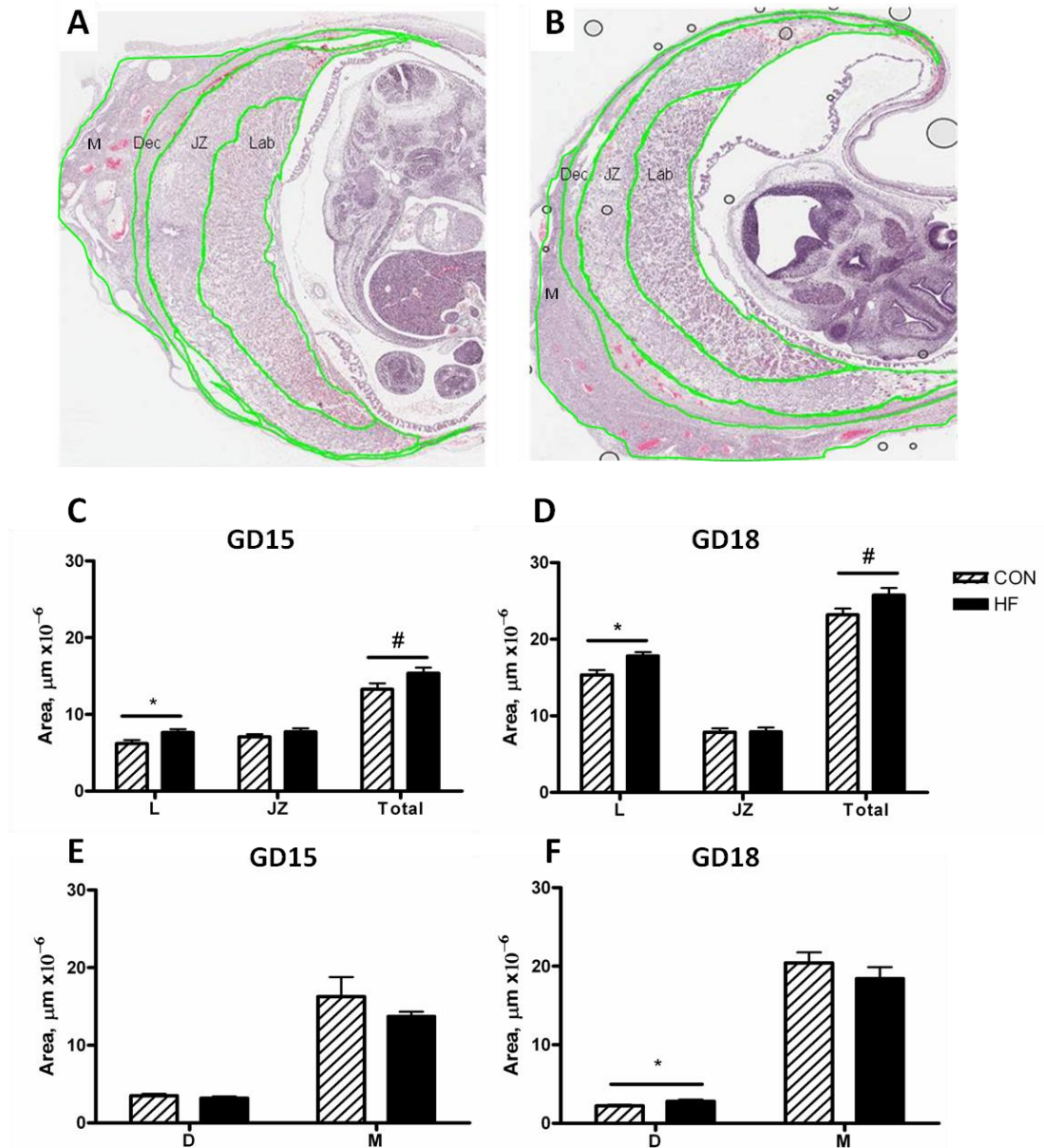


**Figure 11. Placental morphometric parameters are altered in HF-fed dams at gestational days 15 and 18.** Slices (5  $\mu\text{m}$  thick) taken from the widest area of the placenta and stained with hematoxylin and eosin. The borders of the labyrinth, junctional zone, decidua and mesometrium were manually traced. Representative images of GD 15 placenta from CON-fed (A) and HF-fed dams (B) are shown. Morphometric measurements of the placenta proper are shown at GD15 (C) and GD18 (D); L=labyrinth, JZ= junctional zone. Morphometric measurements of the maternal side of the implantation site are shown at GD15 (E) and GD18 (F); D=decidua, M=mesometrial triangle. All values represent mean  $\pm$  SEM. P values were calculated using two-tailed Student's T-tests; \*  $p < 0.05$ ,  $n \geq 7$  dams per group.

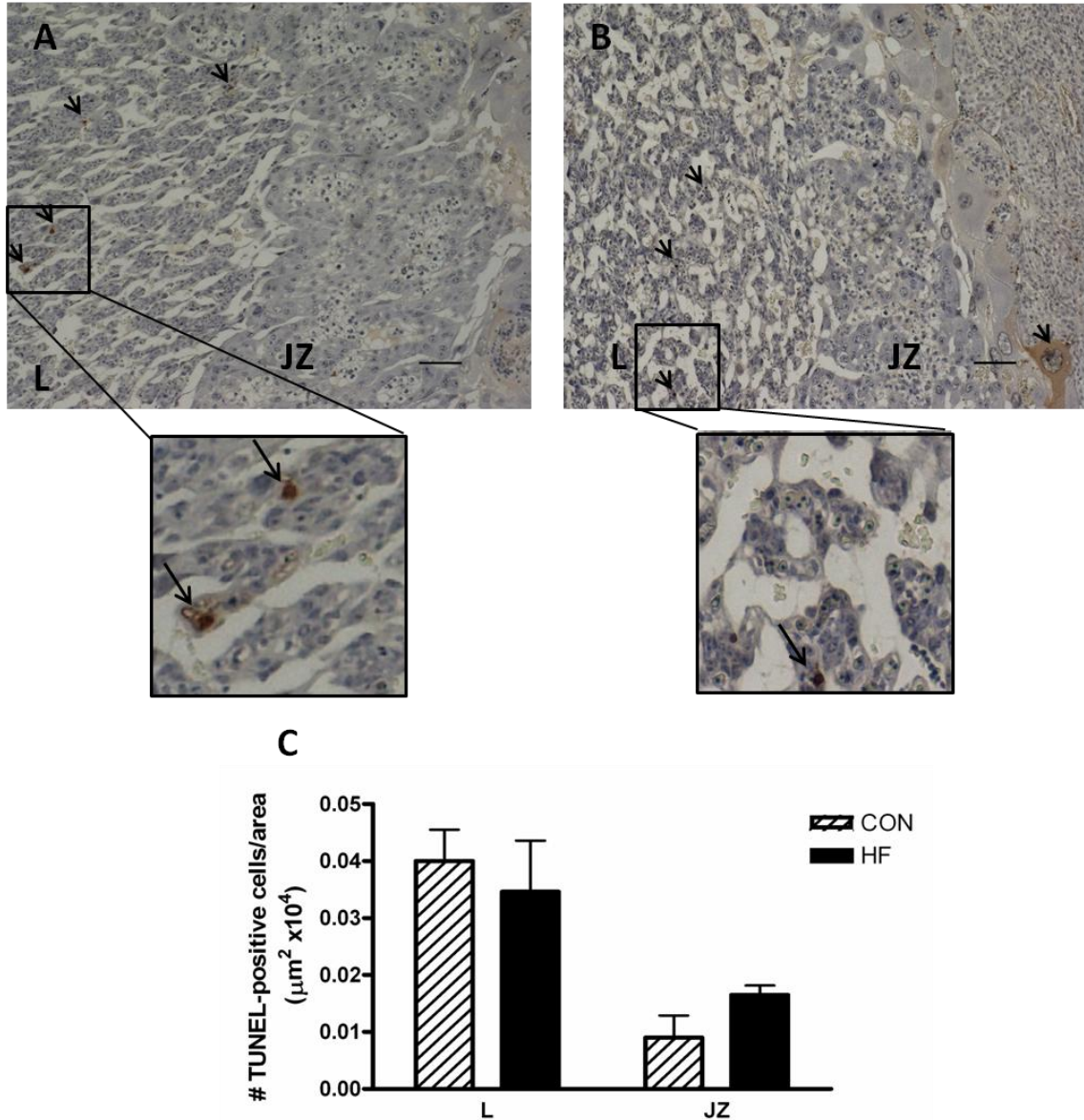


**Figure 12.** The number of apoptotic cells per area is not significantly different in the labyrinth and junctional zones of placentas from CON and HF-fed dams at GD15. 5 μm slices from the central region of each placenta were stained to assess the presence of DNA strand breaks using the TUNEL labelling method, indicative of apoptosis. Whole slides were scanned and positive cells were counted in each region and normalized to the total area of the junctional zone or labyrinth. Representative images of GD 15 placenta from CON-fed (A) and HF-fed dams (B) are shown. L=labyrinth, JZ=junctional zone; scale bar = 100 μm. C, number of positive cells per area in the labyrinth and junctional zone at GD15. All values represent mean ± SEM. P values were calculated using two-tailed Student's T-tests; p ≥0.10; n=4 for CON, 5 for HF.

#### **4.5. Mechanisms behind the alterations in blood vessel structure and morphometry of the placenta: angiogenic growth factors and hypoxia**

To assess the molecular mechanisms behind the increase in blood vessel density and decrease in blood vessel maturity, levels of two placental angiogenic growth factors (vascular endothelial growth factor (VEGF) and placental growth factor (PlGF)) were examined by Western blot (Figure 13). VEGF protein levels were 76% higher in the labyrinth layer of the placenta of HF-fed dams at GD15 ( $p < 0.05$ ), but by GD18 no significant difference was observed ( $p = 0.64$ ). PlGF, a less potent VEGF analog, was 37% lower in the labyrinth layer of the placenta of HF-fed dams at GD15 ( $p < 0.05$ ), but was not significantly different by GD18 ( $p = 0.94$ ).

Placental hypoxia is known to be present in pregnancy complications including preeclampsia and has been connected with growth restriction. It is also known to increase VEGF and decrease PlGF expression by trophoblast cells (Munaut et al, 2008). Therefore levels of carbonic anhydrase, a marker of hypoxia, were quantified at GD15 and GD18 (Figure 14). At GD15, carbonic anhydrase staining intensity was 73% higher in the labyrinth of placentas from HF-fed dams ( $p < 0.05$ ). However, by GD18 carbonic anhydrase levels were no longer significantly different ( $p = 0.55$ ).

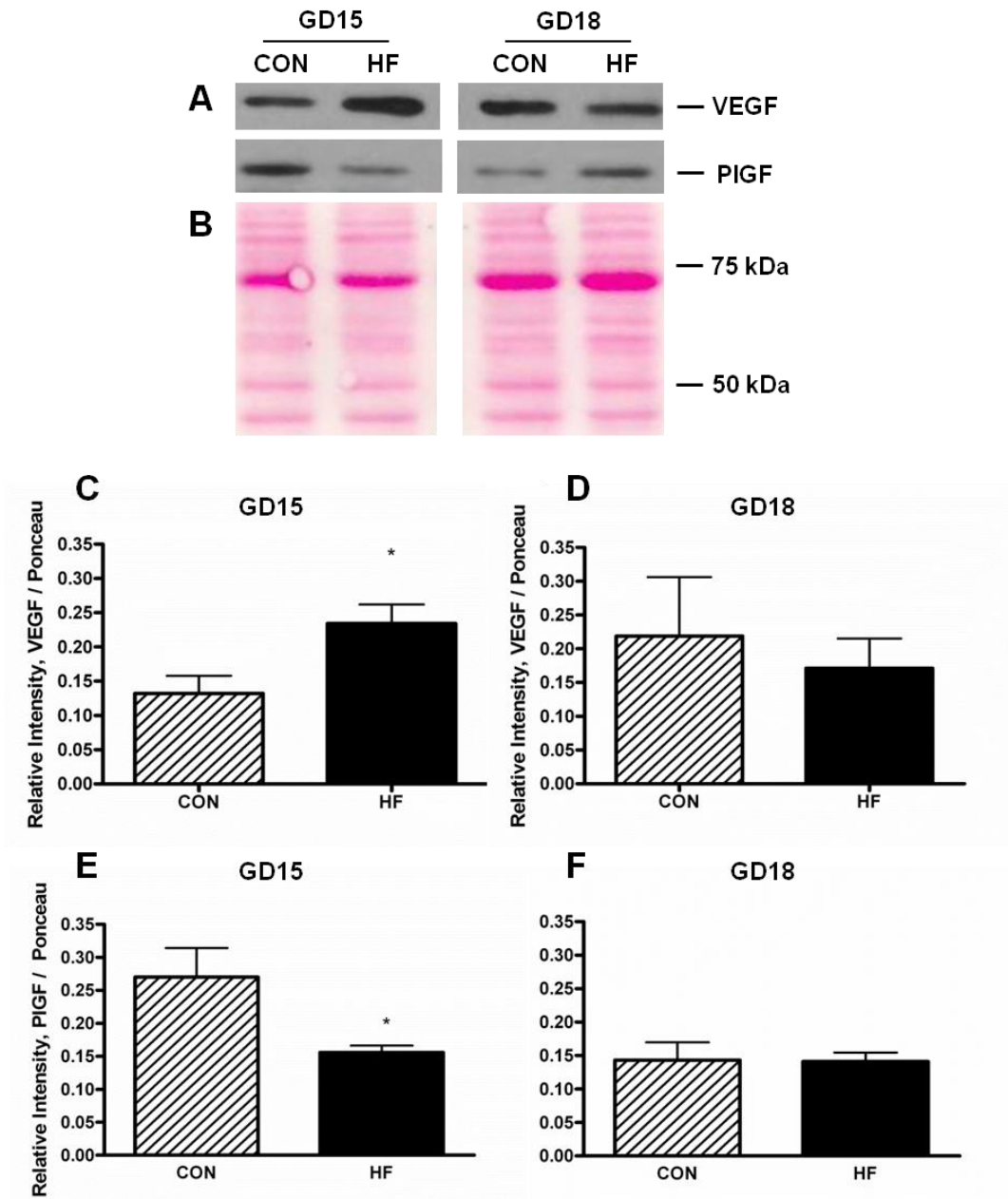


**Figure 13. VEGF protein levels are increased and PlGF levels are decreased in HF GD15 placentas.** Proteins (10  $\mu$ g per lane) were separated on a 12.5% polyacrylamide gel and incubated with anti-VEGF (1:2000) or anti-PlGF (1:2000). Representative Western blots for VEGF and PlGF at GD15 and GD18 are shown (A). A representative segment of Ponceau-S stained nitrocellulose used for normalization is also shown (B). Densitometric quantification of VEGF Western blots at GD15 (C) and GD18 (D), and PlGF Western blot at GD15 (E) and GD18 (F) are shown. All values represent mean  $\pm$  SEM. P values were calculated using two-tailed Student's T-tests; \* $p$ <0.05,  $n$ =6 per group.

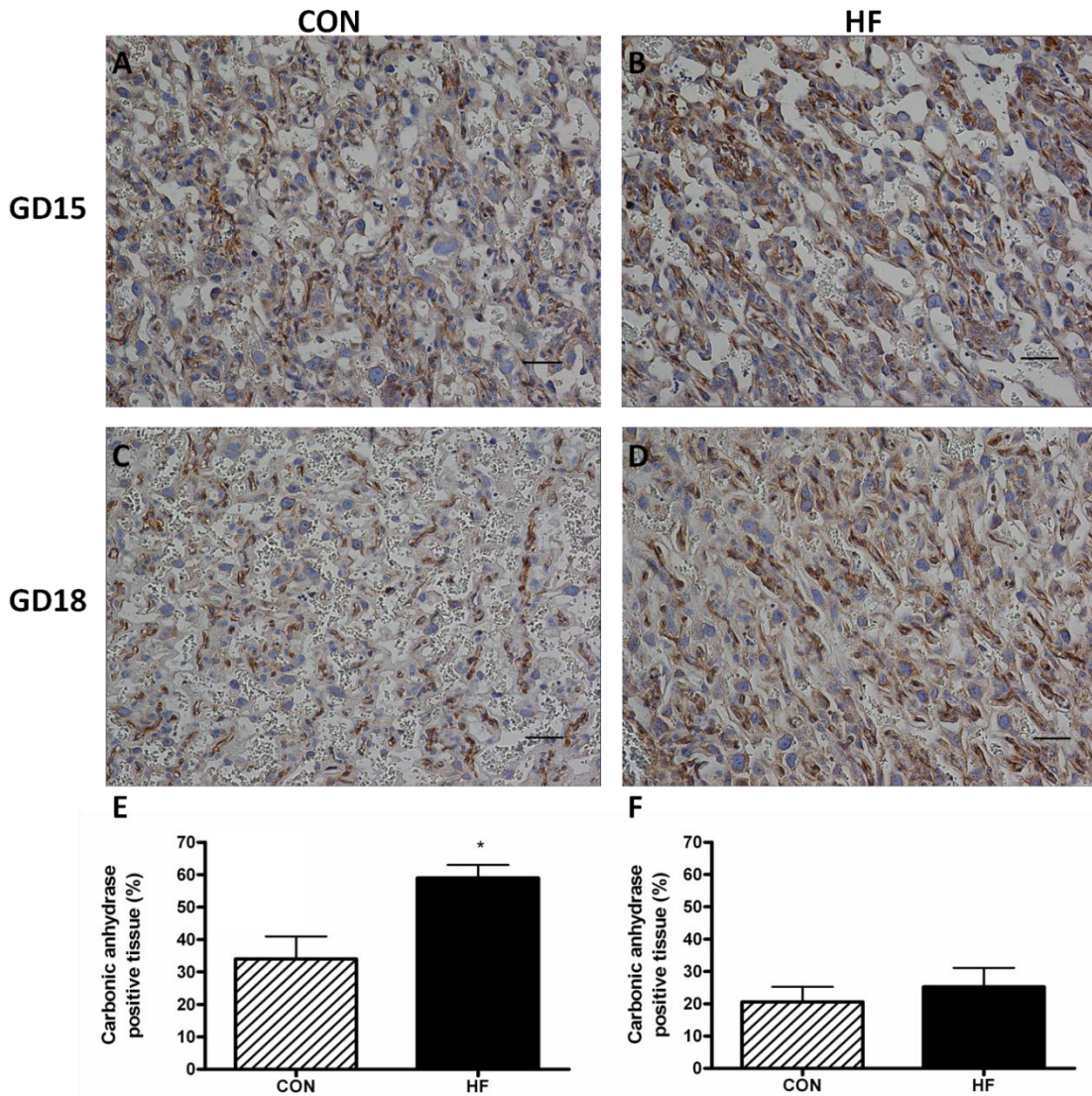


**Figure 14. Labyrinth layers of placentas from HF-fed dams exhibit increased carbonic anhydrase staining intensity at GD15 but not GD18.** 5  $\mu$ m slices were stained with an antibody to carbonic anhydrase (CA). Representative images of placental labyrinth layers from GD15 CON-fed (A) and HF-fed dams (B) and GD18 CON-fed (C) and HF-fed (D) dams are shown. Scale bar = 100 $\mu$ m. At GD15, the percentage of tissue staining positive for CA was calculated in five fields of view taken from across the entire labyrinth. At GD18, the average intensity of the carbonic anhydrase stain was calculated across the entire labyrinth. **C.** Percentage of tissue positive for CA in CON and HF labyrinth layers at GD15; **D.** Percentage of tissue positive for CA in CON and HF placentas at GD18. All values represent mean  $\pm$  SEM. P values were calculated using two-tailed Student's T-tests; \* $p < 0.05$ ;  $n \geq 5$  dams for each group.

#### **4.6 Trophoblast invasion and spiral artery remodelling in the mesometrial triangle**

Trophoblast invasion into the mesometrial triangle is known to be affected by hypoxia and can lead to poor pregnancy outcomes if compromised (Geusens et al, 2008; Rosario et al, 2008). The amount of invasion through the interstitial pathway was quantified by measuring the area covered by interstitial trophoblast cells compared to the entire mesometrial triangle on slides stained with the trophoblast cell marker cytokeratin (Figure 15). At GD15, interstitial trophoblasts covered double the area of the mesometrial triangle in placentas from HF-fed dams compared with those from CON-fed dams ( $p<0.05$ ); by GD18, no difference in area covered by interstitial trophoblasts was observed ( $p=0.42$ ). Analysis by two-way ANOVA showed that the increase between GD15 and GD18 was significant for both diet groups ( $p<0.05$ ).

Endovascular trophoblast invasion was also quantified at GD15 and GD18 (Figure 16). The number of blood vessels fully or partially invaded by EVT was compared with the total number of blood vessels in the entire mesometrial triangle. At GD15, a significantly higher percentage of blood vessels had been invaded by endovascular trophoblast in mesometrial triangles from HF-fed dams ( $p<0.05$ ), but by GD18 there was no significant difference ( $p=0.53$ ). Analysis by two-way ANOVA showed that in the CON group, the percentage of arteries invaded increased significantly between GD15 and GD18 ( $p<0.05$ ), while in the HF group no significant difference between gestational ages was observed.

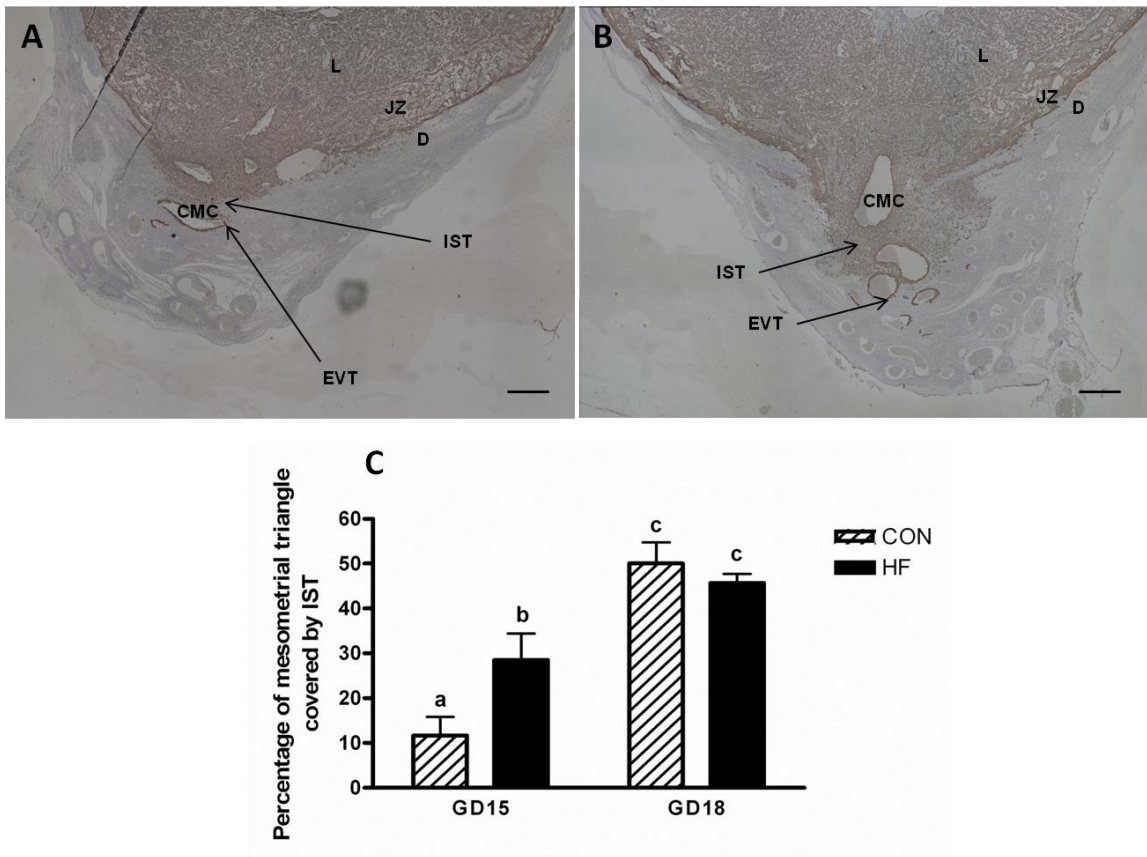


**Figure 15. Area covered by interstitial trophoblast cells in the mesometrial triangle is higher in HF-fed dams at gestational day 15 but not 18 of pregnancy.** Central slides (5  $\mu$ m thick) were stained with anti-pan cytokeratin (1:300). Cytokeratin staining (brown) indicates the presence of trophoblast cells. L=labyrinth, JZ= junctional zone, D= decidua, SA = spiral artery, IST = interstitial trophoblast, EVT = endovascular trophoblast. Representative images of GD 15 placenta from CON-fed (A) and HF-fed dams (B) are shown; scale bar = 600  $\mu$ m. C, the percentage of the mesometrial triangle invaded by interstitial trophoblast cells at GD15 and GD18. All values represent mean  $\pm$  SEM; different letters above bars represent a statistically significant difference ( $p < 0.05$ ). One implantation site was examined per dam. P values were calculated using a two-way ANOVA;  $n \geq 4$  dams per group.

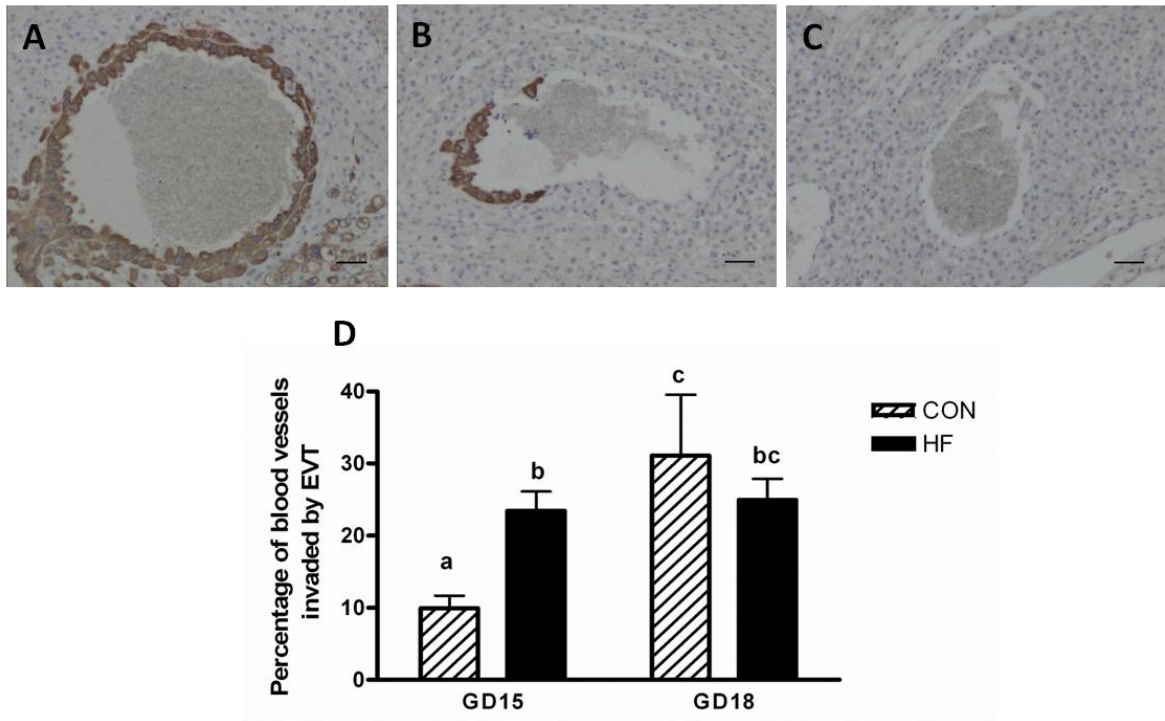


**Figure 16.** The percentage of blood vessels invaded by endovascular trophoblast cells in the entire mesometrial triangle is higher in HF-fed dams at GD15 but not GD18. Central slides (5  $\mu$ m thick) were stained with anti-pan cytokeratin (1:300). All blood vessels in the mesometrial triangle were traced and vessels fully invaded (A), partially invaded (B), and not invaded (C) by endovascular trophoblast were counted. Scale bars = 50  $\mu$ m. D, the percentage of total blood vessels that were fully or partially invaded was calculated for each implantation site before being averaged. All values represent mean  $\pm$  SEM; different letters above bars represent a statistically significant difference ( $p < 0.05$ ). One implantation site was examined per dam. P values were calculated using a two-way ANOVA;  $n \geq 4$  dams per group.

Both endovascular and interstitial trophoblast cells work together to convert the maternal spiral arteries into high-capacity, low-resistance blood vessels. This is accomplished by the replacement of maternal endothelial cells with trophoblasts and the elimination of vascular smooth muscle cells, limiting contractility. The extent of blood vessel remodelling was analyzed on slides stained with the endothelial cell marker CD31

and the vascular smooth muscle cell marker SMA. Invasion of EVT's leads to the loss of maternal endothelial cells in a contact-dependant manner (Caluwaerts et al, 2005).

Therefore, the presence of endothelial cells in the artery contour directly underlying invading endovascular trophoblast cells (the sub-EVT contour) was quantified. There was no significant difference in the percentage of the sub-EVT artery contour that was covered by CD31-positive endothelial cells between the CON and HF-fed groups at GD15 ( $p=0.55$ ) or GD18 ( $p=0.31$ ; Figure 17D).

Maintenance of the vascular smooth muscle cell layer of spiral arteries is another hallmark of a failure of the remodelling process. The percentage of the entire artery contour covered by SMA-positive VSMCs in partially and fully invaded arteries was quantified. There was no significant difference in the % contour covered by VSMC at GD15 ( $p=0.88$ ) or at GD18 ( $p=0.11$ ; Figure 17E).

The matrix metalloproteinases MMP2 and MMP9 are involved in trophoblast invasion and also blood vessel remodelling (Qiu et al, 2004; Xu et al, 2011; Harris and Aplin, 2007). MMP2 and 9 protein and activity levels were assessed in the junctional zones of GD15 placentas, as this section of the placenta contains the precursors to the invasive trophoblast cells. Protein levels were examined via Western blot and protease activities were assessed via gelatin zymography. Activity levels of pro-MMP2 ( $p=0.23$ ) and active MMP2 ( $p=0.18$ ) were not significantly different between junctional zones from CON and HF-fed dams. Protein levels of MMP2 were also not significantly different, although protein levels were three times as high in the HF group (Figure 18;  $p=0.32$ ). MMP9 protein levels were 35% lower in the HF group, though this did not

reach significance (Figure 19;  $p=0.10$ ). However, the activities of pro-MMP9 and total MMP9 were significantly lower in junctional zones from HF-fed dams ( $p<0.05$ ), and active MMP9 trended towards a decrease in the HF group as well ( $p=0.09$ ).

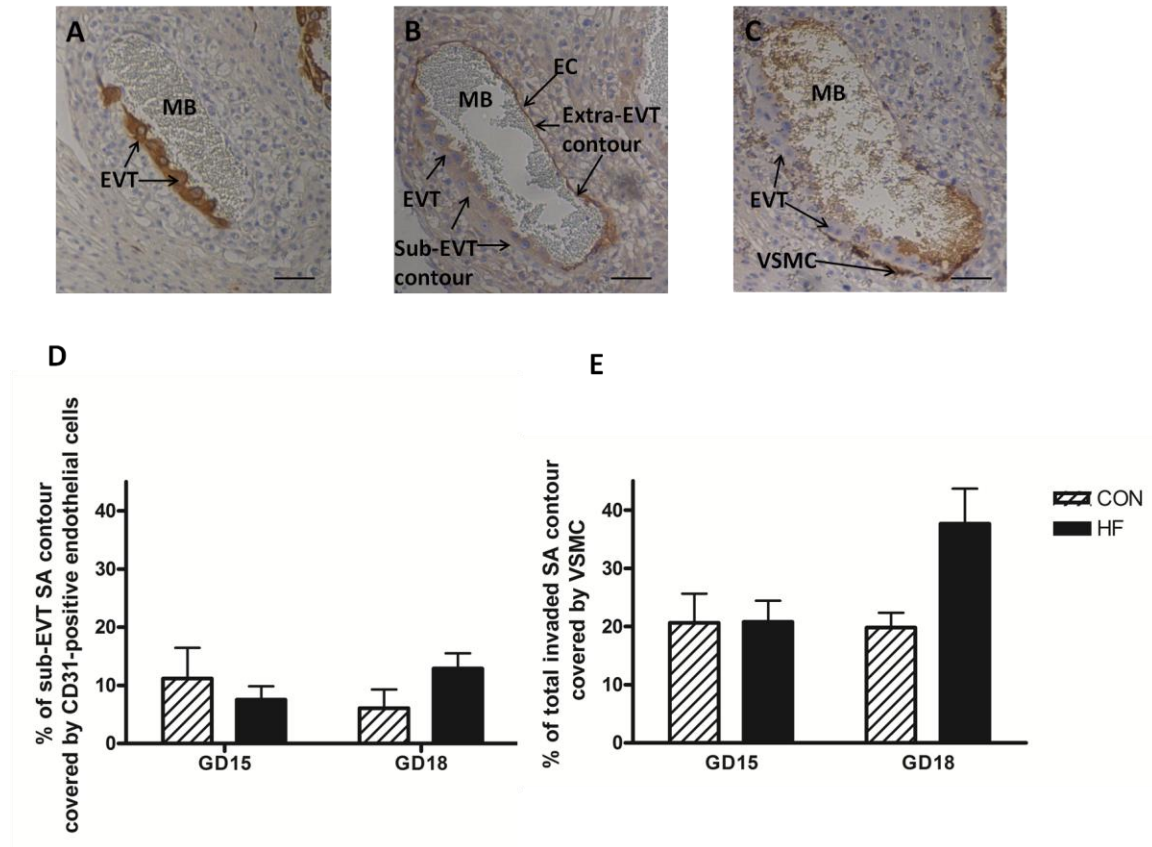


**Figure 17. The degree of spiral artery remodeling is not significantly different between CON and HF-fed dams at GD15 or GD18.** Slides stained with anti-pancytokeratin (1:300; Sigma) were used to identify endovascular trophoblasts, and parallel or near-parallel slides were stained with anti-CD31 (1:200; BD Biosciences) and anti-SMA (1:300; Sigma). Only vessels that were partially or fully invaded by endovascular trophoblasts were analyzed. A representative partially invaded blood vessel is shown stained with cytokeratin (A), CD31 (B), and SMA (C). D, The percentage of contour length covered by CD31-positive endothelial cells was quantified in the artery contour directly beneath EVTs (sub-EVT contour). E, The percentage of contour length covered by SMA-positive VSMCs was quantified in the entire artery contour of fully or partially invaded arteries. All values represent mean  $\pm$  SEM. P values were calculated using two-way ANOVAs;  $p \geq 0.10$ . 1 to 6 spiral arteries were analyzed in each dam;  $n \geq 5$  dams per group.

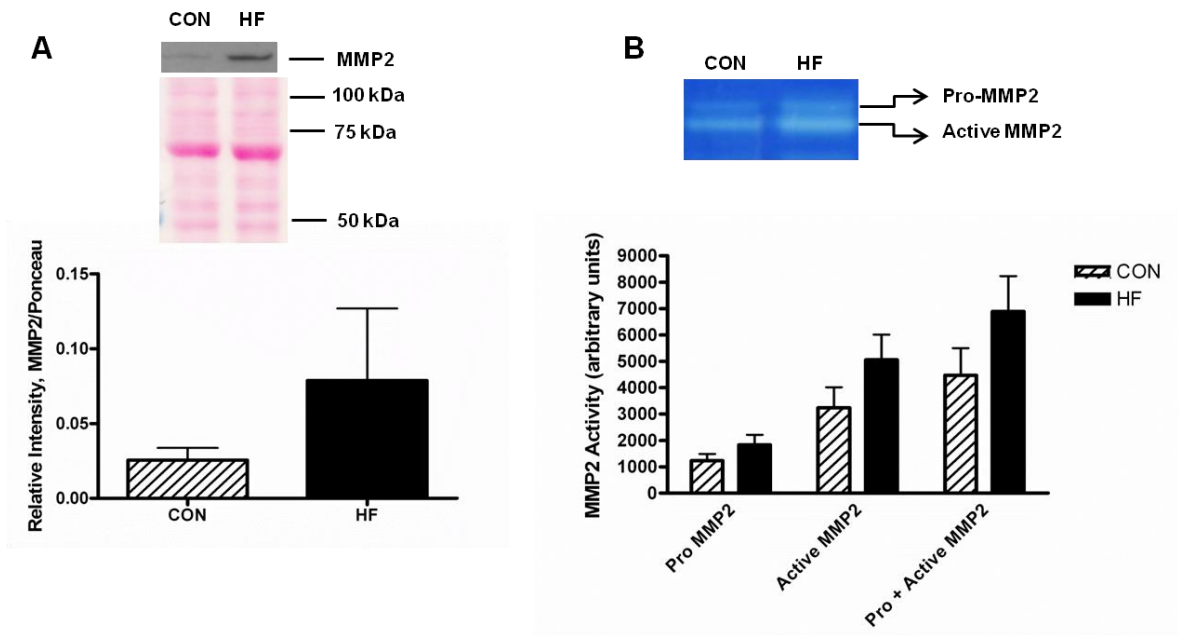


**Figure 18. MMP2 protein and activity levels in junctional zones of placentas from HF and CON-fed dams are not significantly different at GD15.** MMP2 protein levels were measured by Western blot (**A**) and pro- and active MMP2 activity were measured by gelatin zymography (**B**). For Western blot analysis, proteins (10  $\mu$ g per lane) were separated on a 10% polyacrylamide gel, transferred to nitrocellulose and incubated in 3% milk with anti-MMP2 monoclonal antibody (1:5000). Ponceau-S staining was used for normalization. Representative CON and HF lanes as well as the section of the Ponceau-S stained nitrocellulose used for normalization are shown (**A**);  $n=7$  per group. For gelatin zymography, 30  $\mu$ g of protein was loaded in each well of a 10% polyacrylamide gel containing 1 mg/ml gelatin, allowed to incubate, washed and then stained with Coomassie Blue. Pro, active and total MMP2 activities were examined (**B**);  $n = 6$  per group. All values represent mean  $\pm$  SEM. P values were calculated using two-tailed Student's T-tests;  $p \geq 0.10$ .

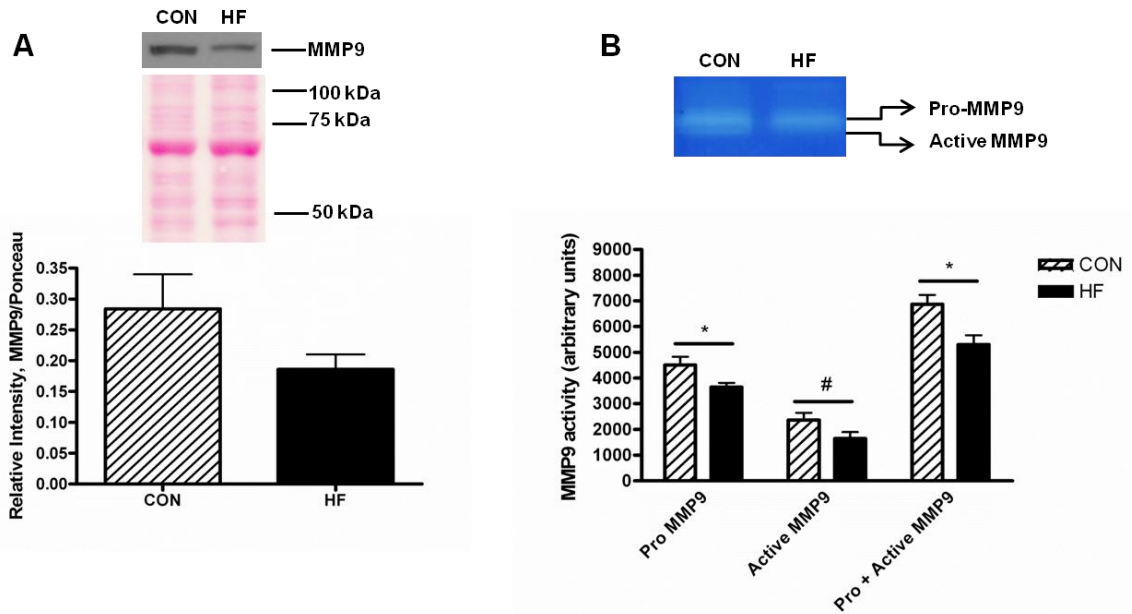


**Figure 19. MMP9 protein and activity levels are lower in junctional zones of placentas from HF-fed dams at GD15.** MMP9 protein levels were measured by Western blot (A) and pro- and active MMP9 activity were measured by gelatin zymography (B). For Western blot analysis, proteins (10 ug per lane) were separated on a 10% polyacrylamide gel, transferred to nitrocellulose and incubated in 3% milk with anti-MMP9 monoclonal antibody (1:20 000). Ponceau-S staining was used for normalization. Representative CON and HF lanes as well as the section of the Ponceau-S stained nitrocellulose used for normalization are shown (A); n=7 per group. For gelatin zymography, 30 µg of protein was loaded in each well of a 10% polyacrylamide gel containing 1 mg/ml gelatin, allowed to incubate, washed and then stained with Coomassie Blue. Pro, active and total MMP9 activities were examined (B); n = 6 per group. All values represent mean ± SEM; p values were calculated using two-tailed Student's T-tests; \* = p <0.05, # = p=0.09.

#### **4.7. Markers of placental oxidative stress**

Placental oxidative stress has been observed in a rat model of maternal obesity (Lin et al, 2011); in addition, placental hypoxia, which we have observed at GD15, is often associated with placental oxidative stress in pregnancy complications in humans (Soleymanlou et al, 2005). Therefore we assessed antioxidant protein levels and markers of oxidative damage in placentas from CON and HF-fed animals.

Antioxidant proteins may be altered in response to excessive ROS production. Levels of several antioxidant proteins were assessed via Western blotting in whole placenta, as well as specific regions including the labyrinth, and junctional zone layers at GD15. Values were normalized to Ponceau-S staining intensity and are expressed as a percentage of control for consistency. MnSOD, CuZnSOD, glutathione peroxidase, and catalase levels were not significantly different in any section of the placenta (Figure 20).

Another marker of oxidative stress is the presence of oxidative damage to cellular components. 4-hydroxynonenal (4-HNE) is an oxidized lipid that attaches to nearby proteins and can be quantified via Western blot. There was a trend towards an increase in 4-HNE levels in GD15 whole placenta (Figure 21; 29% higher in HF,  $p=0.09$ ); however, this trend was not observed when 4-HNE was assessed in the labyrinth and junctional zones of GD15 placentas.

Protein carbonyl formation occurs due to oxidative damage to proteins. Protein carbonyls can be derivatized with dinitrophenylhydrazine (DNP) and can then be detected with an antibody to the derivative. Protein carbonyl formation was measured in the labyrinth and junctional zones of GD15 placentas with an ELISA that uses this

principle of derivatization (Table 6). There was no difference in protein carbonyl levels in the labyrinth or junctional zone of placentas at GD15.

Nitrative damage is a downstream consequence of oxidative stress, occurring after superoxide radicals interact with nitric oxide to produce peroxynitrite, which attacks and nitrosylates proteins. This damage can alter protein function. Nitrotyrosine was measured via Western blot in whole placenta as well as labyrinth and junctional zone fractions at GD15 (Figure 22). No significant differences in nitrotyrosine levels were observed in any fraction measured.

Oxidative stress often originates in the mitochondria due to excessive production of ROS by the electron transport chain; these ROS preferentially attack mitochondrial proteins and lipids due to their close proximity to the site of origin. Therefore we examined oxidative damage in mitochondrially enriched fractions from whole placentas at GD15 (Figure 23). A trend towards an increase in protein carbonyl levels was observed (63% higher in HF;  $p=0.06$ ); no changes in 4-HNE or NTyr levels was observed.

Nitrative damage often occurs around blood vessels because it is dependent on both superoxide and the presence of NO, a vasodilator. Therefore we visualized nitrotyrosine staining via immunohistochemistry on whole implantation sites to assess whether certain regions had an increase in NTyr formation. We found no difference in staining intensity in the labyrinth, junctional zone, decidua or mesometrium (Figure 24). Endovascular trophoblasts, which were identified by their morphology, showed a dark staining intensity for nitrotyrosine (Figure 25). The staining intensity of these cells was measured and no difference was observed between the CON and HF samples.

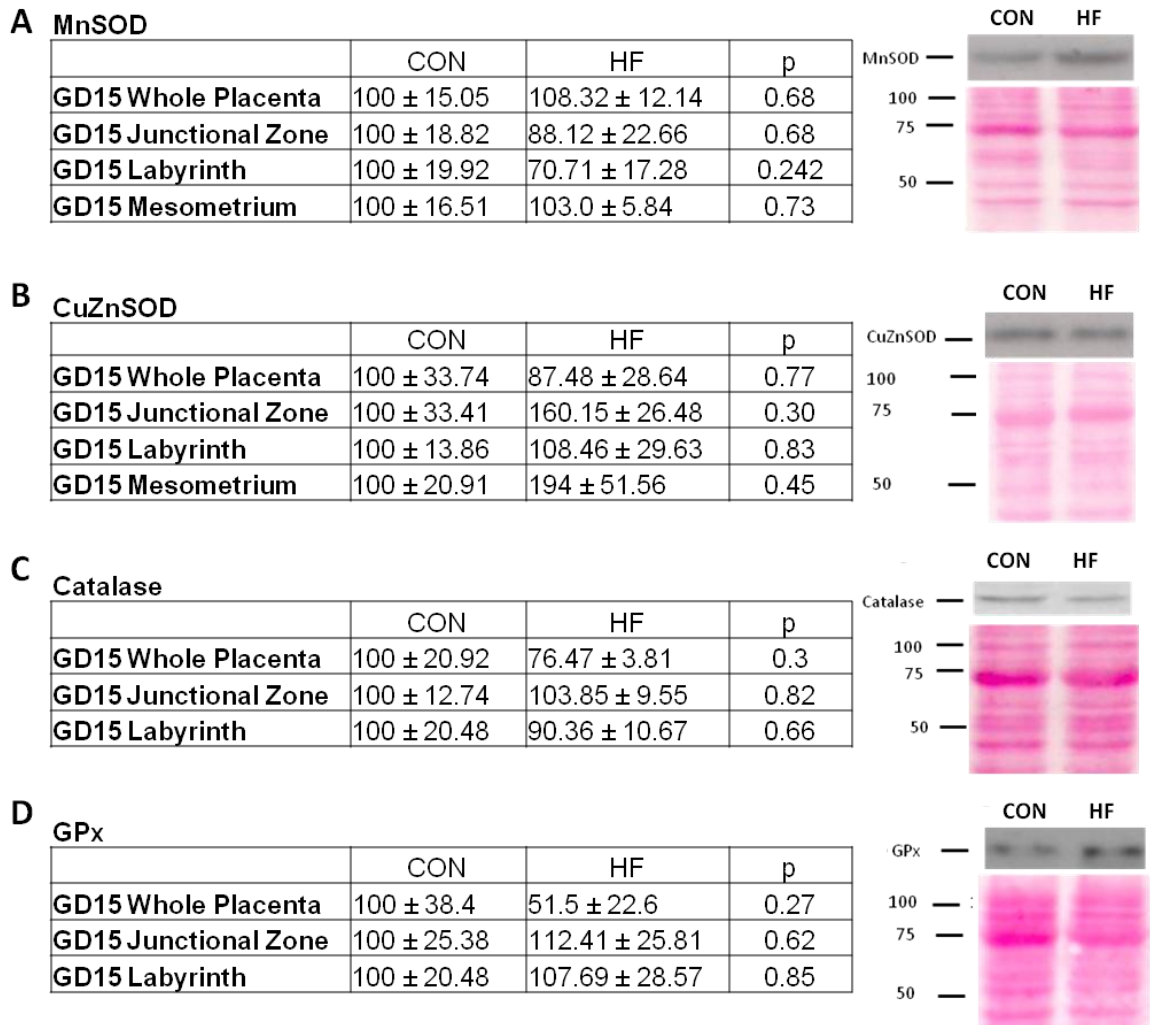


**Figure 20. Levels of antioxidant enzymes are similar in the placentas of CON and HF-fed dams at GD15.** Manganese superoxide dismutase (**A**; MnSOD; 1:50 000, exposure time 10 s), copper zinc superoxide dismutase (**B**; CuZnSOD; 1:100 000, exposure time 10 s), glutathione peroxidase (**C**; GPx; 1:10 000, exposure time 2 min), and catalase (**D**; 1:3000; exposure time 10 s) were all measured in GD15 whole placenta, labyrinth and junctional zone homogenates by Western blotting. Relevant regions from representative Western blots on the labyrinth layer are shown, along with the section of the Ponceau-S stained membrane used for normalization. Values are expressed as a percentage of control values ± SEM. P values were calculated using two-tailed Student's T-tests; n ≥ 5 per group.

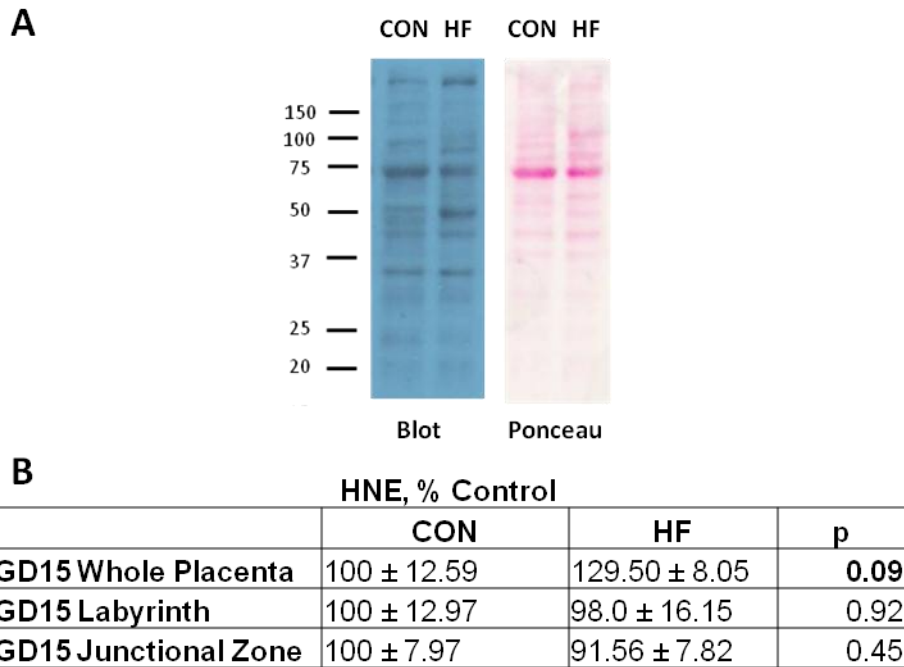


**Figure 21. Levels of lipid peroxidation are similar in the placentas of GD15 CON and HF-fed dams.** Placentas from CON and HF-fed dams at gestational day 15 were either collected whole or dissected into the labyrinth and junctional zone. 4-hydroxynonenal (4-HNE) was measured via Western blot using a monoclonal antibody to 4-HNE (1:2000; exposure times 10-20 seconds). A representative Western blot of HNE and the Ponceau-S stain used for normalization in GD15 whole placenta are shown (A). HNE levels were normalized to Ponceau-S stain and expressed as a percentage of control values ± SEM (B). P values were calculated using two-tailed Student's T-tests; n ≥ 6 per group.

**Protein carbonyl ELISA**

	CON	HF	p
<b>GD15 Junctional Zone</b>	4.30 ± 0.25	4.63 ± 0.34	0.70
<b>GD15 Labyrinth</b>	4.32 ± 0.16	4.49 ± 0.13	0.42

**Table 6. Levels of protein carbonyls are similar in the placentas of GD15 CON and HF-fed dams.** Placentas from CON and HF-fed dams at gestational day 15 were dissected into the labyrinth and junctional zone. Levels of protein carbonyls were measured using a commercially available ELISA according to the manufacturer's instructions; all values represent mean ± SEM. P values were calculated using two-tailed Student's T-tests; n ≥ 6 per group.

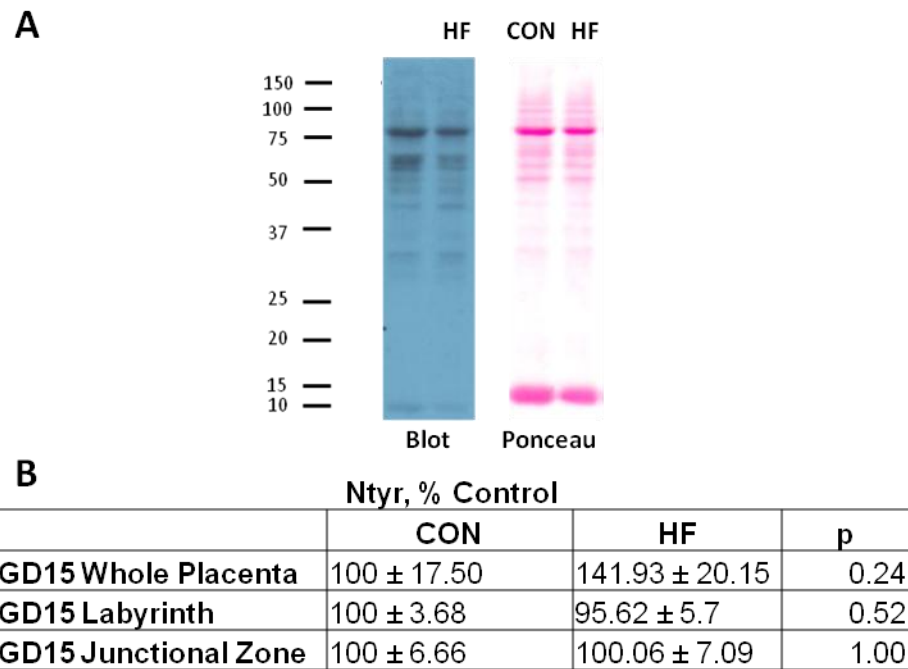


**Figure 22. Levels of nitrotyrosine are similar in the placentas of GD15 CON and HF-fed dams.** Placentas from CON and HF-fed dams at gestational day 15 were either collected whole or dissected into the labyrinth and junctional zone. NTyr damage was measured via western blot using a monoclonal antibody to nitrotyrosine (1:5000, exposure times 10-20 seconds). A representative western blot of NTyr and the Ponceau-S stain used for normalization in GD15 whole placenta are shown (A). NTyr levels were normalized to Ponceau-S stain and expressed as a percentage of control values ± SEM (B). P values were calculated using two-tailed Student's T-tests; n ≥ 6 per group.

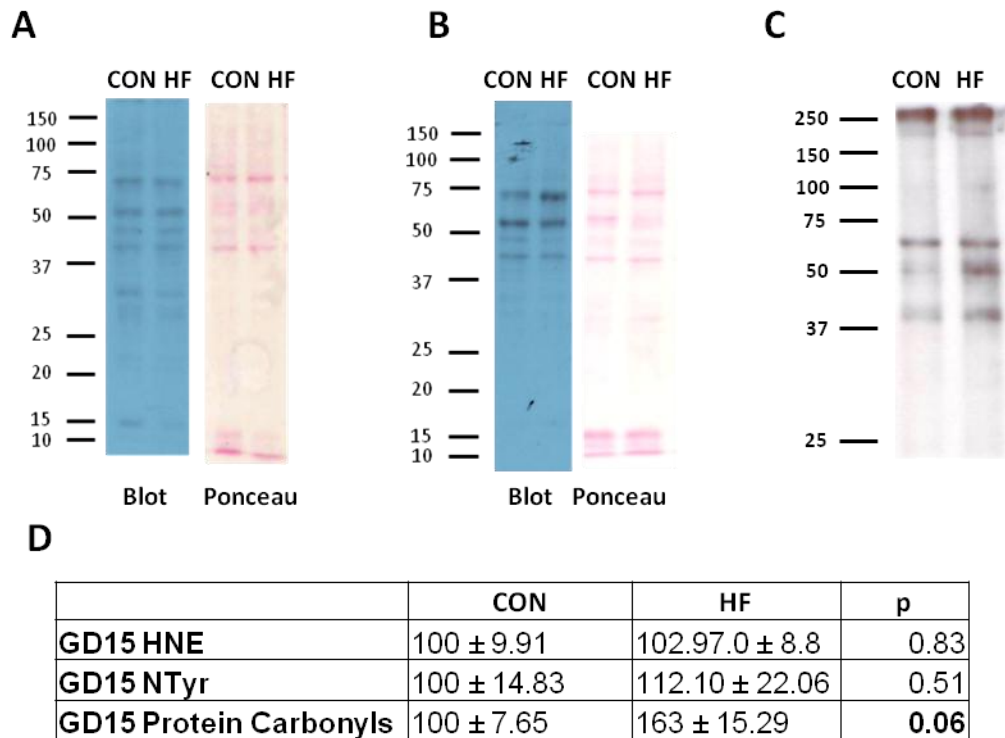


**Figure 23. Levels of oxidative damage in mitochondrially enriched fractions isolated from the whole placentas of CON and HF-fed dams at GD15.** Mitochondrially enriched fractions were prepared through differential centrifugation. Levels of 4-HNE (1:2000, 20 second exposure) (**A**) and NTyr (1:5000, 10 second exposure) (**B**) were quantified via Western blot using monoclonal antibodies to each. Levels of protein carbonyls (**C**) were quantified using the OxyBlot system and developed using ECL (15 s exposure). Values are expressed as a percentage of control values ± SEM. P values were calculated using two-tailed Student's T-tests; n ≥ 5 per group.

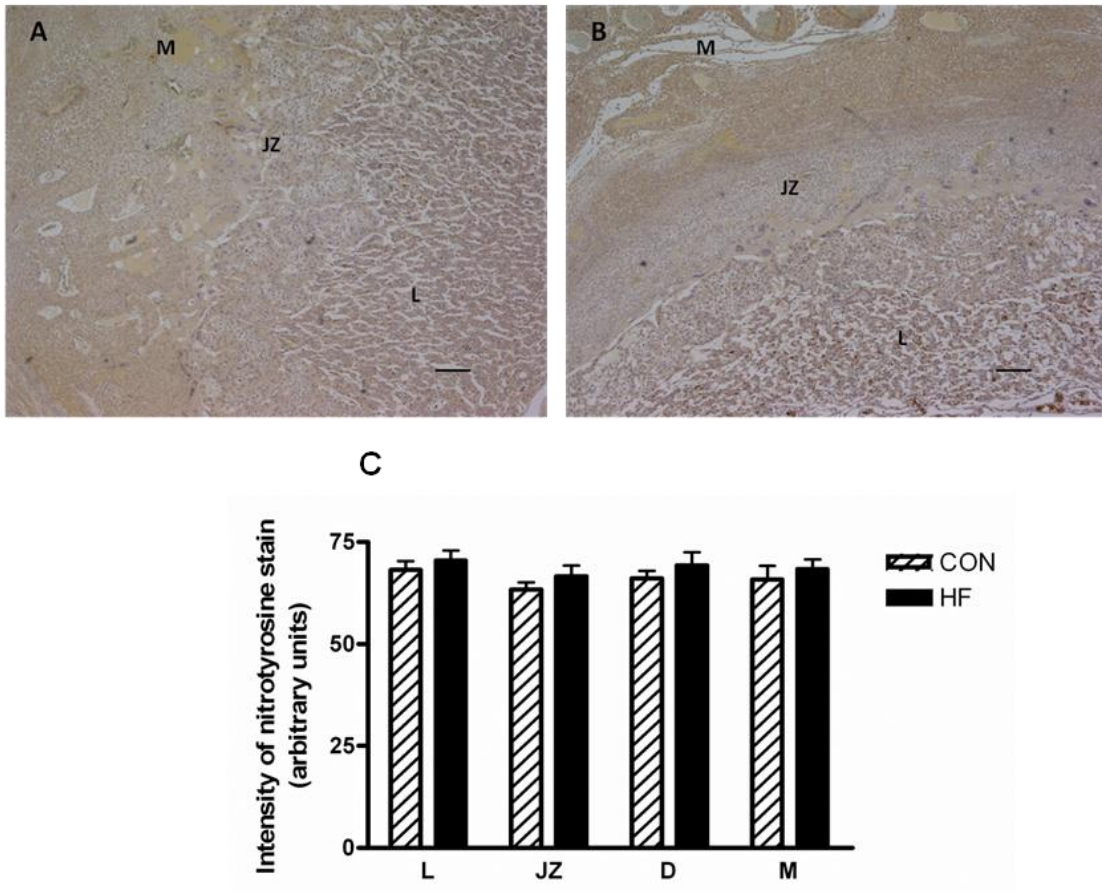


**Figure 24. Immunohistochemical analysis of nitrotyrosine in the placentas of GD15 and GD18 CON and HF-fed dams shows no significant difference.** 5  $\mu$ m slices were taken from the central region of each placenta and stained with a monoclonal antibody to nitrotyrosine (1:300; Millipore). Representative images of CON (A) and HF (B) placentas at gestational day 15 are shown. L=labyrinth, JZ=junctional zone, D= decidua, M=mesometrium. Scale bar = 200  $\mu$ m. C, average staining intensities of placental sections at GD15. Values represent mean  $\pm$  SEM. P values were calculated using two-tailed Student's T-tests;  $p \geq 0.10$ ,  $n \geq 5$  per group.

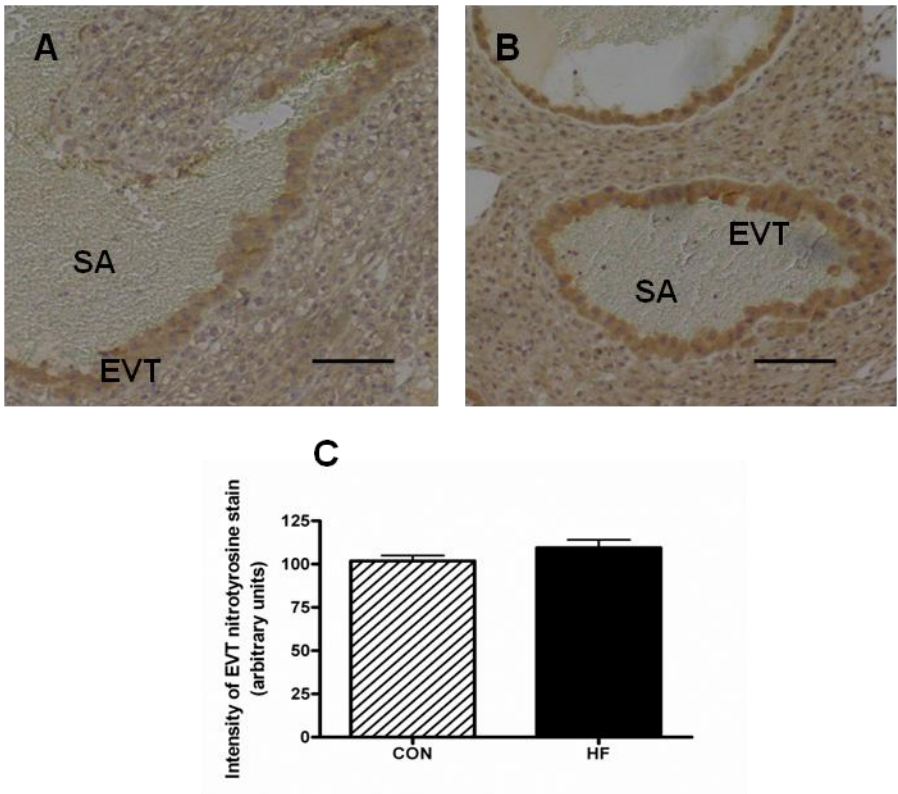


**Figure 25. Nitrotyrosine immunostaining in endovascular trophoblasts at GD15 is not significantly higher in HF-fed dams.** Slices (5  $\mu\text{m}$  thick) from the central area of the placenta were stained with a monoclonal antibody to nitrotyrosine (1:300, Millipore). Endovascular trophoblast cells are visible as darker-staining cells lining maternal spiral arteries. EVT = endovascular trophoblast; SA = maternal spiral artery. Representative images of CON (A) and HF (B) placentas at gestational day 15 are shown; scale bar = 100  $\mu\text{m}$ . C, the average staining intensity of EVT's was calculated. Values represent mean  $\pm$  SEM. P values were calculated using two-tailed Student's T-tests;  $p \geq 0.10$ ,  $n = 5$  per group.

## **DISCUSSION**

Maternal obesity is associated with an increased risk of pregnancy complications in women, including preeclampsia, growth restriction, fetal death, and stillbirth (Rajasingam et al, 2009; Norman and Reynolds, 2011; Perlow et al, 1992). We have developed a rat model of lifelong maternal obesity which results in reduced fetal growth, increased fetal death, and increased incidence of stillbirth. The placentas of these HF-fed dams exhibit altered morphology, with the labyrinth layers covering more area at GD15 and GD18 of gestation. Placentas of HF-fed dams also exhibit changes at GD15 which are no longer present at GD18, including hypoxia and alterations in blood vessel density and maturity in the labyrinth, and increased trophoblast invasion into the mesometrial triangle. No previous work has thoroughly examined the structure of the placenta in the context of maternal obesity. Our observations of early placental dysfunction suggests a role of the placenta in the pregnancy complications associated with maternal obesity.

### **5.1 The model of lifelong maternal obesity**

Our model involves lifelong exposure to a high-fat (HF) diet in Sprague-Dawley dams, starting at weaning. A lifelong exposure to a HF diet is more representative of the trend that occurs in the human population than the short-term feeding that is used in some studies of maternal obesity (Singh et al, 2008). This longer exposure may affect experimental outcomes, as there are metabolic adaptations to a lifelong exposure to a HF diet that do not occur with short-term feeding (Chalkley et al, 2002; Ainslie et al, 2000). In addition, the age at onset of obesity may affect the development of later-life fertility

complications, with obesity prior to puberty being more strongly associated with subsequent fertility issues (Pasquali et al, 2007).

Other rat models of maternal obesity use varying lengths of exposure to obesogenic diets. These studies examine a wide variety of outcomes; however, one measurement that was consistently reported was offspring birth weight. Howie et al demonstrated that lifelong exposure to the same HF diet used in this study showed a decrease in pup weight consistent with what we have observed (Howie et al, 2009). Another study involving lifelong feeding of a high-fat 'cafeteria' diet showed similar decreases in pup and placental weight at GD20 (Akyol et al, 2009). In contrast, short-term exposure to a HF diet starting in adulthood resulted in no difference in pup weight in several other studies (White et al, 2009; Shankar et al, 2011; Shankar et al, 2008). Thus the long-term exposure to an obesogenic diet in our study as well as others may be contributing to the observed decrease in pup weight.

The type of high fat diet used to induce obesity is also important. The diet used in our study has been demonstrated to induce maternal obesity in rats (Howie et al, 2009; Mark et al, 2011) and contains 45% kcal from fat in contrast to the 16% kcal from fat in the control diet. This HF diet is representative of a Western diet, which is characterized by a higher than recommended fat intake (Last and Wilson, 2006). The excess fat in this diet is provided by lard and soybean oil (Appendix 1), leading to an increased percentage of saturated fat, which is associated with obesity and specifically visceral fat accumulation in humans (Coelho et al, 2011).

### **5.1.1 Maternal weight gain, distribution of adipose tissue, systemic oxidative stress and inflammation**

It is important to validate our model of maternal obesity by characterizing the degree of maternal weight gain as well as factors involved in the pathogenicity of obesity, ie. body fat distribution, systemic inflammation and systemic oxidative stress, as these factors may be implicated in the development of pregnancy complications due to obesity (Yamamoto et al, 2001; Denison et al, 2010).

The classification system for obesity in humans is well defined; unfortunately, there is no corresponding scale laid out for rats. Because the term obesity has not been defined in rats, we refer to our animals as ‘HF-fed’ dams and not ‘obese’ dams. However, the weight difference between a lean woman (BMI 23) and an obese woman (BMI 30) of average height is about 30%, and rats fed the high-fat diet in our study weighed 36 % more than the CON-fed group at 19 weeks of age (Figure 1); thus the relative weight gain in our model is comparable to the development of obesity in women.

In the human population, an excess of abdominal fat is associated with a more inflammatory and thus more pathological phenotype of obesity compared with an excess of subcutaneous fat (Despres, 2006). This also appears to be the case in rats (Foster et al, 2011; Roca-Rivada et al, 2011). Our HF-fed rats exhibit this type of abdominal obesity pre-pregnancy, as the volume of abdominal fat depots was eight times higher than controls (Figure 2).

Pregnancy is also a state of elevated inflammation and oxidative stress, independent of obesity (Burton and Jauniaux, 2011; Paulesu et al, 2010). Higher systemic

oxidative stress and inflammation persists during obese pregnancies compared with lean pregnancies (Stewart et al, 2007), and this state may be associated with poor outcomes including the development of growth restriction and preeclampsia (Rajasingam et al, 2009; Schmatz et al, 2010). There is very little data on levels of inflammation and oxidative stress in the obese pregnancy in the rat, though systemic oxidative stress on the day of parturition has been observed in obese dams (Bouanane et al, 2009). We had hypothesized that, like in the obese pregnancy in women, systemic oxidative stress and inflammation persists during pregnancy in our HF-fed rats.

As expected, we observed increased MCP-1 in HF-fed dams during pregnancy. This molecule is a marker of inflammation ((Kalupahana et al, 2011; Nelson et al, 2011), and is known to be elevated in the obese pregnancy in women (Madan et al. 2009). When markers of systemic oxidative stress (urinary 8-OHdG and isoprostanes) were examined at GD15, no significant difference between the groups was observed, though the means of both markers were about 30% higher in HF-fed dams. It is possible that pathways leading to oxidative stress during pregnancy (including inflammation and increased metabolism of glucose and fats) were already activated in the HF-fed dams pre-pregnancy, leading to a proportionally lower increase in oxidative stress in HF-fed dams. This possibility could be resolved by assessing oxidative stress markers pre-pregnancy as well. There are also other means of measuring oxidative stress that may be more sensitive than those performed. We examined markers of oxidative damage, but reduced antioxidant capacity may be another indicator of systemic oxidative stress; means to measure this systemically include measuring oxygen radical absorbance capacity

(ORAC) or reduction of peroxides by blood antioxidants (Horoz et al. 2005). Finally, it is possible that some dams have successfully adapted to the HF diet and do not exhibit systemic oxidative stress at the time of measurement. In the human population, not all individuals exposed to a high-fat diet become obese (Blundell et al, 2005), and the existence of ‘obesity resistant’ rats that show little evidence of oxidative stress when exposed to a HF diet has also been documented (Liu et al, 2011). The adaptation to a high-fat diet in some rats but not others would lead to a greater biological variation; the high standard deviation in oxidative stress measures in the HF-fed dams may be a consequence of this.

## **5.2 Fertility and pregnancy outcomes**

In our model, HF-fed dams exhibited an increased time to copulation and a decline in the proportion of females that copulated. The fertility index (number of matings that resulted in a successful pregnancy) was also reduced (Table 3). This reduction in fertility is similar to trends observed in obese women, who often experience difficulty conceiving. This may be due in part to dysregulated menstrual cycles leading to anovulation in obese women (Friedman and Kim, 1985). The rat equivalent to the menstrual cycle (the estrus cycle) is 4 days in length. In the rat, pheromones are an important contributor to mating success; the male rat is more attracted to the female during the proestrous phase of the estrous cycle, and mating is less likely to occur if the female is not cycling (Lucas et al, 1982). Although we did not directly measure estrous cycling in the rat, the increased number of days to mating and the decline in the mating index suggest that the estrous cycle may be dysregulated. Several other rat models of

maternal obesity have also shown aberrant or reduced estrous cycling (Howie et al, 2009; Marin et al, 1997).

Obstacles to successful pregnancy may remain even after fertilization occurs. In the mouse, maternal obesity leads to oocyte oxidative stress and failure to develop to the blastocyst stage, reducing implantation rates (Igosheva et al, 2010). This may be another factor contributing to the decline in the fertility index observed in our rats.

We observed evidence of reduced fetal and neonatal health in the pups of HF-fed dams, including increased *in utero* death, stillbirth, and smaller birth weights (Tables 4 and 5). These complications are also observed in obese women (Norman and Reynolds, 2011; Perlow et al, 1992). *In utero* death and stillbirth have not been previously reported in rat models of maternal obesity, though stillbirth is more common in macaques fed a high-fat diet (Frias et al, 2011). The placenta has been implicated in these complications in humans (Ball et al, 2006; Sibley et al, 2005), and the reduction in the fetal:placental weight ratio at GD15 is consistent with the presence of placental dysfunction in our model as well. This measurement is often used as a marker of inefficient placental function, as the growth of the fetus is reduced when compared to the size of the placenta (Furukawa et al, 2011). By GD18, the fetal:placental weight ratio was no longer significantly different, though there was a trend towards a lower placental weight in HF-fed dams. The normalization of the fetal:placental ratio may suggest a certain degree of compensation in some parameter of placental function in an attempt to support fetal growth in the face of a reduced placental size. To help explain these trends, we examined parameters of placental structure at GD15 and GD18.

### **5.3 Structural perturbations in the placenta proper**

We measured the area covered by the different sections of the implantation site (including the placental labyrinth and junctional zone as well as the maternal decidua and mesometrial triangle) at the thickest region of the placenta to determine whether the morphometry of these sections were altered (Figure 11). The area of the labyrinth layer was greater in HF-fed dams at GD15; by GD18, both the labyrinth and decidua covered more area. When the area of the labyrinth layer is increased in the rat, it is often as an attempt at compensation for a reduced efficiency of exchange (Furukawa et al, 2011). A larger labyrinth layer has been observed in cases of reduced trophoblast invasion (Crossey, et al 2002) and tissue hypoxia due to maternal anemia (Lewis et al, 2001). A thicker decidual layer has not been reported in the rat in any other models; however, a thinner decidua is observed during spontaneous pregnancy loss in the human, so the increase in decidual thickness may be part of an attempt to maintain the pregnancy in the surviving conceptuses (Wong and Cheung, 2010).

At GD15, we observed an increase in blood vessel density and decrease in blood vessel maturity in the labyrinth (Figures 9 and 10). An increase in vascularisation with obesity has been observed in other tissues; for example, incidence of retinopathy increases with increasing waist:hip ratio (van Leiden et al, 2003), and renal vascular proliferation has been observed in obese animal models (Iliescu and Chade, 2010). These complications are usually but not necessarily associated with the development of type 2 diabetes. These changes may be due to a higher systemic level of VEGF in obesity, which may be secreted by the growing adipose tissue depots (Loebig et al, 2010).

We also observed a decrease in blood vessel maturity in the labyrinth of placentas from HF-fed dams. Blood vessel maturation (measured by the presence of smooth muscle actin-positive VSMCs) depends on the recruitment of pericytes to blood vessels. A reduction in VSMC coverage is associated with hyperdilation and leakiness of blood vessels (Bergers et al, 2005), and in the labyrinth of the placenta, VSMC coverage may play an important role in the integrity and stability of blood vessels (Wang and Zhao, 2010). The process of pericyte recruitment is negatively regulated by VEGF, which inhibits pericyte recruitment while also increasing angiogenesis (Greenberg et al, 2009; Chen et al, 2006). Thus the presence of increased but immature blood vessels is consistent with the pattern expected for elevated VEGF signaling, as this growth factor contributes to vessel growth while decreasing vessel maturation.

We examined VEGF levels in the labyrinth layers of placentas to assess whether this signalling factor may be leading to the increased blood vessel density and decreased maturity in this tissue. As expected, we observed that VEGF protein levels were increased in the labyrinth layers of placentas from HF-fed dams at GD15. This observation coincided with a decrease in PlGF protein levels in the labyrinth layers at this timepoint. PlGF is a VEGF analog that exerts most of its proangiogenic functions by displacing VEGF from its decoy receptor, VEGFR1 (Carmeliet et al, 2001). The displaced VEGF can then exert its angiogenic functions. A decrease in PlGF therefore leads to a decrease in VEGF signalling. However, it appears that the increase in VEGF protein levels outweighs the decrease in PlGF levels, as the increased density and decreased maturity of the vasculature are both supportive of a net increase in free VEGF.

Increased VEGF protein levels in combination with decreased PlGF levels at GD15 can be elegantly explained by the effects of hypoxia, which is known to increase VEGF and decrease PlGF expression in trophoblasts *in vitro* (Lash et al, 2002). *In vivo*, hypoxia (due to high altitude pregnancies) is also associated with elevated placental VEGF signaling (Parraguez et al, 2010), increased vascularization in the labyrinth (Zamudio et al, 2003), and a reduction in blood vessel maturity in the labyrinth (Zhang et al, 2002). Therefore we tested for hypoxia by staining slides for carbonic anhydrase, and observed an increase in staining intensity in placentas from HF-fed dams at GD15 (Figure 14). The carbonic anhydrase enzyme is involved in the conversion of carbonic acid to bicarbonate, and its main transcriptional activator is the HIF-1 transcription factor (Kaluz et al, 2009). A direct measurement of the activation of the HIF-1 transcription factor by assessing the nuclear localization of the subunit HIF-1 $\alpha$  would have been valuable as well; however, attempts to measure this proved unsuccessful (data not shown).

#### **5.4 Trophoblast invasion into the mesometrial triangle**

We next examined trophoblast invasion and remodelling of the maternal spiral arteries. We initially hypothesized that the placental hypoxia at GD15 may be caused by decreased invasion of trophoblast cells into the mesometrial triangle. Decreased invasion of trophoblasts is associated with a reduction in placental perfusion in rats, and both growth restriction and preeclampsia, complications which are more likely to occur in obese women, are associated with reduced trophoblast invasion (Geusens et al, 2008; Silasi et al, 2010; Pardi et al, 2002). However, we observed that both endovascular and

interstitial trophoblasts showed more extensive invasion into the mesometrial triangle at GD15 (Figures 15 and 16). Thus it is clear that decreased trophoblast invasion is not the cause of the placental hypoxia in our model. Interestingly, preexisting hypoxia in both animal models (caused by reduction of environmental O<sub>2</sub> or chronic aortic constriction) and human subjects (caused by maternal anemia) is associated with increased trophoblast invasion through both the endovascular and interstitial pathways (Rosario et al, 2008) (Zhou et al, 1993) (Kadyrov et al, 2003). It appears likely that placental hypoxia may be contributing to the increased trophoblast invasion in our model, rather than reduced trophoblast invasion leading to placental hypoxia.

### **5.5 Temporal changes in the placenta**

Our results show that several aspects of placental physiology are altered at GD15, but these effects are no longer observed at GD18. The placental hypoxia at GD15 likely leads to the increase in blood vessel density and decrease in maturity in the labyrinth at this timepoint, mediated by elevated VEGF expression. It appears that adequate blood flow to the placenta is established between GD15 and GD18, as carbonic anhydrase staining intensity normalizes. This likely leads to the normalization of VEGF signaling, preventing the VEGF-induced inhibition of blood vessel maturation. It is interesting to note that the blood vessel density in the labyrinth also normalizes in the HF group by GD18. This may suggest that the developmental trajectory of the placentas from HF-fed dams is altered; vascular growth may be occurring earlier in HF-fed dams but may level off at the same point as in placentas from CON-fed dams. The increase in invasion early in gestation can be viewed in the same manner; invasion may be occurring earlier in HF-

fed dams but reach the same intrinsic peak as CON-fed dams. Supportive of this theory is research performed on obese ewes, where it was discovered that the vasculature of the placenta is more developed mid-gestation, yet this increase is no longer observed at late gestation; these placental changes were associated with increased fetal weight in obese ewes at midgestation, which also normalized by late gestation (Ma et al, 2010). Another possibility is that the conceptuses with the most severe pathology at GD15 are dying in HF-fed dams and would be counted as absorption sites at GD18, leading to an apparent correction of pathology.

## **5.6 Spiral artery remodeling in the mesometrial triangle**

Invasive trophoblasts work to remodel spiral arteries and convert them into high-capacity vessels to increase blood flow to the placenta. A failure of the remodelling process is associated with reduced placental perfusion (Geusens et al, 2008), and we hypothesized that this may be altered in our HF-fed dams, contributing to hypoxia in early gestation. Therefore we examined loss of CD31-positive maternal endothelial cells as well as SMA-positive VSMCs in the spiral arteries of the mesometrial triangle.

We observed no significant difference in the presence of CD31-positive maternal endothelial cells underneath invading EVT's at GD15 or GD18, suggesting that the ability of trophoblasts to induce endothelial cell death on contact is not compromised at this timepoint. We also observed no significant difference in the percentage of invaded spiral artery contour covered by VSMCs at GD15 (CON and HF-fed dams both exhibited approximately 20% coverage). This percentage of invaded spiral artery contour covered by VSMCs is consistent with the findings of Caluwaerts et al., who observed a similar

value in their control group (Caluwaerts et al, 2005). No significant difference in VSMC coverage was observed at GD18 either, though the mean % coverage by SMA per invaded artery contour in the HF-fed group was 40% higher than in the CON group ( $p=0.11$ ). In the CON-fed group, the mean percent contour covered by SMA in invaded blood vessels was very similar from GD15 to GD18 (Figure 17E). This suggests that endovascular trophoblast cells may eliminate VSMCs soon after their arrival in the blood vessel, with no additional loss of VSMCs in invaded blood vessels between GD15 and GD18. This is, to our knowledge, the first time that this analysis has been performed comparing multiple gestational ages.

The connection between decreased VSMC coverage and increased spiral artery lumen area has, surprisingly, not been proven in rats, though it is well established in humans (Cartwright et al, 2007). Therefore we examined the correlation between spiral artery lumen area and percentage contour covered by VSMC. Decreased coverage of blood vessels by VSMCs was indeed associated with increased blood vessel lumen area at GD18 (Supplemental Figure 1).

It is clear that early placental hypoxia cannot be explained by a decrease in spiral artery remodelling. It is possible that the remaining vascular smooth muscle cells surrounding spiral arteries maintain a more contractile phenotype compared to controls; indeed, obesity is associated with impaired vascular relaxation in humans (Sivitz et al, 2007). An examination of the total lumen area of spiral arteries in HF vs CON rats showed no significant difference (data not shown); however, evidence of vasoconstriction may be lost during processing, and these parameters may be better assessed *in vivo*.

### **5.7 Matrix metalloproteinases 2 and 9 in the junctional zone**

Metalloproteinases are important in the placenta for both the invasion of trophoblast cells into the mesometrium and the subsequent remodeling of spiral arteries (Xu et al, 2011). MMP9 in the junctional zone is primarily expressed by glycogen cells, which later leave the junctional zone to become interstitial trophoblast cells (Coan et al, 2006). We assessed protein and activity levels of MMP2 and MMP9 in the junctional zone of GD15 placentas to examine whether the increase in IST invasion at this point could be explained by increased MMPs. We did not observe a significant increase in MMP2 levels in the junctional zones of HF-fed dams, although the mean levels of MMP2 protein and activity were 50% higher. We did observe a significant decrease in total MMP9 and pro-MMP9 activity levels in junctional zones from HF-fed dams, and a trend towards a decrease in active MMP9. This result suggests that the increase in interstitial trophoblast invasion is not due to elevated MMP9 levels. When total MMP2+9 activity levels were quantified on the zymogram, no significant difference was observed, suggesting that the increase in MMP2 levels, though not statistically significant, may be compensating for the reduced MMP9 levels.

### **5.8 Placental oxidative stress**

Placental oxidative stress is often observed alongside placental dysfunction in women, and may contribute to the pathogenicity of pregnancy complications (Burton and Jauniaux, 2011). The placentas of obese women are associated with elevated inflammatory markers (Challier et al, 2008) as well as increased nitrate stress (Roberts et al, 2009). In rats, placental oxidative stress has not been assessed in any models of

maternal obesity; however, obesity is associated with expression of inflammatory genes by the uterus and blastocyst in rats (Shankar et al, 2011), and inflammation is often associated with oxidative stress (Redman et al, 2003). In addition, exposure to a high-fat diet during gestation (in the absence of pre-pregnancy high-fat diet) is associated with placental oxidative stress in the rat. Since comparison of GD15 placentas between CON and HF groups exhibited the most significant changes we examined markers of oxidative stress in these tissues.

Antioxidant levels are an important indicator of oxidative stress. An increase in antioxidant levels would suggest a compensation for an increased production of ROS, while a decrease in antioxidant levels in conjunction with oxidative damage suggests a failure of regulation of the defense system (Burton and Jauniaux, 2011). We observed no significant differences in levels of four important antioxidant proteins (MnSOD, CuZnSOD, GPx, catalase) in whole placental homogenates or labyrinth and junctional zone homogenates at GD15.

We also examined markers of oxidative damage (HNE, protein carbonyls) and a marker of nitrative damage, nitrotyrosine. We observed a weak trend towards an increase in 4-HNE in the whole placentas of HF GD15 dams ( $p=0.09$ ) which was not observed in the labyrinth or junctional zone sections. It is possible that there is mild oxidative stress occurring but these experiments were too weak to reliably detect it. To clarify this we assessed oxidative damage in mitochondrially enriched fractions of whole placental homogenates.

Mitochondria are the main source of cellular ROS and are therefore usually the first site of increased oxidative damage (Burton and Jauniaux, 2011). Mitochondria show increased lipid peroxidation and protein carbonyl formation compared to whole cell fractions in various situations of oxidative stress (Zhang et al, 2010). In our model, an increase in protein carbonyl levels was observed in GD15 mitochondrially enriched fractions prepared from whole placentas, but no statistically significant difference was observed in mitochondrial 4-HNE or nitrotyrosine levels, though average values for these measures were consistently higher (Figure 23). It is known that the processing of tissue samples can cause oxidative damage through exposure to oxygen, light and temperature variations; this effect may be particularly strong in mitochondrially enriched fractions due to the longer preparation time (Anson et al, 2000). The amount of oxidative damage due to sample processing would presumably be the same between HF and CON samples, as they were processed at the same time. However, the semi-quantitative nature of the Western blotting techniques means that a quantitative increase of the same increment will be more easily detected if the baseline values are low, as opposed to if the baseline values are higher. It is possible that damage during processing is increasing baseline values for oxidative damage markers, and this effect may be contributing to the lack of significant differences between CON and HF placentas. In the future, treatment of samples with a free radical scavenger such as butylated hydroxytoluene (BHT) may help to combat this issue (Murray et al, 2007). There are also other markers of oxidative stress that are commonly used (including malondialdehyde and total GSH:GSSG ratio) which may

prove to be more sensitive and should be examined in these samples (Madazli et al, 2002).

In obese women, placental 'nitrative stress' (characterized by an increase in nitrotyrosine formation) was observed, but oxidative stress was not (Roberts et al, 2009). Though nitrotyrosine levels were not increased in whole tissues or mitochondrially enriched fractions, we decided to examine the tissues immunohistochemically. This allowed us to examine whether the maternal side of the implantation site (decidua and mesometrial triangle) showed evidence of nitrative stress, as well as whether there may have been an increase in a certain cell type or region that was diluted during the homogenization process. Nitrotyrosine formation appeared to be fairly equal across the tissue, though it appeared to be slightly darker in regions surrounding blood vessels; however, there were no differences between placentas from CON and HF-fed dams (Figure 24). It was interesting to observe that at GD15 endovascular trophoblast cells appear to stain more intensely than other cell types for nitrotyrosine, suggesting elevated nitrative damage in these cells; however, this pattern was observed in both control and HF-fed dams with no significant difference between the two groups (Figure 25).

It is apparent that a high level of oxidative stress is not occurring in the placentas of HF-fed rats. It is possible that low-grade oxidative stress is occurring, judging by the trends towards increased 4-HNE in whole placental homogenates and increased protein carbonyls in GD15 mitochondrially enriched fractions. It must also be taken into consideration that the placenta is an organ with a relatively fast turnover rate. Increased

degradation of damaged proteins by the proteasome cannot be ruled out; this process may reduce evidence of oxidative damage while also contributing to reduced fetal growth.

## **6. FUTURE DIRECTIONS**

We have observed that placentas from HF-fed dams show alterations at GD15 (including altered vascularisation and evidence of hypoxia in the labyrinth, and increased trophoblast invasion into the mesometrial triangle), that appear to be resolved by GD18. Changes in these parameters can lead to a decreased efficiency of exchange. These changes are rectified by GD18, yet fetal growth is still compromised later in gestation. This could be explained by a change to the developmental trajectory of the fetus due to the early placental dysregulation. Also, we have primarily focused on placental vascular development in these experiments, but it is possible that other aspects of placental function may be impacted by obesity. The transport capabilities of the placenta have been examined briefly in the past in our lab; no difference in glucose transporters was observed, but a decrease in the amino acid transporter SNAT2 was observed in HF placentas (unpublished data). A more thorough assessment of the transport of nutrients across the placenta may explain the observed reduced fetal growth. It is also important to examine the endocrine function of the placenta, as secretion of hormones such as leptin, IGF-I and IGF-II into the fetal circulation may affect fetal growth (Hoggard et al, 2001; Gluckman and Pinal, 2003). By examining these effects, we will be able to better understand the mechanism of how lifelong maternal obesity results in growth restriction and compromised fetal and neonatal health in this model.

## REFERENCES

- Adelman, D. M., M. Gertsenstein, A. Nagy, M. C. Simon, and E. Maltepe. 2000. Placental cell fates are regulated in vivo by HIF-mediated hypoxia responses. *Genes & Development* 14 (24): 3191-203.
- Ain, R., L. N. Canham, and M. J. Soares. 2003. Gestation stage-dependent intrauterine trophoblast cell invasion in the rat and mouse: Novel endocrine phenotype and regulation. *Developmental Biology* 260 (1): 176-90.
- Ain, R., and M. J. Soares. 2004. Is the metrial gland really a gland? *Journal of Reproductive Immunology* 61 (2): 129-31.
- Ainslie, D. A., J. Proietto, B. C. Fam, and A. W. Thorburn. 2000. Short-term, high-fat diets lower circulating leptin concentrations in rats. *The American Journal of Clinical Nutrition* 71 (2): 438-42.
- Akyol, A., S. C. Langley-Evans, and S. McMullen. 2009. Obesity induced by cafeteria feeding and pregnancy outcome in the rat. *The British Journal of Nutrition* 102 (11): 1601-10.
- Anson, R. M., E. Hudson, and V. A. Bohr. 2000. Mitochondrial endogenous oxidative damage has been overestimated. *The FASEB Journal : Official Publication of the Federation of American Societies for Experimental Biology* 14 (2): 355-60.
- Apel-Sarid, L., A. Levy, G. Holcberg, and E. Sheiner. 2010. Term and preterm (<34 and <37 weeks gestation) placental pathologies associated with fetal growth restriction. *Archives of Gynecology and Obstetrics* 282 (5): 487-92.
- Arita, Y., S. Kihara, N. Ouchi, M. Takahashi, K. Maeda, J. Miyagawa, K. Hotta, et al. 1999. Paradoxical decrease of an adipose-specific protein, adiponectin, in obesity. *Biochemical and Biophysical Research Communications* 257 (1): 79-83.
- Armitage, J. A., L. Poston, and P. D. Taylor. 2008. Developmental origins of obesity and the metabolic syndrome: The role of maternal obesity. *Frontiers of Hormone Research* 36 : 73-84.
- Ball, E., J. N. Bulmer, S. Ayis, F. Lyall, and S. C. Robson. 2006. Late sporadic miscarriage is associated with abnormalities in spiral artery transformation and trophoblast invasion. *The Journal of Pathology* 208 (4): 535-42.
- Bauer, S., J. Pollheimer, J. Hartmann, P. Husslein, J. D. Aplin, and M. Knofler. 2004. Tumor necrosis factor-alpha inhibits trophoblast migration through elevation of

- plasminogen activator inhibitor-1 in first-trimester villous explant cultures. *The Journal of Clinical Endocrinology and Metabolism* 89 (2): 812-22.
- Belo, L., M. Caslake, A. Santos-Silva, E. M. Castro, L. Pereira-Leite, A. Quintanilha, and I. Rebelo. 2004. LDL size, total antioxidant status and oxidised LDL in normal human pregnancy: A longitudinal study. *Atherosclerosis* 177 (2): 391-9.
- Belobrajdic, D. P., Y. Y. Lam, M. Mano, G. A. Wittert, and A. R. Bird. 2011. Cereal based diets modulate some markers of oxidative stress and inflammation in lean and obese zucker rats. *Nutrition & Metabolism* 8: 27.
- Benaitreau, D., E. Dos Santos, M. C. Leneuve, N. Alfaidy, J. J. Feige, P. de Mazancourt, R. Pecquery, and M. N. Dieudonne. 2010. Effects of adiponectin on human trophoblast invasion. *The Journal of Endocrinology* 207 (1): 45-53.
- Bergers, G., and S. Song. 2005. The role of pericytes in blood-vessel formation and maintenance. *Neuro-Oncology* 7 (4): 452-64.
- Bilbo, S. D. 2011. How cytokines leave their mark: The role of the placenta in developmental programming of brain and behavior. *Brain, Behavior, and Immunity* 25 (4): 602-3.
- Blundell, J.E., Stubbs, R.J., Golding, C., Croden, F., Alam, R., Whybrow, S., Le Noury, J., Lawton, C.L. 2005. Resistance and susceptibility to weight gain: Individual variability in response to a high-fat diet. *Physiol and Behavior* 86 (5): 614-622
- Bohler, H., Mokshagundam, S., Winters, S.J. 2010. Adipose tissue and reproduction in women. *Fertility and Sterility* 94(3); 795-825
- Bouanane, S., N. B. Benkalfat, F. Z. Baba Ahmed, H. Merzouk, N. S. Mokhtari, S. A. Merzouk, J. Gresti, C. Tessier, and M. Narce. 2009. Time course of changes in serum oxidant/antioxidant status in overfed obese rats and their offspring. *Clinical Science (London, England : 1979)* 116 (8): 669-80.
- Bournat, J. C., and C. W. Brown. 2010. Mitochondrial dysfunction in obesity. *Current Opinion in Endocrinology, Diabetes, and Obesity* 17 (5): 446-52.
- Burton, G. J., and I. Caniggia. 2001. Hypoxia: Implications for implantation to delivery-a workshop report. *Placenta* 22 Suppl A: S63-5.
- Burton, G.J., Woods, A.W., Jauniaux, E., Kingdom, J.C. 2009. Rheological and physiological consequences of conversion of the maternal spiral arteries for uteroplacental blood flow during human pregnancy. *Placenta* 30 (6): 473-82

- Burton, G. J., and E. Jauniaux. 2011. Oxidative stress. *Best Practice & Research. Clinical Obstetrics & Gynaecology* 25 (3): 287-99.
- Caluwaerts, S., L. Vercruyse, C. Luyten, and R. Pijnenborg. 2005. Endovascular trophoblast invasion and associated structural changes in uterine spiral arteries of the pregnant rat. *Placenta* 26 (7): 574-84.
- Caniggia, I., J. Winter, S. J. Lye, and M. Post. 2000. Oxygen and placental development during the first trimester: Implications for the pathophysiology of pre-eclampsia. *Placenta* 21 Suppl A: S25-30.
- Carayannopoulos, M. O., M. M. Chi, Y. Cui, J. M. Pingsterhaus, R. A. McKnight, M. Mueckler, S. U. Devaskar, and K. H. Moley. 2000. GLUT8 is a glucose transporter responsible for insulin-stimulated glucose uptake in the blastocyst. *Proceedings of the National Academy of Sciences of the United States of America* 97 (13): 7313-8.
- Carmeliet, P., V. Ferreira, G. Breier, S. Pollefeyt, L. Kieckens, M. Gertsenstein, M. Fahrig, et al. 1996. Abnormal blood vessel development and lethality in embryos lacking a single VEGF allele. *Nature* 380 (6573): 435-9.
- Carmeliet, P., L. Moons, A. Lutun, V. Vincenti, V. Compernelle, M. De Mol, Y. Wu, et al. 2001. Synergism between vascular endothelial growth factor and placental growth factor contributes to angiogenesis and plasma extravasation in pathological conditions. *Nature Medicine* 7 (5): 575-83.
- Carter, AM. 2007. Animal models of human placentation-a review. *Placenta* 28 : S41-7.
- Cartwright, J. E., R. J. Keogh, and M. C. Tissot van Patot. 2007. Hypoxia and placental remodelling. *Advances in Experimental Medicine and Biology* 618 : 113-26.
- Catalan, V., J. Gomez-Ambrosi, B. Ramirez, F. Rotellar, C. Pastor, C. Silva, A. Rodriguez, M. J. Gil, J. A. Cienfuegos, and G. Fruhbeck. 2007. Proinflammatory cytokines in obesity: Impact of type 2 diabetes mellitus and gastric bypass. *Obesity Surgery* 17 (11): 1464-74.
- Cetin, I., and P. Antonazzo. 2009. The role of the placenta in intrauterine growth restriction (IUGR). *Zeitschrift Fur Geburtshilfe Und Neonatologie* 213 (3): 84-8.
- Chakravarty, E.F., Nelson, L., Krishnan, E. 2006. Obstetric hospitalizations in the United States for women with systemic lupus erythromatosis and rheumatoid arthritis. *Arthritis and Rheumatism* 54 (3): 899-907

- Chalkley, S. M., M. Hettiarachchi, D. J. Chisholm, and E. W. Kraegen. 2002. Long-term high-fat feeding leads to severe insulin resistance but not diabetes in wistar rats. *American Journal of Physiology. Endocrinology and Metabolism* 282 (6): E1231-8.
- Challier, J. C., S. Basu, T. Bintein, J. Minium, K. Hotmire, P. M. Catalano, and S. Hauguel-de Mouzon. 2008a. Obesity in pregnancy stimulates macrophage accumulation and inflammation in the placenta. *Placenta* 29 (3): 274-81.
- . 2008b. Obesity in pregnancy stimulates macrophage accumulation and inflammation in the placenta. *Placenta* 29 (3): 274-81.
- Chen, B., K. S. Lam, Y. Wang, D. Wu, M. C. Lam, J. Shen, L. Wong, R. L. Hoo, J. Zhang, and A. Xu. 2006. Hypoxia dysregulates the production of adiponectin and plasminogen activator inhibitor-1 independent of reactive oxygen species in adipocytes. *Biochemical and Biophysical Research Communications* 341 (2): 549-56.
- Chen, Q., P. R. Stone, L. M. McCowan, and L. W. Chamley. 2005. Interaction of jar choriocarcinoma cells with endothelial cell monolayers. *Placenta* 26 (8-9): 617-25.
- Christiansen, T., B. Richelsen, and J. M. Bruun. 2005. Monocyte chemoattractant protein-1 is produced in isolated adipocytes, associated with adiposity and reduced after weight loss in morbid obese subjects. *International Journal of Obesity (2005)* 29 (1): 146-50.
- Coan, P. M., N. Conroy, G. J. Burton, and A. C. Ferguson-Smith. 2006. Origin and characteristics of glycogen cells in the developing murine placenta. *Developmental Dynamics : An Official Publication of the American Association of Anatomists* 235 (12): 3280-94.
- Coelho, D. F., L. O. Pereira-Lancha, D. S. Chaves, D. Diwan, R. Ferraz, P. L. Campos-Ferraz, J. R. Poortmans, and A. H. Lancha Junior. 2011. Effect of high-fat diets on body composition, lipid metabolism and insulin sensitivity, and the role of exercise on these parameters. *Brazilian Journal of Medical and Biological Research = Revista Brasileira De Pesquisas Medicas e Biologicas / Sociedade Brasileira De Biofisica ...[Et Al.]* 44 (10): 966-72.
- Conde-Agudelo, A., Villar, J., Lindheimer, M. 2008. Maternal infection and risk of preeclampsia: systematic review and metaanalysis. *American Journal of Obstetrics and Gynecology* 198 (1): 7-22
- Conus, F., D. B. Allison, R. Rabasa-Lhoret, M. St-Onge, D. H. St-Pierre, A. Tremblay-Lebeau, and E. T. Poehlman. 2004. Metabolic and behavioral characteristics of metabolically obese but normal-weight women. *The Journal of Clinical Endocrinology and Metabolism* 89 (10): 5013-20.

- Cowden Dahl, K. D., S. E. Robertson, V. M. Weaver, and M. C. Simon. 2005. Hypoxia-inducible factor regulates alphavbeta3 integrin cell surface expression. *Molecular Biology of the Cell* 16 (4): 1901-12.
- Crossey, P. A., C. C. Pillai, and J. P. Miell. 2002. Altered placental development and intrauterine growth restriction in IGF binding protein-1 transgenic mice. *The Journal of Clinical Investigation* 110 (3): 411-8.
- de Rijk, E. P., E. van Esch, and G. Flik. 2002. Pregnancy dating in the rat: Placental morphology and maternal blood parameters. *Toxicologic Pathology* 30 (2): 271-82.
- Demir, R., Y. Seval, and B. Huppertz. 2007. Vasculogenesis and angiogenesis in the early human placenta. *Acta Histochemica* 109 (4): 257-65.
- Denison, F. C., K. A. Roberts, S. M. Barr, and J. E. Norman. 2010. Obesity, pregnancy, inflammation, and vascular function. *Reproduction (Cambridge, England)* 140 (3): 373-85.
- Despres, J. P. 2006. Is visceral obesity the cause of the metabolic syndrome? *Annals of Medicine* 38 (1): 52-63.
- Despres, J. P., I. Lemieux, J. Bergeron, P. Pibarot, P. Mathieu, E. Larose, J. Rodes-Cabau, O. F. Bertrand, and P. Poirier. 2008. Abdominal obesity and the metabolic syndrome: Contribution to global cardiometabolic risk. *Arteriosclerosis, Thrombosis, and Vascular Biology* 28 (6): 1039-49.
- Donnelly, Leo, and Gillian Campling. 2008. Functions of the placenta. *Anaesthesia & Intensive Care Medicine* 9 (3) (3): 124-7.
- Dunwoodie, S. L. 2009. The role of hypoxia in development of the mammalian embryo. *Developmental Cell* 17 (6) : 755-73.
- Eder, K., N. Baffy, A. Falus, and A. K. Fulop. 2009. The major inflammatory mediator interleukin-6 and obesity. *Inflammation Research : Official Journal of the European Histamine Research Society ...[Et Al.]* 58 (11): 727-36.
- Eriksson, J., T. Forsen, J. Tuomilehto, C. Osmond, and D. Barker. 2001. Size at birth, childhood growth and obesity in adult life. *International Journal of Obesity and Related Metabolic Disorders : Journal of the International Association for the Study of Obesity* 25 (5): 735-40.
- Fain, J. N. 2006. Release of interleukins and other inflammatory cytokines by human adipose tissue is enhanced in obesity and primarily due to the nonfat cells. *Vitamins and Hormones* 74 : 443-77.

- Fain, J. N., S. W. Bahouth, and A. K. Madan. 2004. TNFalpha release by the nonfat cells of human adipose tissue. *International Journal of Obesity and Related Metabolic Disorders : Journal of the International Association for the Study of Obesity* 28 (4): 616-22.
- Fain, J. N., D. S. Tichansky, and A. K. Madan. 2005. Transforming growth factor beta1 release by human adipose tissue is enhanced in obesity. *Metabolism: Clinical and Experimental* 54 (11): 1546-51.
- Fernandez-Sanchez, A., E. Madrigal-Santillan, M. Bautista, J. Esquivel-Soto, A. Morales-Gonzalez, C. Esquivel-Chirino, I. Durante-Montiel, G. Sanchez-Rivera, C. Valadez-Vega, and J. A. Morales-Gonzalez. 2011. Inflammation, oxidative stress, and obesity. *International Journal of Molecular Sciences* 12 (5): 3117-32.
- Figueras, F., and J. Gardosi. 2011. Intrauterine growth restriction: New concepts in antenatal surveillance, diagnosis, and management. *American Journal of Obstetrics and Gynecology* 204 (4): 288-300.
- Foster, M. T., H. Shi, R. J. Seeley, and S. C. Woods. 2011. Removal of intra-abdominal visceral adipose tissue improves glucose tolerance in rats: Role of hepatic triglyceride storage. *Physiology & Behavior* 104 (5): 845-54.
- Frias, A. E., T. K. Morgan, A. E. Evans, J. Rasanen, K. Y. Oh, K. L. Thornburg, and K. L. Grove. 2011. Maternal high-fat diet disturbs uteroplacental hemodynamics and increases the frequency of stillbirth in a nonhuman primate model of excess nutrition. *Endocrinology* 152 (6): 2456-64.
- Friedman, C. I., and M. H. Kim. 1985. Obesity and its effect on reproductive function. *Clinical Obstetrics and Gynecology* 28 (3): 645-63.
- Fujiwara, S., K. Nakagawa, H. Harada, S. Nagato, K. Furukawa, M. Teraoka, T. Seno, K. Oka, S. Iwata, and T. Ohnishi. 2007. Silencing hypoxia-inducible factor-1alpha inhibits cell migration and invasion under hypoxic environment in malignant gliomas. *International Journal of Oncology* 30 (4): 793-802.
- Furukawa, S., S. Hayasha, K. Usuda, M. Abe, S. Hagio, and I. Ogawa. 2011. Toxicologic pathology in the rat placenta. *Journal of Toxicologic Pathology* 24 (2): 95-111.
- Furukawa, S., T. Fujita, M. Shimabukuro, M. Iwaki, Y. Yamada, Y. Nakajima, O. Nakayama, M. Makishima, M. Matsuda, and I. Shimomura. 2004. Increased oxidative stress in obesity and its impact on metabolic syndrome. *The Journal of Clinical Investigation* 114 (12): 1752-61.

- Furuya, M., Ishida, J., Inaba, S., Kasuya, Y., Kimura, S., Nemori, R., Fukamizu, A. 2008. Impaired placental neovascularization in mice with pregnancy-associated hypertension. *Laboratory investigation* 88 (4): 419-29
- Gautron, L., and J. K. Elmquist. 2011. Sixteen years and counting: An update on leptin in energy balance. *The Journal of Clinical Investigation* 121 (6): 2087-93.
- Genbacev, O., and R. K. Miller. 2000. Post-implantation differentiation and proliferation of cytotrophoblast cells: In vitro models--a review. *Placenta* 21 Suppl A: S45-9.
- Geusens, N., L. Hering, S. Verlohren, C. Luyten, K. Drijkoningen, M. Taube, L. Vercruyse, M. Hanssens, R. Dechend, and R. Pijnenborg. 2010. Changes in endovascular trophoblast invasion and spiral artery remodelling at term in a transgenic preeclamptic rat model. *Placenta* 31 (4): 320-6.
- Geusens, N., S. Verlohren, C. Luyten, M. Taube, L. Hering, L. Vercruyse, M. Hanssens, J. W. Dudenhausen, R. Dechend, and R. Pijnenborg. 2008. Endovascular trophoblast invasion, spiral artery remodelling and uteroplacental haemodynamics in a transgenic rat model of pre-eclampsia. *Placenta* 29 (7): 614-23.
- Gluckman, P. D., and C. S. Pinal. 2003. Regulation of fetal growth by the somatotrophic axis. *The Journal of Nutrition* 133 (5 Suppl 2): 1741S-6S.
- Gore, A., M. Muralidhar, M. G. Espey, K. Degenhardt, and L. L. Mantell. 2010. Hyperoxia sensing: From molecular mechanisms to significance in disease. *Journal of Immunotoxicology* 7 (4): 239-54.
- Green, D. R., and J. C. Reed. 1998. Mitochondria and apoptosis. *Science (New York, N.Y.)* 281 (5381): 1309-12.
- Greenberg, J. I., D. J. Shields, S. G. Barillas, L. M. Acevedo, E. Murphy, J. Huang, L. Schepke, et al. A role for VEGF as a negative regulator of pericyte function and vessel maturation. *Nature* 456, 809-813.
- Grune, T., T. Reinheckel, and K. J. Davies. 1996. Degradation of oxidized proteins in K562 human hematopoietic cells by proteasome. *The Journal of Biological Chemistry* 271 (26): 15504-9.
- Guh, D. P., W. Zhang, N. Bansback, Z. Amarsi, C. L. Birmingham, and A. H. Anis. 2009. The incidence of co-morbidities related to obesity and overweight: A systematic review and meta-analysis. *BMC Public Health* 9: 88.

- Han, H. J., Y. J. Lee, S. H. Park, J. H. Lee, and M. Taub. 2005. High glucose-induced oxidative stress inhibits Na<sup>+</sup>/glucose cotransporter activity in renal proximal tubule cells. *American Journal of Physiology. Renal Physiology* 288 (5): F988-96.
- Harris, L. K., and J. D. Aplin. 2007. Vascular remodeling and extracellular matrix breakdown in the uterine spiral arteries during pregnancy. *Reproductive Sciences (Thousand Oaks, Calif.)* 14 (8 Suppl) (Dec): 28-34.
- Harris, L. K., R. J. Keogh, M. Wareing, P. N. Baker, J. E. Cartwright, J. D. Aplin, and G. S. Whitley. 2006. Invasive trophoblasts stimulate vascular smooth muscle cell apoptosis by a fas ligand-dependent mechanism. *The American Journal of Pathology* 169 (5) (Nov): 1863-74.
- Hass, M. A., J. Iqbal, L. B. Clerch, L. Frank, and D. Massaro. 1989. Rat lung cu,zn superoxide dismutase. isolation and sequence of a full-length cDNA and studies of enzyme induction. *The Journal of Clinical Investigation* 83 (4): 1241-6.
- Heazell, A. E., A. N. Sharp, P. N. Baker, and I. P. Crocker. 2011. Intra-uterine growth restriction is associated with increased apoptosis and altered expression of proteins in the p53 pathway in villous trophoblast. *Apoptosis : An International Journal on Programmed Cell Death* 16 (2): 135-44.
- Hensley, K., K. A. Robinson, S. P. Gabbita, S. Salsman, and R. A. Floyd. 2000. Reactive oxygen species, cell signaling, and cell injury. *Free Radical Biology & Medicine* 28 (10) : 1456-62.
- Hiratsuka, S., O. Minowa, J. Kuno, T. Noda, and M. Shibuya. 1998. Flt-1 lacking the tyrosine kinase domain is sufficient for normal development and angiogenesis in mice. *Proceedings of the National Academy of Sciences of the United States of America* 95 (16): 9349-54.
- Hoggard, N., J. Crabtree, S. Allstaff, D. R. Abramovich, and P. Haggarty. 2001. Leptin secretion to both the maternal and fetal circulation in the ex vivo perfused human term placenta. *Placenta* 22 (4): 347-52.
- Horoz, M., C. Bolukbas, F. F. Bolukbas, T. Sabuncu, M. Aslan, S. Sarifakiogullari, N. Gunaydin, and O. Erel. 2005. Measurement of the total antioxidant response using a novel automated method in subjects with nonalcoholic steatohepatitis. *BMC Gastroenterology* 5: 35.
- Howard, R. B., T. Hosokawa, and M. H. Maguire. 1987. Hypoxia-induced fetoplacental vasoconstriction in perfused human placental cotyledons. *American Journal of Obstetrics and Gynecology* 157 (5): 1261-6.

- Howie, G. J., D. M. Sloboda, T. Kamal, and M. H. Vickers. 2009. Maternal nutritional history predicts obesity in adult offspring independent of postnatal diet. *The Journal of Physiology* 587 (Pt 4): 905-15.
- Hu, D., and J. C. Cross. 2010. Development and function of trophoblast giant cells in the rodent placenta. *The International Journal of Developmental Biology* 54 (2-3): 341-54.
- Hutchinson, E.S., Brownbill, P., Jones, N.W., Abrahams, V.M., Baker, P.N., Sibley, C.P., Crocker, I.P. 2009. Uteroplacental hemodynamics in the pathogenesis of preeclampsia. *Placenta* 30 (7): 634-41
- Igosheva, N., A. Y. Abramov, L. Poston, J. J. Eckert, T. P. Fleming, M. R. Duchon, and J. McConnell. 2010. Maternal diet-induced obesity alters mitochondrial activity and redox status in mouse oocytes and zygotes. *PloS One* 5 (4): e10074.
- Iliescu, R., Chade, A.R. 2010. Progressive renal vascular proliferation and injury in obese Zucker rats. *Microcirculation* 17 (4): 250-8
- Jauniaux, E., N. Greenwold, J. Hempstock, and G. J. Burton. 2003. Comparison of ultrasonographic and doppler mapping of the intervillous circulation in normal and abnormal early pregnancies. *Fertility and Sterility* 79 (1): 100-6.
- Jauniaux, E., A. L. Watson, J. Hempstock, Y. P. Bao, J. N. Skepper, and G. J. Burton. 2000. Onset of maternal arterial blood flow and placental oxidative stress. A possible factor in human early pregnancy failure. *The American Journal of Pathology* 157 (6): 2111-22.
- Jones, M. L., P. J. Mark, J. L. Lewis, T. A. Mori, J. A. Keelan, and B. J. Waddell. 2010. Antioxidant defenses in the rat placenta in late gestation: Increased labyrinthine expression of superoxide dismutases, glutathione peroxidase 3, and uncoupling protein 2. *Biology of Reproduction* 83 (2): 254-60.
- Jovanovic, M., I. Stefanoska, L. Radojic, and L. Vicovac. 2010. Interleukin-8 (CXCL8) stimulates trophoblast cell migration and invasion by increasing levels of matrix metalloproteinase (MMP)2 and MMP9 and integrins alpha5 and beta1. *Reproduction (Cambridge, England)* 139 (4): 789-98.
- Jovanovic, M., and L. Vicovac. 2009. Interleukin-6 stimulates cell migration, invasion and integrin expression in HTR-8/SVneo cell line. *Placenta* 30 (4): 320-8.
- Kadyrov, M., C. Schmitz, S. Black, P. Kaufmann, and B. Huppertz. 2003. Pre-eclampsia and maternal anaemia display reduced apoptosis and opposite invasive phenotypes of extravillous trophoblast. *Placenta* 24 (5): 540-8.

- Kalinderis, M., A. Papanikolaou, K. Kalinderi, E. Ioannidou, C. Giannoulis, V. Karagiannis, and B. C. Tarlatzis. Elevated serum levels of Interleukin-6, Interleukin-1 $\beta$  and human chorionic gonadotropin in Pre-eclampsia. *American Journal of Reproductive Immunology*.
- Kalupahana, N. S., B. H. Voy, A. M. Saxton, and N. Moustaid-Moussa. 2011. Energy-restricted high-fat diets only partially improve markers of systemic and adipose tissue inflammation. *Obesity (Silver Spring, Md.)* 19 (2): 245-54.
- Kaluz, S., M. Kaluzova, S. Y. Liao, M. Lerman, and E. J. Stanbridge. 2009. Transcriptional control of the tumor- and hypoxia-marker carbonic anhydrase 9: A one transcription factor (HIF-1) show? *Biochimica Et Biophysica Acta* 1795 (2): 162-72.
- Khalid, M. E. M., M. E. Ali, and K. Z. M. Ali. 1997. Full-term birth weight and placental morphology at high and low altitude. *International Journal of Gynecology & Obstetrics* 57 (3) (6): 259-65.
- Khaliq, A., C. Dunk, J. Jiang, M. Shams, X. F. Li, C. Acevedo, H. Weich, M. Whittle, and A. Ahmed. 1999. Hypoxia down-regulates placenta growth factor, whereas fetal growth restriction up-regulates placenta growth factor expression: Molecular evidence for "placental hyperoxia" in intrauterine growth restriction. *Laboratory Investigation; a Journal of Technical Methods and Pathology* 79 (2): 151-70.
- Khong, T. Y., F. De Wolf, W. B. Robertson, and I. Brosens. 1986. Inadequate maternal vascular response to placentation in pregnancies complicated by pre-eclampsia and by small-for-gestational age infants. *British Journal of Obstetrics and Gynaecology* 93 (10): 1049-59.
- Kingdom, J. C., and P. Kaufmann. 1999. Oxygen and placental vascular development. *Advances in Experimental Medicine and Biology* 474 : 259-75.
- Kolamunne, R. T., M. Clare, and H. R. Griffiths. 2011. Mitochondrial superoxide anion radicals mediate induction of apoptosis in cardiac myoblasts exposed to chronic hypoxia. *Archives of Biochemistry and Biophysics* 505 (2): 256-65.
- Kwak-Kim, J., J. C. Park, H. K. Ahn, J. W. Kim, and A. Gilman-Sachs. 2010. Immunological modes of pregnancy loss. *American Journal of Reproductive Immunology (New York, N.Y.: 1989)* 63 (6): 611-23.
- Lam, C., K. H. Lim, and S. A. Karumanchi. 2005. Circulating angiogenic factors in the pathogenesis and prediction of preeclampsia. *Hypertension* 46 (5): 1077-85.
- Lam, S. Y., Y. Liu, K. M. Ng, C. F. Lau, E. C. Liong, G. L. Tipoe, and M. L. Fung. 2011. Chronic intermittent hypoxia induces local inflammation of the rat carotid body via

- functional upregulation of proinflammatory cytokine pathways. *Histochemistry and Cell Biology* (Dec 21).
- Lash, G. E., C. M. Taylor, A. J. Trew, S. Cooper, F. W. Anthony, T. Wheeler, and P. N. Baker. 2002. Vascular endothelial growth factor and placental growth factor release in cultured trophoblast cells under different oxygen tensions. *Growth Factors (Chur, Switzerland)* 20 (4): 189-96.
- Last, A. R., and S. A. Wilson. 2006. Low-carbohydrate diets. *American Family Physician* 73 (11): 1942-8.
- Lee, K. Y., and F. J. DeMayo. 2004. Animal models of implantation. *Reproduction (Cambridge, England)* 128 (6): 679-95.
- Lewis, R. M., C. B. Doherty, L. A. James, G. J. Burton, and C. N. Hales. 2001. Effects of maternal iron restriction on placental vascularization in the rat. *Placenta* 22 (6): 534-9.
- Librach, C. L., S. L. Feigenbaum, K. E. Bass, T. Y. Cui, N. Verastas, Y. Sadovsky, J. P. Quigley, D. L. French, and S. J. Fisher. 1994. Interleukin-1 beta regulates human cytotrophoblast metalloproteinase activity and invasion in vitro. *The Journal of Biological Chemistry* 269 (25): 17125-31.
- Lin, Y., X. F. Han, Z. F. Fang, L. Q. Che, D. Wu, X. Q. Wu, and C. M. Wu. 2011. The beneficial effect of fiber supplementation in high- or low-fat diets on fetal development and antioxidant defense capacity in the rat. *European Journal of Nutrition* (Mar 22).
- Liu, A.X., He, W.H., Yin, L.J., Lv, P.P., Zhang, Y., Sheng, J.Z., Leung, P.C., Huang, H.F. 2011. Sustained endoplasmic reticulum stress as a cofactor of oxidative stress in decidual cells from patients with early pregnancy loss. *Journal of Clinical Endocrinology and Metabolism* 96 (3): E493-7
- Liu, X., Wang, F., Li, Y., Sun, C. 2011. Oxidative stress and the susceptibility to obesity in rats. *Wei Sheng Yan Jiu* 40(4): 420-2
- Lockwood, C. J., C. F. Yen, M. Basar, U. A. Kayisli, M. Martel, I. Buhimschi, C. Buhimschi, S. J. Huang, G. Krikun, and F. Schatz. 2008. Preeclampsia-related inflammatory cytokines regulate interleukin-6 expression in human decidual cells. *The American Journal of Pathology* 172 (6): 1571-9.
- Loebig, M., Klement, J., Schmoller, A., Betz, S., Heuck, N., Schweiger, U., Peters, A., Schultes, B., Oltmanns, K.M. 2010. Evidence for a relationship between VEGF and BMI independent of insulin sensitivity by glucose clamp procedure in a homogenous group of healthy young men. *PLoS ONE* 9 (5): e12610

- Lucas, P. D., S. M. Donohoe, and A. J. Thody. 1982. The role of estrogen and progesterone in the control of preputial gland sex attractant odors in the female rat. *Physiology & Behavior* 28 (4): 601-7.
- Ma, Y., Zhu, M.J., Zhang, L., Hein, S.M., Nathanielsz, P.W., Ford, S.P. 2010. Maternal obesity and overnutrition alter fetal growth rate and cotyledonary vascularity and angiogenic factor expression in the ewe. *Am J Physiol Regul Integr Comp Physiol* 299 (1): R249-58.
- Madan, J. C., J. M. Davis, W. Y. Craig, M. Collins, W. Allan, R. Quinn, and O. Dammann. 2009. Maternal obesity and markers of inflammation in pregnancy. *Cytokine* 47 (1): 61-4.
- Madazli, R., Benian, A., Aydin, S., Uzun, H., Tolun, N. 2002. The plasma and placental levels of malondialdehyde, glutathione and superoxide dismutase in preeclampsia. *Journal of Obstetrics and Gynecology* 22 (5): 477-480
- Maglione, D., V. Guerriero, G. Viglietto, P. Delli-Bovi, and M. G. Persico. 1991. Isolation of a human placenta cDNA coding for a protein related to the vascular permeability factor. *Proceedings of the National Academy of Sciences of the United States of America* 88 (20): 9267-71.
- Marin Bivens, C. L., and D. H. Olster. 1997. Abnormal estrous cyclicity and behavioral hyporesponsiveness to ovarian hormones in genetically obese Zucker female rats. *Endocrinology* 138 (1): 143-8.
- Mark, P. J., C. Sisala, K. Connor, R. Patel, J. L. Lewisa, M. H. Vickers, B. J. Waddell, and D. M. Sloboda. 2011. A maternal high-fat diet in rat pregnancy reduces growth of the fetus and the placental junctional zone, but not placental labyrinth zone growth. *Journal of Developmental Origins of Health and Disease* 2 (1): 63-70.
- Mayhew, T. M., C. Ohadike, P. N. Baker, I. P. Crocker, C. Mitchell, and S. S. Ong. 2003. Stereological investigation of placental morphology in pregnancies complicated by pre-eclampsia with and without intrauterine growth restriction. *Placenta* 24 (2-3): 219-26.
- Maynard, S.E., Min, J.Y., Merchan, J., Lim, K.H., Mondal, S., Libermann, T.A., Morgan, J.P., Sellke, F.W., Stillman, I.E., Epstein, F.H., Sukhatme, V.P., Karumanchi, S.A. 2003. Excess placental soluble fms-like tyrosine kinase 1 (s-Flt1) may contribute to endothelial dysfunction, hypertension, and proteinuria in preeclampsia. *Journal of Clinical Investigation* 111 (5): 649-58
- McMillen, I. C., and J. S. Robinson. 2005. Developmental origins of the metabolic syndrome: Prediction, plasticity, and programming. *Physiological Reviews* 85 (2): 571-633.

- Meisser, A., P. Cameo, D. Islami, A. Campana, and P. Bischof. 1999. Effects of interleukin-6 (IL-6) on cytotrophoblastic cells. *Molecular Human Reproduction* 5 (11): 1055-8.
- Metwally, M., T. C. Li, and W. L. Ledger. 2007. The impact of obesity on female reproductive function. *Obesity Reviews : An Official Journal of the International Association for the Study of Obesity* 8 (6): 515-23.
- Munaut, C., S. Lorquet, C. Pequeux, S. Blacher, S. Berndt, F. Frankenne, and J. M. Foidart. 2008. Hypoxia is responsible for soluble vascular endothelial growth factor receptor-1 (VEGFR-1) but not for soluble endoglin induction in villous trophoblast. *Human Reproduction (Oxford, England)* 23 (6): 1407-15.
- Murray, I. V., L. Liu, H. Komatsu, K. Uryu, G. Xiao, J. A. Lawson, and P. H. Axelsen. 2007. Membrane-mediated amyloidogenesis and the promotion of oxidative lipid damage by amyloid beta proteins. *The Journal of Biological Chemistry* 282 (13): 9335-45.
- Myatt, L., and X. Cui. 2004. Oxidative stress in the placenta. *Histochemistry and Cell Biology* 122 (4): 369-82.
- Naicker, T., S. M. Khedun, J. Moodley, and R. Pijnenborg. 2003. Quantitative analysis of trophoblast invasion in preeclampsia. *Acta Obstetrica Et Gynecologica Scandinavica* 82 (8): 722-9.
- Nash, P., and U. J. Eriksson. 2007. Suramin-restricted blood volume in the placenta of normal and diabetic rats is normalized by vitamin E treatment. *Placenta* 28 (5-6): 505-15.
- Nelson, K., I. Thethi, J. Cunanan, D. Hoppensteadt, R. Bajwa, J. Fareed, and V. Bansal. 2011. Upregulation of surrogate markers of inflammation and thrombogenesis in patients with ESRD: Pathophysiologic and therapeutic implications. *Clinical and Applied thrombosis/hemostasis : Official Journal of the International Academy of Clinical and Applied Thrombosis/Hemostasis* 17 (3): 302-4.
- Norman, J. E., and R. M. Reynolds. 2011. The consequences of obesity and excess weight gain in pregnancy. *The Proceedings of the Nutrition Society* 70 (4): 450-6.
- Osol, G., G. Celia, N. Gokina, C. Barron, E. Chien, M. Mandala, L. Luksha, and K. Kublickiene. 2008. Placental growth factor is a potent vasodilator of rat and human resistance arteries. *American Journal of Physiology.Heart and Circulatory Physiology* 294 (3): H1381-7.

- Pardi, G., A. M. Marconi, and I. Cetin. 2002. Placental-fetal interrelationship in IUGR fetuses--a review. *Placenta* 23 Suppl A: S136-41.
- Park, Y., S. Kanekal, and J. P. Kehrer. 1991. Oxidative changes in hypoxic rat heart tissue. *The American Journal of Physiology* 260 (5 Pt 2): H1395-405.
- Parr, E. L., H. N. Tung, and M. B. Parr. 1987. Apoptosis as the mode of uterine epithelial cell death during embryo implantation in mice and rats. *Biology of Reproduction* 36 (1): 211-25.
- Parraguez, V. H., M. A. Atlagich, B. Urquieta, M. Galleguillos, M. De Los Reyes, D. L. Kooyman, S. Araneda, and L. A. Raggi. 2010. Expression of vascular endothelial growth factor and endothelial nitric oxide synthase is increased in the placenta of sheep at high altitude in the andes. *Canadian Journal of Veterinary Research = Revue Canadienne De Recherche Veterinaire* 74 (3): 193-9.
- Pasquali, R., L. Patton, and A. Gambineri. 2007. Obesity and infertility. *Current Opinion in Endocrinology, Diabetes, and Obesity* 14 (6): 482-7.
- Paulesu, L., J. Bhattacharjee, N. Bechi, R. Romagnoli, S. Jantra, and F. Ietta. 2010. Pro-inflammatory cytokines in animal and human gestation. *Current Pharmaceutical Design* 16 (32): 3601-15.
- Perlow, J. H., M. A. Morgan, D. Montgomery, C. V. Towers, and M. Porto. 1992. Perinatal outcome in pregnancy complicated by massive obesity. *American Journal of Obstetrics and Gynecology* 167 (4 Pt 1): 958-62.
- Petanovski, Z., G. Dimitrov, B. Ajdin, M. Hadzi-Lega, V. Sotirovska, V. Matevski, S. Stojkovska, S. Saltirovski, D. Suslevski, and E. Petanovska. 2011. Impact of body mass index (BMI) and age on the outcome of the IVF process. *Prilozi / Makedonska Akademija Na Naukite i Umetnostite, Oddelenie Za Bioloski i Medicinski Nauki = Contributions / Macedonian Academy of Sciences and Arts, Section of Biological and Medical Sciences* 32 (1): 155-71.
- Pfarrer, C., L. Macara, R. Leiser, and J. Kingdom. 1999. Adaptive angiogenesis in placentas of heavy smokers. *Lancet* 354 (9175): 303.
- Picut, C. A., C. L. Swanson, R. F. Parker, K. L. Scully, and G. A. Parker. 2009. The metrial gland in the rat and its similarities to granular cell tumors. *Toxicologic Pathology* 37 (4): 474-80.
- Pijnenborg, R., L. Vercruysse, and M. Hanssens. 2006. The uterine spiral arteries in human pregnancy: Facts and controversies. *Placenta* 27 (9-10): 939-58.

- Qiu, Q., M. Yang, B. K. Tsang, and A. Gruslin. 2004. EGF-induced trophoblast secretion of MMP-9 and TIMP-1 involves activation of both PI3K and MAPK signalling pathways. *Reproduction (Cambridge, England)* 128 (3): 355-63.
- Rajasingam, D., P. T. Seed, A. L. Briley, A. H. Shennan, and L. Poston. 2009a. A prospective study of pregnancy outcome and biomarkers of oxidative stress in nulliparous obese women. *American Journal of Obstetrics and Gynecology* 200 (4): 395.e1,395.e9.
- . 2009b. A prospective study of pregnancy outcome and biomarkers of oxidative stress in nulliparous obese women. *American Journal of Obstetrics and Gynecology* 200 (4): 395.e1,395.e9.
- Ray, J. G., M. J. Vermeulen, M. J. Schull, S. McDonald, and D. A. Redelmeier. 2005. Metabolic syndrome and the risk of placental dysfunction. *Journal of Obstetrics and Gynaecology Canada : JOGC = Journal d'Obstetrique Et Gynecologie Du Canada : JOGC* 27 (12): 1095-101.
- Reynolds, L. P., P. P. Borowicz, J. S. Caton, K. A. Vonnahme, J. S. Luther, C. J. Hammer, K. R. Maddock Carlin, A. T. Grazul-Bilska, and D. A. Redmer. 2010. Developmental programming: The concept, large animal models, and the key role of uteroplacental vascular development. *Journal of Animal Science* 88 (13 Suppl): E61-72.
- Reynolds, L. P., P. P. Borowicz, K. A. Vonnahme, M. L. Johnson, A. T. Grazul-Bilska, J. M. Wallace, J. S. Caton, and D. A. Redmer. 2005. Animal models of placental angiogenesis. *Placenta* 26 (10): 689-708.
- Roberts, V. H. J., J. Smith, S. A. McLea, A. B. Heizer, J. L. Richardson, and L. Myatt. 2009. Effect of increasing maternal body mass index on oxidative and nitrate stress in the human placenta. *Placenta* 30 (2): 169-75.
- Robinson, G. E. 2011. Dilemmas related to pregnancy loss. *The Journal of Nervous and Mental Disease* 199 (8): 571-4.
- Roca-Rivada, A., J. Alonso, O. Al-Massadi, C. Castela, J. R. Peinado, L. M. Seoane, F. F. Casanueva, and M. Pardo. 2011. Secretome analysis of rat adipose tissues shows location-specific roles for each depot type. *Journal of Proteomics* 74 (7): 1068-79.
- Rosario, G. X., T. Konno, and M. J. Soares. 2008. Maternal hypoxia activates endovascular trophoblast cell invasion. *Developmental Biology* 314 (2): 362-75.
- Rossant, J., and J. C. Cross. 2001. Placental development: Lessons from mouse mutants. *Nature Reviews Genetics* 2 (7): 538-48.

- Said, H. M., C. Hagemann, A. Staab, J. Stojic, S. Kuhnel, G. H. Vince, M. Flentje, K. Roosen, and D. Vordermark. 2007. Expression patterns of the hypoxia-related genes osteopontin, CA9, erythropoietin, VEGF and HIF-1alpha in human glioma in vitro and in vivo. *Radiotherapy and Oncology : Journal of the European Society for Therapeutic Radiology and Oncology* 83 (3): 398-405.
- Schmatz, M., J. Madan, T. Marino, and J. Davis. 2010. Maternal obesity: The interplay between inflammation, mother and fetus. *Journal of Perinatology : Official Journal of the California Perinatal Association* 30 (7): 441-6.
- Schulz, L. C., and E. P. Widmaier. 2004. The effect of leptin on mouse trophoblast cell invasion. *Biology of Reproduction* 71 (6): 1963-7.
- Sebire, N. J., and D. Talbert. 2001. 'Cor placentale': Placental intervillous/intravillous blood flow mismatch is the pathophysiological mechanism in severe intrauterine growth restriction due to uteroplacental disease. *Medical Hypotheses* 57 (3): 354-7.
- Seed, P. T., L. C. Chappell, M. A. Black, K. K. Poppe, Y. C. Hwang, N. Kasabov, L. McCowan, et al. 2011. Prediction of preeclampsia and delivery of small for gestational age babies based on a combination of clinical risk factors in high-risk women. *Hypertension in Pregnancy : Official Journal of the International Society for the Study of Hypertension in Pregnancy* 30 (1): 58-73.
- Shankar, K., A. Harrell, X. Liu, J. M. Gilchrist, M. J. Ronis, and T. M. Badger. 2008. Maternal obesity at conception programs obesity in the offspring. *American Journal of Physiology.Regulatory, Integrative and Comparative Physiology* 294 (2): R528-38.
- Shankar, K., Y. Zhong, P. Kang, F. Lau, M. L. Blackburn, J. R. Chen, S. J. Borengasser, M. J. Ronis, and T. M. Badger. 2011. Maternal obesity promotes a proinflammatory signature in rat uterus and blastocyst. *Endocrinology* 152 (11): 4158-70.
- Shields, M. 2006. Overweight and obesity among children and youth. *Statistics Canada Catalogue: Health Reports* 17 (3): 27-42.
- Sibley, C. P., M. A. Turner, I. Cetin, P. Ayuk, C. A. Boyd, S. W. D'Souza, J. D. Glazier, S. L. Greenwood, T. Jansson, and T. Powell. 2005. Placental phenotypes of intrauterine growth. *Pediatric Research* 58 (5): 827-32.
- Siddiqui, I.A., Jaleel, A., Tamimi, W., Al Khadri, H.M. 2010. Role of oxidative stress in the pathogenesis of preeclampsia. *Archives of Gynecology and Obstetrics* 282 (5): 469-74

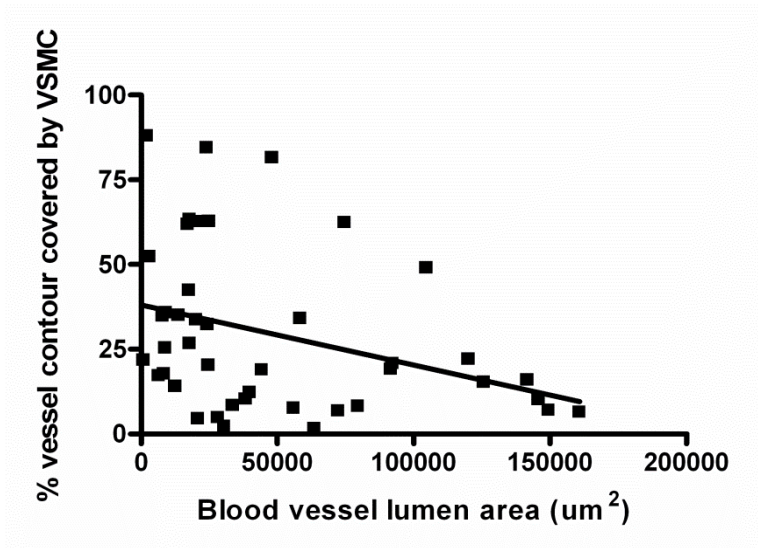
- Silasi, M., B. Cohen, S. A. Karumanchi, and S. Rana. 2010. Abnormal placentation, angiogenic factors, and the pathogenesis of preeclampsia. *Obstetrics and Gynecology Clinics of North America* 37 (2): 239-53.
- Singh, A. S., C. Mulder, J. W. Twisk, W. van Mechelen, and M. J. Chinapaw. 2008. Tracking of childhood overweight into adulthood: A systematic review of the literature. *Obesity Reviews : An Official Journal of the International Association for the Study of Obesity* 9 (5): 474-88.
- Sirimi, N., and D. G. Goulis. 2010. Obesity in pregnancy. *Hormones (Athens, Greece)* 9 (4): 299-306.
- Sivitz, W. I., S. M. Wayson, M. L. Bayless, C. A. Sinkey, and W. G. Haynes. 2007. Obesity impairs vascular relaxation in human subjects: Hyperglycemia exaggerates adrenergic vasoconstriction arterial dysfunction in obesity and diabetes. *Journal of Diabetes and its Complications* 21 (3): 149-57.
- Smith, J., M. Al-Amri, P. Dorairaj, and A. Sniderman. 2006. The adipocyte life cycle hypothesis. *Clinical Science (London, England : 1979)* 110 (1): 1-9.
- Soares, M. J., and J. S. Hunt, eds. 2006. *Placenta and trophoblast: Methods and protocols volume 1*. Totowa, NJ: Humana Press Inc.
- Sohlberg, S., Stephansson, O., Cnattingius, S., Wikstrom, A.K. 2012. Maternal body mass index, height, and risks of preeclampsia. *American Journal of Hypertension* 25 (1): 120-5
- Soleymanlou, N., I. Jurisica, O. Nevo, F. Ietta, X. Zhang, S. Zamudio, M. Post, and I. Caniggia. 2005. Molecular evidence of placental hypoxia in preeclampsia. *The Journal of Clinical Endocrinology and Metabolism* 90 (7): 4299-308.
- Souter, I., L. M. Baltagi, D. Kuleta, J. D. Meeker, and J. C. Petrozza. 2011. Women, weight, and fertility: The effect of body mass index on the outcome of superovulation/intrauterine insemination cycles. *Fertility and Sterility* 95 (3): 1042-7.
- Srinivas, S. K., L. M. Ernst, A. G. Edlow, and M. A. Elovitz. 2008. Can placental pathology explain second-trimester pregnancy loss and subsequent pregnancy outcomes? *American Journal of Obstetrics and Gynecology* 199 (4): 402.e1,402.e5.
- Staff, A. C., T. Ranheim, T. Henriksen, and B. Halvorsen. 2000. 8-iso-prostaglandin f(2alpha) reduces trophoblast invasion and matrix metalloproteinase activity. *Hypertension* 35 (6): 1307-13.

- Stewart, F. M., D. J. Freeman, J. E. Ramsay, I. A. Greer, M. Caslake, and W. R. Ferrell. 2007. Longitudinal assessment of maternal endothelial function and markers of inflammation and placental function throughout pregnancy in lean and obese mothers. *Journal of Clinical Endocrinology & Metabolism* 92 (3): 969.
- Stewart, F. M., D. J. Freeman, J. E. Ramsay, I. A. Greer, M. Caslake, and W. R. Ferrell. 2007. Longitudinal assessment of maternal endothelial function and markers of inflammation and placental function throughout pregnancy in lean and obese mothers. *The Journal of Clinical Endocrinology and Metabolism* 92 (3): 969-75.
- Stillbirth Collaborative Research Network Writing Group. 2011. Causes of death among stillbirths. *JAMA : The Journal of the American Medical Association* 306 (22): 2459-68.
- Strackowski, M., S. Dzienis-Strackowska, A. Stepien, I. Kowalska, M. Szelachowska, and I. Kinalska. 2002. Plasma interleukin-8 concentrations are increased in obese subjects and related to fat mass and tumor necrosis factor-alpha system. *The Journal of Clinical Endocrinology and Metabolism* 87 (10): 4602-6.
- Sucak, A., M. Kanat-Pektas, T. Gungor, and L. Mollamahmutoglu. 2010. Leptin levels and antihypertensive treatment in preeclampsia. *Singapore Medical Journal* 51 (1): 39-43.
- Szarka, A., J. Rigo Jr, L. Lazar, G. Beko, and A. Molvarec. 2010. Circulating cytokines, chemokines and adhesion molecules in normal pregnancy and preeclampsia determined by multiplex suspension array. *BMC Immunology* 11: 59.
- Takata, K., K. Fujikura, and B. Shin. 1997. Ultrastructure of the rodent placental labyrinth: A site of barrier and transport. *Journal of Reproduction and Development* 43 (1): 13-24.
- Tayade, C., D. Hilchie, H. He, Y. Fang, L. Moons, P. Carmeliet, R. A. Foster, and B. A. Croy. 2007. Genetic deletion of placenta growth factor in mice alters uterine NK cells. *Journal of Immunology (Baltimore, Md.: 1950)* 178 (7): 4267-75.
- Thaete, L. G., E. R. Dewey, and M. G. Neerhof. 2004. Endothelin and the regulation of uterine and placental perfusion in hypoxia-induced fetal growth restriction. *Journal of the Society for Gynecologic Investigation* 11 (1): 16-21.
- Thornburg, K. L., P. F. O'Tierney, and S. Louey. 2010. Review: The placenta is a programming agent for cardiovascular disease. *Placenta* 31 Suppl: S54-9.

- Tissot van Patot, M., A. Grilli, P. Chapman, E. Broad, W. Tyson, D. S. Heller, L. Zwerdinger, and S. Zamudio. 2003. Remodelling of uteroplacental arteries is decreased in high altitude placentae. *Placenta* 24 (4) (Apr): 326-35.
- Tjempkema, M. 2006. Adult obesity. *Health Rep.* 17(3): 9-25
- Turpa, A. B. N. B. A., M. Kavutçub, and Ö. H. İ. Durakç. 2007. Role of oxidative stress in intrauterine growth restriction. *Gynecol Obstet Invest* 64 : 187-92.
- Um, J. Y., H. S. Chung, M. Y. Song, H. D. Shin, and H. M. Kim. 2004. Association of interleukin-1beta gene polymorphism with body mass index in women. *Clinical Chemistry* 50 (3): 647-50.
- Vahratian, A., and Y. R. Smith. 2009. Should access to fertility-related services be conditional on body mass index? *Human Reproduction (Oxford, England)* 24 (7): 1532-7.
- van Lieden, H.A., Dekker, J.M., Moll, A.C., Nijpels, G., Heine, R.J., Bouter, L.M., Stehouwer, C.D., Polak, B.C. 2003. Risk factors for incident retinopathy in a diabetic and nondiabetic population: the Hoorn study. *Arch Ophthalmol* 121 (2): 245-51
- Veilleux, A., M. Caron-Jobin, S. Noel, P. Y. Laberge, and A. Tchernof. 2011. Visceral adipocyte hypertrophy is associated with dyslipidemia independent of body composition and fat distribution in women. *Diabetes* 60 (5): 1504-11.
- Vercruyse, L., S. Caluwaerts, C. Luyten, and R. Pijnenborg. 2006. Interstitial trophoblast invasion in the decidua and mesometrial triangle during the last third of pregnancy in the rat. *Placenta* 27 (1): 22-33.
- Verlohren, S., N. Geusens, J. Morton, I. Verhaegen, L. Hering, F. Herse, J. W. Dudenhausen, et al. 2010. Inhibition of trophoblast-induced spiral artery remodeling reduces placental perfusion in rat pregnancy. *Hypertension* 56 (2): 304-10.
- Visner, G. A., S. E. Chesrown, J. Monnier, U. S. Ryan, and H. S. Nick. 1992. Regulation of manganese superoxide dismutase: IL-1 and TNF induction in pulmonary artery and microvascular endothelial cells. *Biochemical and Biophysical Research Communications* 188 (1): 453-62.
- Wang, Y., and S. Zhao. 2010. *Vascular biology of the placenta*, eds. N. Granger, J. Granger. NJ: Morgan and Claypool Life Sciences.
- Watson, A. L., J. N. Skepper, E. Jauniaux, and G. J. Burton. 1998. Susceptibility of human placental syncytiotrophoblastic mitochondria to oxygen-mediated damage in

- relation to gestational age. *The Journal of Clinical Endocrinology and Metabolism* 83 (5): 1697-705.
- Watson, E. D., and J. C. Cross. 2005. Development of structures and transport functions in the mouse placenta. *Physiology (Bethesda, Md.)* 20: 180-93.
- White, C. L., M. N. Purpera, and C. D. Morrison. 2009. Maternal obesity is necessary for programming effect of high-fat diet on offspring. *American Journal of Physiology.Regulatory, Integrative and Comparative Physiology* 296 (5): R1464-72.
- Whitley, G. S., and J. E. Cartwright. 2010. Cellular and molecular regulation of spiral artery remodelling: Lessons from the cardiovascular field. *Placenta* 31 (6): 465-74.
- Wong, H. S., and Y. K. Cheung. 2010. Sonographic study of the decidua basalis in early pregnancy loss. *Ultrasound in Obstetrics & Gynecology : The Official Journal of the International Society of Ultrasound in Obstetrics and Gynecology* 36 (3): 362-7.
- World Health Organization. 2000. Obesity: Preventing and managing the global epidemic. report of a WHO consultation. *World Health Organization Technical Report Series* 894 : i,xii, 1-253.
- Xu, J., H. Liu, Y. Wu, X. Gong, Q. Zhou, and F. Qiao. 2011. Proapoptotic effect of metalloproteinase 9 secreted by trophoblasts on endothelial cells. *The Journal of Obstetrics and Gynaecology Research* 37 (3): 187-94.
- Yamamoto, S., T. Douchi, N. Yoshimitsu, M. Nakae, and Y. Nagata. 2001. Waist to hip circumference ratio as a significant predictor of preeclampsia, irrespective of overall adiposity. *The Journal of Obstetrics and Gynaecology Research* 27 (1): 27-31.
- Yoshioka, T., T. Homma, B. Meyrick, M. Takeda, T. Moore-Jarrett, V. Kon, and I. Ichikawa. 1994. Oxidants induce transcriptional activation of manganese superoxide dismutase in glomerular cells. *Kidney International* 46 (2): 405-13.
- Yung, H.W., Calabrese, S., Hynx, D., Hemmings, B.A., Cetin, I., Charnock-Jones, D.S., Burton, G.J. 2008. Evidence of placental translation inhibition and endoplasmic reticulum stress in the etiology of human intrauterine growth restriction. *American Journal of Pathology* 173 (2): 451-62
- Zahorska-Markiewicz, B. 2006. Metabolic effects associated with adipose tissue distribution. *Advances in Medical Sciences* 51 : 111-4.
- Zamudio, S. 2003. The placenta at high altitude. *High Altitude Medicine & Biology* 4 (2) (Summer): 171-91.

- Zavalza-Gomez, A. B. 2011. Obesity and oxidative stress: A direct link to preeclampsia? *Archives of Gynecology and Obstetrics* 283 (3): 415-22.
- Zhang, E. G., G. J. Burton, S. K. Smith, and D. S. Charnock-Jones. 2002. Placental vessel adaptation during gestation and to high altitude: Changes in diameter and perivascular cell coverage. *Placenta* 23 (10): 751-62.
- Zhang, K. 2010. Integration of ER stress, oxidative stress and the inflammatory response in health and disease. *International Journal of Clinical and Experimental Medicine* 3 (1): 33-40.
- Zhou, Y., K. Chiu, R. J. Brescia, C. A. Combs, M. A. Katz, J. L. Kitzmiller, D. C. Heilbron, and S. J. Fisher. 1993. Increased depth of trophoblast invasion after chronic constriction of the lower aorta in rhesus monkeys. *American Journal of Obstetrics and Gynecology* 169 (1): 224-9.



**Supplemental Figure 1. Decreased VSMC coverage is associated with increased lumen area in invaded blood vessels.** A. Slides stained with anti-pancytokeratin (1:300; Sigma) were used to identify endovascular trophoblasts, and parallel or nearby slides were stained with anti-SMA (1:200; Sigma). Only vessels that were partially or fully invaded by endovascular trophoblasts were analyzed. The percentage of contour length covered by SMA-positive VSMCs was quantified in the entire artery contour of fully or partially invaded arteries and compared to the lumen area for each artery.

**Diet composition, % kcal**

	<b>CON</b>	<b>HF</b>
<b>Protein</b>	29	20
<b>Carbohydrate</b>	54	35
<b>Fat</b>	17	45

**Appendix 1. Macronutrient composition of CON diet (Harlan Teklad 22/5 Rodent Diet 8640) and HF diet (Research Diets D12451)**